



POLITECNICO DI TORINO

DIPARTIMENTO DI INGEGNERIA MECCANICA E AEROSPAZIALE
(DIMEAS)

Master's Degree in Biomedical Engineering

**Design and Implementation of Wearable
Devices for sEMG Detection and
Analysis of Muscle Synergies**

Supervisors

Prof. Danilo DEMARCHI
Dott. Paolo MOTTO ROS

Candidate

Giovanni MANZELLA

TORINO, October 2019

Abstract

This thesis is part of a larger project, called *MITOR* (a collaboration between Politecnico di Torino (*POLITO*), Massachusetts Institute of Technology (*MIT*) and *Spaulding Rehabilitation Hospital's Motion Analysis Laboratory* (an affiliate of Harvard Medical School)). This project aims to develop a wearable, wireless, low-power surface *ElectroMyoGraphy* (sEMG) acquisition system for long-term monitoring of muscle synergies and diagnostic motor rehabilitation.

The system's hardware specification was defined specifically for sEMG acquisition channels. Where the resulting signals are stored locally on a microSD card.

The circuit diagrams were drawn referencing the schematics of the previous version of the MITOR system. In this revision, the most significant changes from the previous MITOR is an upgraded microcontroller and additional components in the acquisition channel (so the board can detect *Threshold Crossing* (TC) signals). The TC signal is a quasi-digital signal obtained by comparing sEMG signal and a threshold. Each time the sEMG signal exceeds this threshold an event is generated. The number of events is proportional to the electrical muscle activity. From this signal, it is possible to calculate the *Average Threshold Crossing* (ATC) by noting the number of TC events into a fixed window of time. Applying this approach to sEMG is innovative as it involves a considerable reduction in power consumption due to drastically reducing the volume of data in need of processing, saving and transmission.

Using *Altium Design*[®], a two-layer *Printed Circuit Board* (PCB) was created. In this phase, all the electronic components were placed in order to minimize board size by optimizing its dimensions (50mm x 37.5mm). Most of the components were soldered manually or with the use of a pick-and-place machine. Once the components were set, the electrical connections were checked.

A case for the PCB was created to ease the process of placing the devices on human subjects for sEMG signal recording.

The microcontroller firmware was written in C++, using the *IAR Embedded Workbench IDE*[®]. The firmware allows three different working modes: classic sEMG signal, sEMG envelope (using digital filters in the firmware), and ATC signal.

The main feature of the firmware is wireless synchronization between the different MITOR boards (possible due to a PCB antenna). This is the crucial element that needed to be tested to guarantee long-term analysis. The results showed a maximum delay of 10 μ s with a synchronization period of 5s. Another important aspect to analyze is power consumption. Each developed board, with a battery supply of 450mA/h, can store data for more than 42 hours in classic sEMG mode; or for more than 80 hours in ATC mode.

A commercially available multi-channel EMG system from *Motion Lab Systems* was used to validate the sEMG signal recorded by the MITOR system. For the tests, muscles of the upper-limbs performing grasping movement and of the lower-limbs during gait were selected.

The developed boards, in combination with the Motion Lab Systems' probes, were used to extract muscle synergies during gait in a healthy subject. In addition to the classic method, the ATC approach was also tested to extract the synergies. The synergies with ATC signal, compared with the synergies of the classic method, showed good results. The performance was evaluated in terms of zero lag cross-correlation between the time activations and of cosine similarity between the muscle weights.

Summary

This thesis is part of a larger project, called *MITOR* (a collaboration between Politecnico di Torino (*POLITO*), Massachusetts Institute of Technology (*MIT*) and *Spaulding Rehabilitation Hospital's Motion Analysis Laboratory* (an affiliate of Harvard Medical School)). This project aims to develop a wearable, wireless, low-power surface *ElectroMyoGraphy* (sEMG) acquisition system for long-term monitoring of muscle synergies and diagnostic motor rehabilitation.

In this thesis, a new version of the *MITOR* acquisition system, consisting of 6 wearable devices, has been designed, implemented and tested. Each board can synchronously record the sEMG signal, envelope or Average Threshold Crossing (ATC) signal.

The recorded signal was validated using a system on the EMG market.

In addition, a data collection has been carried out on a healthy patient so that muscle synergies can be extracted during the journey. In addition to the classic synergy extraction approach, an innovative approach using the ATC signal has also been tested. This document is composed by 10 chapters:

1. **Background Information:** This chapter provides all introductory information on all topics of interest to the thesis. This begins with a purely physiological part in which the muscle system is analyzed so that the EMG signal can be introduced and justified. The attention then passes on the surface EMG signal. The last two paragraphs deal instead with the ATC signal and an introduction to what is meant by muscle synergies.
2. **State of Art:** This chapter analyses the state of the art of wearable sEMG acquisition systems and the literature of ATC applied to the sEMG signal and muscle synergies. The last part of the chapter analyzes previous versions of the *MITOR* system.
3. **Hardware Design:** This chapter analyses and justifies all the hardware design steps taken to make the devices. It also contains a short guide explaining the main steps to make PCBs with Altium Design[®].

4. **Software Design:** In this chapter are shown the main flowcharts of the firmware, written in C++ of the MITOR system. In particular, the algorithms of ATC, DAC, synchronization, and ADC are discussed.
5. **Operation Testing:** This chapter shows the tests performed after assembling the boards. First, the synchronization between the boards has been tested. In addition, the quality of the signal recorded in the three modes.
6. **System Validation:** The signals recorded with MITOR devices have been validated using the Motion Lab System in terms of SNR and time activations.
7. **Electrical Characterization:** This part discusses power consumption and impedance measurement tests.
8. **Muscles Synergies Analysis:** This chapter begins with a brief introduction to gait analysis and then analyzes in detail the procedures carried out to carry out the data collection, process data, and extract muscle synergies during walking.
9. **Conclusion:** This final chapter summarizes all the steps taken in the thesis to show the final level of the work done.
10. **Future Steps:** As part of an unfinished project, this chapter is useful to show what future changes could be made to the system in later versions.

Acknowledgements

First of all, I would like to thank Danilo Demarchi and Paolo Motto ROS for allowing me to work on this thesis and for motivating and guiding me throughout the project.

I would also like to thank Paolo Bonato for allowing me to spend six months in his laboratory: Motion Analysis Lab, at Spaulding Rehabilitation Hospital in Boston. This experience has allowed me to grow personally and professionally, making me understand the direction to take in my future career. A special thanks go to Stefano Sapienza for having supported and endured me during the months spent at the MAL and for having always encouraged me to give the maximum.

I cannot fail to thank all my friends and colleagues who have been close to me during my studies. Finally, I am truly grateful to my family for having always been close to me, regardless of physical distances, and for having taught me the value of sacrifice. Thank you!

Prima di tutto, vorrei ringraziare Danilo Demarchi e Paolo Motto ROS per avermi dato l'opportunità di lavorare a questa tesi e per avermi motivato e guidato lungo tutto il progetto.

Inoltre vorrei ringraziare Paolo Bonato per avermi permesso di trascorrere sei mesi nel suo laboratorio: Motion Analysis Lab, presso Spaulding Rehabilitation Hospital in Boston. Questa esperienza mi ha permesso di crescere dal punto di vista personale e lavorativo facendomi capire la direzione da prendere nella mia futura carriera. Un ringraziamento speciale va a Stefano Sapienza per avermi supportato e sopportato durante i mesi trascorsi al MAL e per avermi sempre incitato a dare il massimo.

Non posso inoltre non ringraziare tutti i miei amici e colleghi che mi sono stati vicini durante questo mio percorso di studi. Infine sono veramente grato alla mia famiglia per essermi stato sempre vicino, indipendentemente dalle distanze fisiche, e per avermi insegnato il valore dei sacrifici. Grazie.

Giovanni Manzella

Contents

Abstract	IV
Summary	VI
Acknowledgements	VII
List of Tables	XII
List of Figures	XIII
1 Background Information	1
1.1 Basis of Muscular System	1
1.1.1 The Skeletal Muscle	2
1.2 ElectroMyoGraphy (EMG)	7
1.3 Surface ElectroMyoGraphy (sEMG)	10
1.3.1 Technique	10
1.3.2 Electrical Noise in sEMG Signal	11
1.3.3 sEMG Acquisition Properties	12
1.4 Average Threshold Crossing (ATC)	13
1.5 Muscle Synergies	15
1.5.1 Extraction and Evaluation of Muscle Synergies	17
2 State of Art	19
2.1 ATC used to sEMG Application	19
2.2 Muscle Synergies Analysis	21
2.3 MITOR Project previous versions	22
3 Hardware Design	25
3.1 Design Specification	25
3.1.1 Device Architecture	26

3.2	Analog Front-End	28
3.2.1	sEMG Acquisition Chain	29
3.2.2	TC Events Detection	36
3.2.3	RC Debounce Circuit	39
3.3	Power Supply Unit	40
3.4	Antenna	41
3.5	Local Storage Unit	41
3.6	Accelerometer and Gyroscope	42
3.7	Microcontroller	43
3.7.1	Other component	44
3.7.2	nRF52840 Vs nRF52832	45
3.8	Device Development	45
3.8.1	Case Design	48
4	Firmware Design	50
4.1	Overview	50
4.2	Slave Firmware	50
4.2.1	Initialization: General	51
4.2.2	Initialization: ATC	53
4.2.3	Synchronization routine	56
4.2.4	ADC Management	58
4.3	Master Firmware	60
5	Operation Testing	62
5.1	Electrical test	62
5.2	Synchronization Test	62
5.2.1	Data Pre-Processing	65
5.3	Recording Data Analysis	66
5.3.1	sEMG Signal	66
5.3.2	sEMG Envelope	70
5.3.3	ATC Parameters	70
6	System Validation	73
6.1	Methods and Materials	73
6.1.1	Motion Lab Systems	73
6.1.2	Test Protocol	74
6.2	Validation Results	75

7	Electrical Characterization	78
7.1	Power Consumption	78
7.1.1	Comparison With Other Devices	81
7.1.2	ATC consumption: Hardware VS Firmware	82
7.2	Impedance Measurements	83
7.3	Potential Risk	83
8	Muscles Synergies Analysis	85
8.1	Gait Analysis	85
8.2	Materials And Methods	87
8.2.1	Muscle Selection	87
8.2.2	Data Collection Protocol	91
8.2.3	Initial processing	91
8.3	Traditional Approach	92
8.4	ATC Approach	95
9	Conclusion	100
10	Future Steps	102
A	Circuit Diagram and Altium Design® Project	104
	Acronyms	114
	Bibliography	117

List of Tables

3.1	AD5621 characteristics	38
3.2	nRF52840 nRF52832 comparison	45
5.1	Comparison of Peak Artifact Amplitude	68
6.1	MA-300 EMG System, Motion Lab System, System Specification .	74
6.2	MA-411 EMG Preamplifier probe Specification	75
6.3	SNR values: Motion Lab System Vs MITOR board	76
7.1	Current Consumption	81
7.2	Current Consumption previous version	82
7.3	Current Consumption ATC: Hardware vs Firmware	82
7.4	Impedance Checks: acquisition channel and supply track	83

List of Figures

1.1	Type of muscle fibers.	2
1.2	Skeletal muscle overview.	3
1.3	Physiology of the contractile mechanism of muscle fibers.	4
1.4	Mechanism of muscular contraction.	5
1.5	Type of Muscle Actions.	7
1.6	Intramuscular ElectroMyoGraphy <i>iEMG</i>	8
1.7	Surface ElectroMyoGraphy <i>sEMG</i>	9
1.8	Electrodes Positions	11
1.9	Example of the frequency spectrum of the sEMG signal	12
1.10	Average Threshold Crossing transmission	13
1.11	Example of output signal of the comparator	14
1.12	Example of TC signals	16
2.1	ATC, Force, ARV signals in time domain	20
2.2	PCB Layout MITOR board version 1	23
2.3	PCB Layout MITOR board version 2 (Digital Part)	24
2.4	PCB Layout MITOR board version 2 (AFE Part)	24
3.1	nRF52840-DK	26
3.2	PCB slave overview	27
3.3	Block diagram of the custom slave boards	27
3.4	Block diagram of analog front-ends	28
3.5	Block diagram of EMG conditioning circuit	29
3.6	Schematic: overvoltage protection	29
3.7	Voltage follower configuration and schematic	30
3.8	Schematic: overvoltage protection	31
3.9	Schematic: Instrumentation amplifier	32
3.10	Schematic: Initial reset	33
3.11	Initial reset LTSPICE®	34
3.12	Schematic: active low pass filter (feedback)	35
3.13	Schematic: voltage follower (reference)	35

3.14 Schematic: active low pass filter (Sallen-Key)	36
3.15 Block diagram of TC events detection	36
3.16 Hysteresis comparator	37
3.17 Schematic: DAC	39
3.18 Force Sensing Resistor	39
3.19 Schematic: RC Debounce Circuit	40
3.20 Schematic: Power Supply Unit	40
3.21 Antenna layout	41
3.22 Schematic: μ SD card slot	42
3.23 Schematic: Accelerometer and Gyroscope	42
3.24 Schematic: Microcontroller	43
3.25 J-Link EDU Mini	44
3.26 Schematic: LEDs	44
3.27 IPC [®] Compliant Footprint Wizard	46
3.28 Schematic editing	47
3.29 PCB layout	48
3.30 Case Design	49
4.1 Flowchart: main high level	51
4.2 Flowchart: Threshold Calibration	54
4.3 AD5621 input register contents	56
4.4 Flowchart: Synchronization routine	57
4.5 Flowchart: High level sampling routine and raw-data routine	59
4.6 Flowchart: envelope and ATC routine	60
4.7 Flowchart: master main high level	61
5.1 Test delay without synchronization	63
5.2 Test delay with synchronization	64
5.3 Missing Synchronization Event	64
5.4 Correct Synchronization Event	65
5.5 Flowchart: Data Pre-processing	65
5.6 Recorded sEMG signal	66
5.7 Peaks analysis with TPS61099	67
5.8 Load Regulation comparison between TPS61099 and TPS63070	67
5.9 Peaks analysis with TPS63070	68
5.10 Peaks analysis with TPS63070 and 20 μ F Capacitor	69
5.11 PSD comparison between the three different test	69
5.12 Recorded sEMG Envelope	70
5.13 Selected Threshold (ATC mode)	71
5.14 Comparison ATC value Hardware vs Software	71

5.15	Borderline peak Hardware vs Software	72
6.1	MA-300 EMG System, Motion Lab System	73
6.2	Motion Lab System probes and Covidien Electrode for MITOR board	74
6.3	Signal recorded during maximum voluntary contraction of: a)Biceps Long Head by Motion Lab System; b)Triceps Brachii Lateral by Mo- tion Lab System; c)Biceps Long Head by MITOR system; d)Triceps Brachii Lateral by MITOR system	76
6.4	Comparison between the sEMG signal from Gastrocnemius Medialis	77
7.1	Block diagram of the power consumption test connection	78
7.2	Elaboration data supply current	79
7.3	Behavior of current consumption in three different working mode . .	80
7.4	Zone time/current of AC current on human body	84
8.1	Mains phases during gait cycle	85
8.2	Bipolar electrodes placement	87
8.3	Timing of muscle activity during normal gait	90
8.4	Data collection signals pre-processing flowchart	92
8.5	Block diagram of traditional synergies extraction method	93
8.6	Comparison between original envelope and reconstructed envelope (using R^2)	93
8.7	Extracted Synergies during the gait Left Vs Right Leg	94
8.8	Zero-Lag Cross-correlation and cosine similarity: Traditional Approach	95
8.9	Block diagram of ATC synergies extraction method	95
8.10	Similarity coefficient of classic envelope and ATC envelope	96
8.11	Example of ATC envelope Vs Classic envelope	97
8.12	synergies extraction with ATC approach	98
8.13	Zero-Lag Cross-correlation and Cosine similarity: ATC Approach .	99

Chapter 1

Background Information

1.1 Basis of Muscular System

The muscular system is composed by several muscles that interacting allow the human body movement, but also stabilize and maintain posture, protect underlying organs, produce of heat and permit the transport of organic substances like blood and food.

All this functions are controlled by the *Nervous System* through electrical stimuli, called *action potential* (AP). After receiving it, the muscle contracts it, and the contraction force determines the movement that can be involuntary or voluntary. This link between the Muscular system and the Nervous system has led to the creation, in physiology, of the *Neuromuscular System*.

It is possible make an initial categorization of the muscular system based on the type of muscles tissue that compose it. There are three different types of muscle tissue in the body [1]:

- **Skeletal (or Voluntary) Tissue**

The skeletal muscles are voluntary muscles controlled by the peripheral portion of the *Central Nervous System* (CSN). In Figure 1.1A, we can see that this type of tissue appear as striped with multi-nuclei. they are the only cells in the human body that are multinucleated. These muscles are responsible for body mobility. In fact the main functions are allow the movement of bones, maintaining the body's posture and moves lymph and blood. The ends of the skeletal muscles usually are linked to bones, skin or other muscles. In the subsection 1.1.1 there is a more details about this muscles type.

- **Smooth (or Involuntary) Tissue**

The Smooth Tissue are called Involuntary because these are controlled by the

autonomous nervous system. The cells of this muscle type are non-striated and have a spindle shape (Figure 1.1B). Each cell has a single, centrally located nucleus. This type of muscles has slow but sustained contraction in fact their principal functions are move organic substances trough digestive and urinary tracts. The smooth tissue is find in the walls of hollow visceral organs in the body, except in the heart.

- **Cardiac Tissue**

The cardiac muscle or myocardium, work autonomously and rhythmically. This muscle is characterized by a self-exciting and rhythmic repeating that define the heart's rhythmic contraction. This muscle is made up of striated cell connected in a network (Figure 1.1C). This particular structure allow that the stimulation of one part passes to another part of the heart muscle. It's this event that gives rise to the rhythmic movement introduced above. As its name suggests, this type of muscle is only present in the walls of the heart.

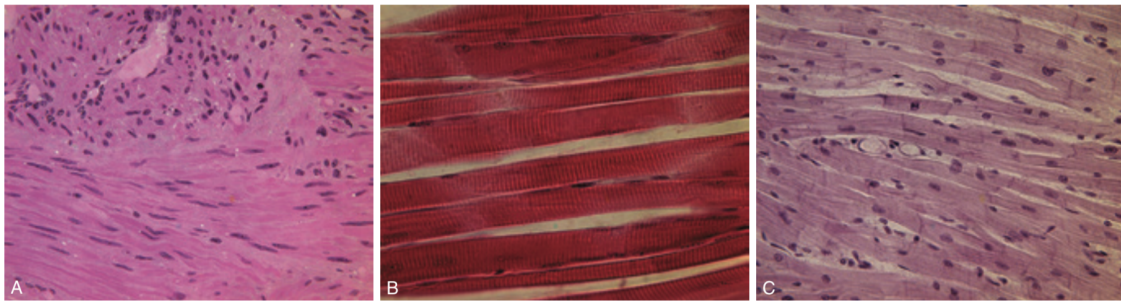


Figure 1.1: Type of muscle fibers:(A) skeletal, (B) smooth, and (C) cardiac [2].

1.1.1 The Skeletal Muscle

For this study is very important clearly understand the main features of the skeletal muscle, because these are related to the body movement and therefore of *ElectroMyoGraphy* (EMG). In fact the EMG signal represent the skeletal muscles' electric activity.

Skeletal Muscle makes up about 40% of the body weight, and another 10% is for smooth and cardiac tissue. So in an healthy body half of the total weight are muscles. These are composed by water (about 75%), protein (25%) and other organic and inorganic components like salt, carbohydrates, fat, glycogen ... (5%).

In this chapter, the several functions of the skeletal muscles will be analyzed in two different point of view: *Metabolic* and *Mechanical*. From a Metabolic prospective, skeletal muscles has an important role in the basal energy metabolism. In

fact this type of muscles works as a deposit for substrate such as amino acids and carbohydrates, but also like consumer of nutrients and oxygen during the contraction or to maintain the internal temperature. From Mechanical point of view the principal goal of the skeletal muscles is convert chemical energy into mechanical energy in order to generate force and power during the physical activity.

Physiology of Skeletal Muscles

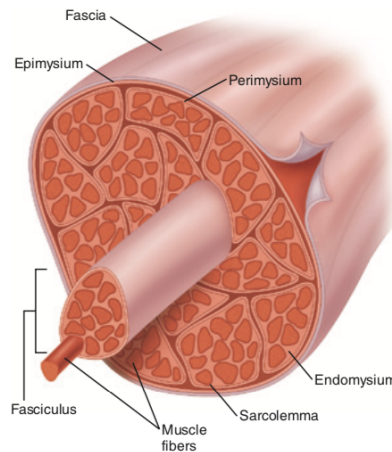


Figure 1.2: Skeletal muscle overview [2].

The skeletal muscles are made up of numerous muscle fibers with varied diameter (from 10 to 100 μm), hold together by fibrous connective tissue. The external structure take the name of *muscle fascia* that inside is composed by smaller elements. The *epimysium* is a connective tissue capsule that wraps the *perimysium*. The latter groups in turn the muscle fibers in *fasciculi*. The single muscular fiber is covered by the *sarcolemma* (a transparent plasma membrane). At the fiber extremities, sarcolemma and tendon fibers merge to giving rise to inelastic parts (*tendon*) that link the muscle to the bone.

Each muscular fiber is made up of *myofibril* that in turn is composed by about 3000 *filament of Actin* and 1500 *filament of Myosin* [3]. Between myofibril there is the *sarcoplasm*, a intracellular liquid rich of magnesium, phosphate, magnesium and numerous *mitochondria* that supply energy in form of ATP during contraction. These filaments are responsible for the muscle contractions as a result of their sliding movement. A longitudinal section of myofibril show that the inside structure is organized in different areas:

- **I** bands are made up of filaments of actin. These bands are bright because are

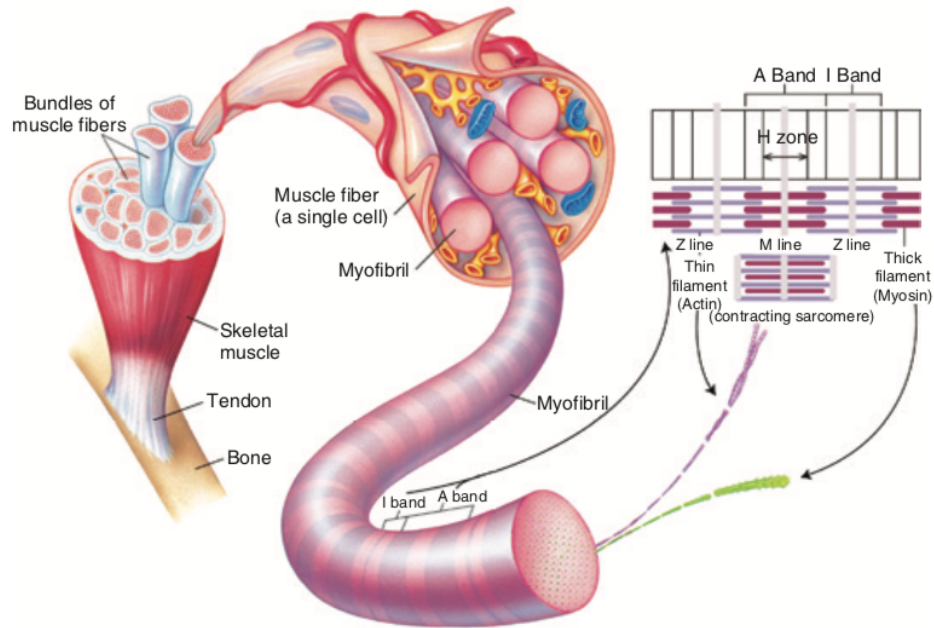


Figure 1.3: Physiology of the contractile mechanism of muscle fibers [2].

isotropic to polarized light.

- **A** bands are dark bands made up of filaments of Myosin that are isotropic to polarized light.
- **Z** disks are composed by mostly alpha-actinin. This protein fix the filaments of actin. The portion of myofibril between two disks *Z* is called *sarcomere*.
- **H** zone is the central part of the sarcomere. It is composed by thick filament.
- **M** line is a thickened area inside of the H zone that consists of proteins that hold the filament in place.

The position of the filaments of actin and myosin is fixed by the *titin*. This protein has a elastic filamentous structure. These filaments are placed among the *Z* disk and the *M* line, and work as a spring during the contraction.

Contraction Mechanism

The muscle contraction start when the CNS send an electrical stimulus via a motor nerve. The AP is spread through the *motor neuron* until the muscular fibers. Each ending the nerve free *acetylcholine*. This neurotransmitter opens the cationic

channels of the muscular membrane. This means that a significant amount of sodium ions (Na^+) enter inside that cause a local depolarization of the membrane. For this reason there is a AP generation inside the membrane that reaches the center of muscular fiber where the sarcoplasmic reticulum release calcium ions (Ca^+). These ions give rise to attractive force between the filaments of actin and myosin, that cause the sliding each other. Another essential characteristic of the myosin for the contraction, is the enzymatic property to obtain energy from the phosphate bond with high energy content of ATP (that became ADP). The contraction finish with rebalancing of Ca^{++} inside the sarcoplasmic reticulum.

Figure 1.4 shows what happens to actin and myosin during the contraction.

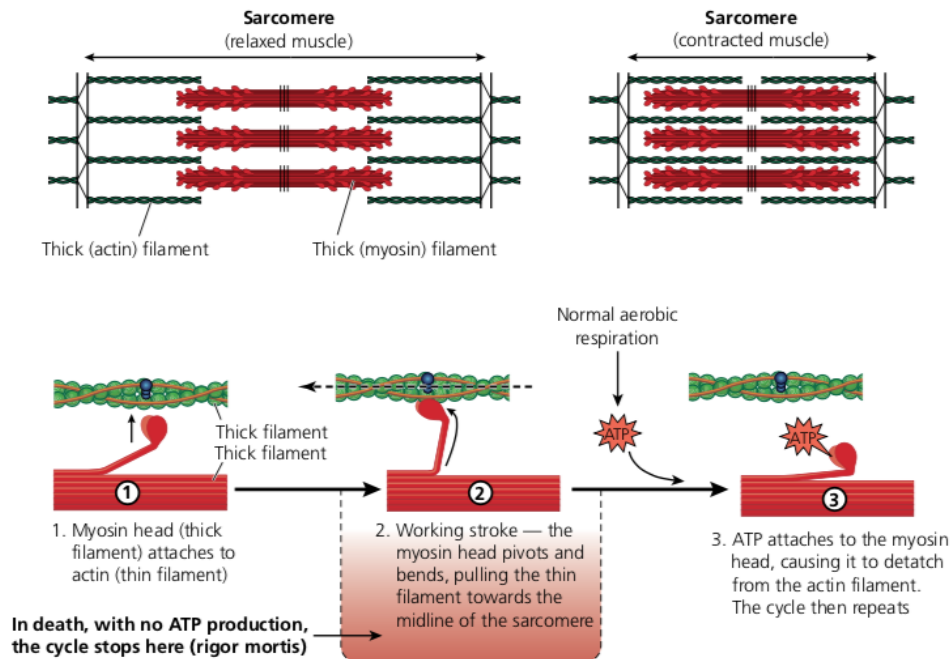


Figure 1.4: Mechanism of muscular contraction [1].

Type of Muscular Fiber

Each skeletal muscle is formed by different types of fibers, classified, in 3 types, based of their resistance and contraction speed. Another different between these types of fibers is the amount of *myosin* that determines a change of color of the fibers.

- **Type I or Red fibers**

These are suitable for slow and long lasting work, because they have a good tolerance to fatigue and have the capacity to remain contracted. This type of fiber involved in intense and long efforts. They are the first type of fiber to be recruited during the muscle contraction and they are able to produce a small force. The red fibers come with *aerobic metabolism*.

- **Type IIa or Intermediate fibers**

The intermediate fibers are able to perform rapid and medium-term contraction before expend effort. They are remarkably resilient. This type of fiber have an *anaerobic metabolism*.

- **Type IIb or White fibers**

The white fibers are the most powerful muscle fibers. They are suitable for strong and short-term efforts. They are characterized by a higher *conduction velocity* and for this reason have a rapid answer but a small resistance to fatigue. The fibers IIb are useful for maximum contractions. Also this type of fiber, as fiber IIa, have an *anaerobic metabolism*.

Muscle Movement

During the movement each muscles don't work alone but every movement is the result of the action of a group of muscles. It's possible classified, this groups, by functions. The muscles that are main activating during the movement take the name of *agonists* or prime movers. Instead, the muscles that oppose the movement are called *antagonists*. The role of the muscles is not fix, but a same group can be agonist or antagonist based on the type of move.

There are muscles that stabilize the origin (they hold a bone) of the prime movers. These muscles are the *fixator*. The *synergists* muscles help the agonist in the execution of the same movement.

The two main type of muscle contraction are static, also called *isometric contraction* of dynamic, defined as *isotonic contraction*. In the first type of contraction, the length of the muscles don't change. When a muscle contracts isometrically, a tension is generated without shortening or lengthening of the muscle fibers even if his sarcomeres became shorter. Instead, the isometric contraction are those in which there is a variation of length of the muscles. These can be *eccentric* or *concentric*. Eccentric occurs when the muscles is stretched and develops tension. As opposed the concentric in which the muscles shortens to move the attachment closer.

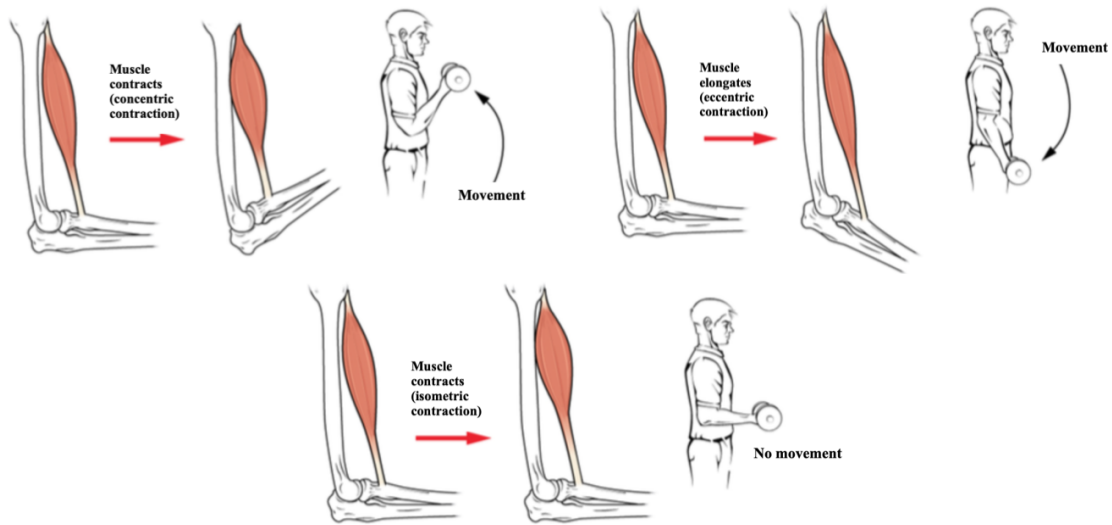


Figure 1.5: Type of muscle actions [1].

1.2 ElectroMyoGraphy (EMG)

The electromyographic signal is a bioelectrical information generated by the muscles during its contraction, representing neuronal and muscular activities. The smallest unit of the muscle activation signals are the *Motor Unit* (MU), these functional units are the smallest parts of the muscle that can be voluntarily contracted. One MU is composed by all the muscle fibers innervated by the same motor neuron. One collection of MUs, that is activated together during a low moderate force contraction, create a *Motor Unit Action Potential* (MUAP), which waveform shows how the MU are organized in that MUAP.

The EMG signal is the result of the electrical potentials generated by the depolarization/repolarization of the external membrane of muscle fibers. The amplitude of these potentials depends not only on the anatomical characteristics of the muscles but also on the position and properties of the electrodes used for the collection. The resulting signal at the detection point is the spatial-temporal sum of the individual action potentials produced by the depolarizations of the muscle fibers of a motor unit and is called MUAP (motor unit action potential)

Generally, in the electrode detection zone, there are contributions from other motor units, so a series of MUAPs are detected. Depending on the electrode used, there are variations in the shape, phase, and duration of MUAPs. The amplitude and shape of an observed MUAP are, therefore, a function of the geometric arrangement of the MU, muscle tissue and electrode properties used. The MUAPs generate a

contribution so much greater the closer they are to the area of withdrawal giving rise to the electromyographic signal.

There are two different types of EMG signal:

- **Intramuscular ElectroMyoGraphy (*iEMG*)**

This is the classic technique for recording and evaluating the EMG signal. The electrodes used are small needles embedded directly on the muscle. This technique has high selectivity and it is possible to study the single MUAP. The extracted signal allows us to distinguish the contributions of the single units (figure 1.6).

For this reason, it can be used to study both the morphology of the signal and

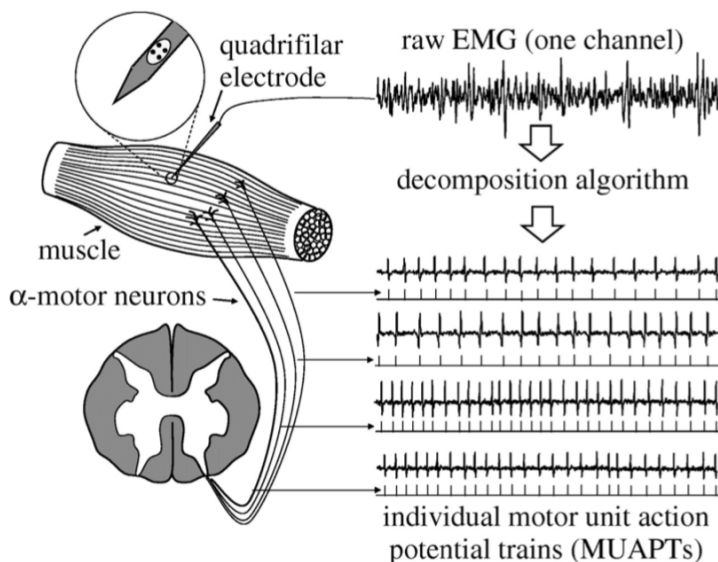


Figure 1.6: Intramuscular ElectroMyoGraphy (*iEMG*) [4].

the temporal activation. Another advantage of this technique is the absence of any kind of filtration and artifact caused by the tissue, as the electrode is directly placed in the muscle. The disadvantages of this technique are certainly the invasiveness of electrodes and the need to sterilize needles. Moreover, this type of sampling cannot be applied to dynamic motor activity. Nowadays, this technique is widely used in neurophysiology for the diagnosis of myopathies.

- **Surface ElectroMyoGraphy (*sEMG*)**

This is a non-invasive technique that involves recording the EMG by placing

the electrodes on the surface of the skin. The biosignal recorded in this way is an interference signal given by all the AP of all the motor units recruited. The signal obtained is affected by tissue filtration between the muscle and the electrodes. It is not useful to study the morphology of the sEMG signal as this because of the multiple sources that generate it giving it a noise aspect. This technique is suitable for dynamic analysis but to obtain good signals it is important to position the electrodes correctly.

When a surface electrode sample is made, the total potential generated by the motor units that they can detect is recorded and it is defined as the potential for interference. Generally, the surface electrodes can know the activity of about ten motor units regardless of the total amount that makes up the muscle. From the EMG signal of interference, it is possible to trace back to those generated by the individual motor units and to the instant of time in which they are activated, it is necessary to carry out the decomposition of the EMG signal. This procedure is carried out to know the method of recruitment of the motor units and therefore the specific functioning of the analyzed muscle.

The sEMG is widely used in rehabilitation because it allows to easily have

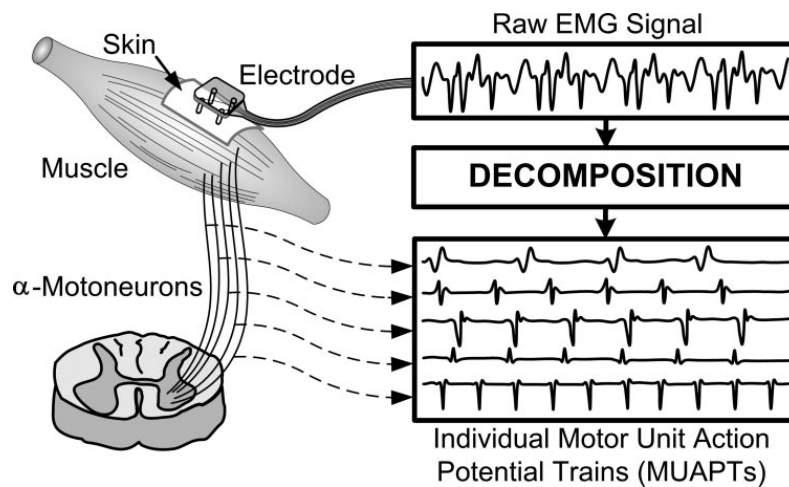


Figure 1.7: Surface ElectroMyoGraphy (*sEMG*) [5]

information both on the timing of the muscle activation during a movement both on the degree of contraction and on the relationship between muscle groups.

1.3 Surface ElectroMyoGraphy (sEMG)

1.3.1 Technique

When an sEMG signal is acquired it is necessary to define the recording mode (monopolar or bipolar), the electrodes configuration (single or double differential), the type of electrodes to be used and especially their position.

Electrodes

The most used electrodes are made of silver/silver chloride (Ag / AgCl), silver chloride (AgCl), silver (Ag) or gold (Au). The Ag/AgCl electrodes are the most used and have the ability not to be polarized. In addition, thanks to the use of a conductive gel layer, it is possible to reduce the sensitivity' to the movement artifacts caused by the sliding between electrode and skin. So these electrodes have good stability at the electrode-skin interface. Low-cost disposable electrodes exist with the built-in gel state to simplify and lessen the timing of electrode positioning. As for the size of the surface electrodes, they vary from millimeters to a few centimeters in diameter or length. Each electrode has its particular field of application, and the size depends on both the area of acquisition and the distance between two electrodes. So the size of the electrodes determines the spatial resolution.

Recording mode

For the sEMG, there are two recording modes: monopolar and bipolar. The monopolar mode consists of placing an active electrode at the muscle to be examined and a reference one at a neutral point. The bipolar mode instead requires the use of two active electrodes placed both on the examined muscle. The bipolar recording provides better immunity to disturbances but is characterized by less selectivity than the monopolar mode. In addition, more complex positioning is necessary for small muscles.

Electrodes Configuration

There are two electrode configurations: single or double differential. In the single differential, the sEMG signal is equal to the output voltage of an Operational Amplifier that makes the difference between its inputs. Three amplifiers are used in the dual differential. This mode allows to create a spatial filter and therefore allows to pick up signal more on the surface. The single differential sampling has

smaller dimensions and is less noisy but less selective. The double differential requires an extra electrode and this increases space but is more selective.

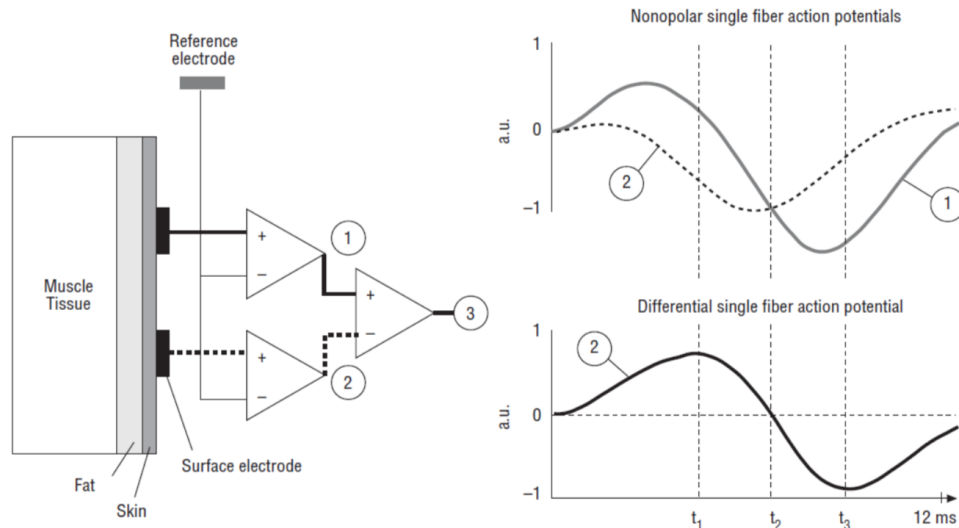


Figure 1.8: Electrodes positions[6]

1.3.2 Electrical Noise in sEMG Signal

During the acquisition of the sEMG signal the sources of noise that afflict the quality of the signal are multiple [7]:

- **Inherent Noise (electronic Components):** All electronic components generate noise throughout the band (white noise). This noise cannot be eliminated but can be reduced with high-quality components and by properly designing a circuit.
- **Environmental Noise:** This noise is caused by interference between the acquisition device and the external environment (antennas, power supply, etc.). One of the most interesting interferences of the sEMG signal is network interference (50Hz in the EU, 60Hz in the USA). ambient noise
- **Motion Artefact:** This noise can be generated either by the electrode sliding on the skin or by the movement of the cables connecting the electrodes to the amplification circuits. This noise is low frequency (below 15Hz).
- **Inherent Instability of the sEMG signal:** The sEMG signal between 0Hz and 20Hz is influenced by the almost physical nature of the firing rate of muscle

fibers. For this reason, it is appropriate not to consider this frequency band.

- **Muscle Cross-Talk:** This noise is caused by the activation of more muscles during the same movement. So during the recording of the sEMG signal of one muscle, the electrodes detect also the activation of another muscle. This causes a wrong interpretation of the recorded sEMG signal. The factors that most influence this phenomenon are the inter-electrode distance and their size.
- **Electrocardiographic (ECG) Artefacts:** The activity of the heart is a strong source of the noise. There is no way to eliminate, completely, this noise. This can be reduced using a high CMRR acquisition channel with bipolar recording.

1.3.3 sEMG Acquisition Properties

The sEMG signal is a stochastic signal, reasonably representative with a Gaussian distribution. The signal amplitude varies between 0mVpp and 10mVpp (Vpp: amplitude peak to peak), or from 0 to 1.5mV in rms. Spectral components are generally between 0Hz and 500Hz, but those with a higher power are in the 0Hz-150Hz band. A typical example of an sEMG signal is shown in the figure .

To acquire a signal sEMG is typically used as a biopotential acquisition chain

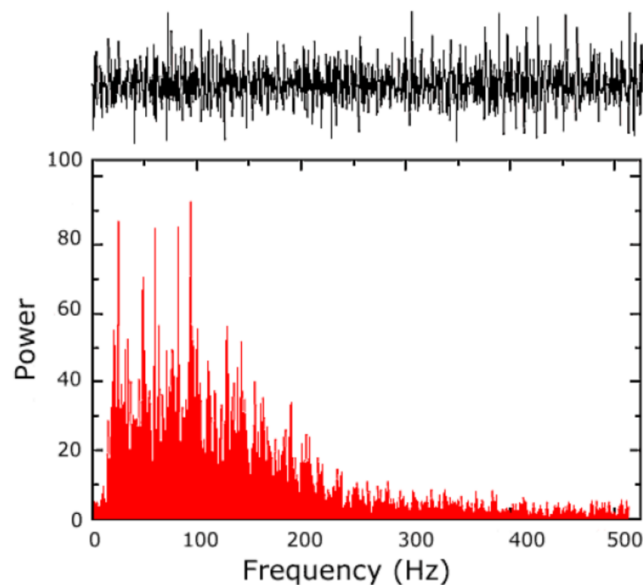


Figure 1.9: Example of the frequency spectrum of the sEMG signal [6]

composed of a series of alternating filtering and amplification blocks. The filtering

blocks are used to record only the sEMG signal in the most interesting band (usually 15Hz-400Hz) and to attenuate the previously analyzed noise. The amplification is necessary to adapt the sEMG signal (usually under 10mVpp) to the dynamics of ADC useful for digitizing the signal. So the typical acquisition channel consists of 4 main steps: *detection*, *amplification*, *conditioning*, and *digitizing*.

1.4 Average Threshold Crossing (ATC)

The *Threshold Crossing* (TC) is a technique in which an event is generated each time that an input signal crosses a fixed threshold. Many papers in literature show the advantages of using this approach for sEMG signal [8] [9] [10].

A comparison between the classic way of transmitting data and the innovative TC technique is shown in figure 1.10. The classic method involves the acquisition and the generation of TX Packets each fix time (T_s) with a sampling frequency of $1/T_s$. Meanwhile, with the TC approach, only when the signal crosses the threshold (V_{th}), the TX events are created.

On electronic point of view, this technique (applied to sEMG) is very easy to

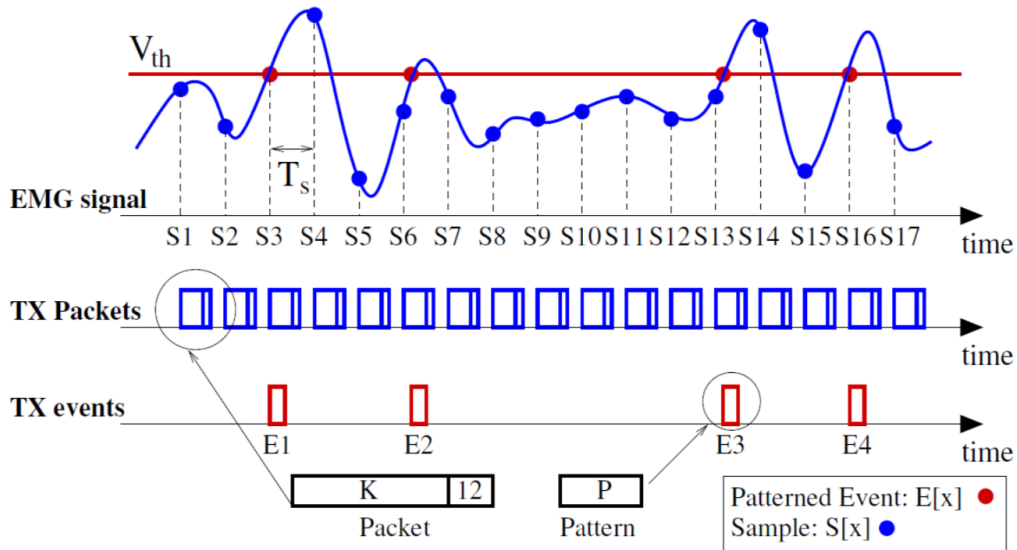


Figure 1.10: Comparison between classic sEMG transmission way and ATC technique [10].

implement, in fact, in addition to the classic acquisition channel only a operational amplifier comparator is required. This type of component are able to compare two analog voltage or current inputs. The sEMG signal and a voltage reference are the

inputs of this component, so in this way, every time that the signal is higher than the reference (threshold) the output take the value of the voltage supply. The output maintain this level until the signal falls below the threshold. Therefore, the outputs signals of the comparator has the same shape of a digital signal like in figure 1.11. It's more correct define this signal a *Quasi-Digital Signal*, because the information is contained in the time between two consecutive events. The TC signal can be given directly as input to a micro-controller or a wireless transmission module, without using an *Analog-to-Digital Converter* (ADC). This allow to reduce the number of component, and hence the space occupied by electronic components, in the device. The quasi digital signal allows to decrease the amount of data to be sent or in

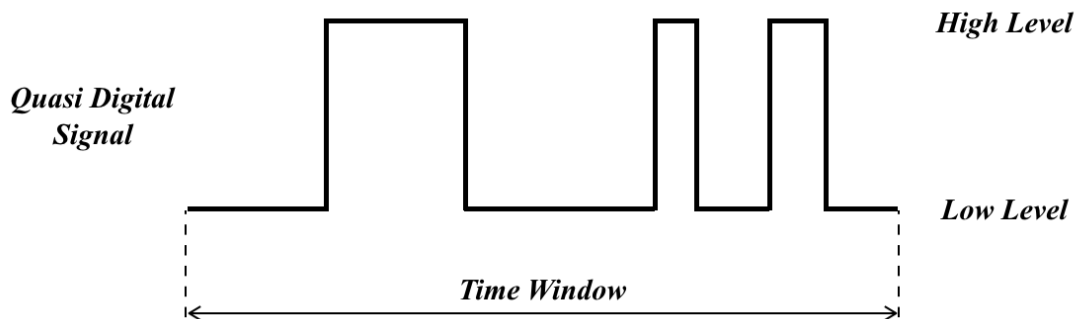


Figure 1.11: Example of output signal of the comparator.

general, that to be saved. Furthermore the ATC technique permits to obtain a low power consumption on transmitter perspective, compared to the standard way to process data. The shape of TC signal is optimal to be combined with *Impulse Radio Ultra Wide Band* (IR-UWB). This is a low power and robustness against interference radio technology that in the last years, has become very popular in *Wireless Body Area Networks* (WBAN), and in general in bio applications. The consumption of the TC technique are very dependent on the choice of the threshold, because a threshold level too low would cause many events to send, but a too high level would be the cause of few information. For this reason, the correct selection of threshold is a critical point of this technique. To obtain a good compromise between power consumption and amount of data, it could be useful use a *Dynamic Threshold*. In this way, the level of the threshold and so, also the number of events would be more controlled.

Starting to TC (figure 1.11), a time window can be fixed, in order to define the ATC parameter. This parameter give information about the average behavior of the signal into a fix windows. With this approach the amount of data significantly

decreases.

To sum up, the advantages of the TC technique are:

- ultra low power consumption;
- robust to noise;
- reduced data transmitted or saved;
- reduced component circuitry;
- applicable to WBAN application.

In opposition to these advantages, there are also some disadvantages that restrict the application fields of this technique:

- loss of the morphological properties of the signals;
- difficulty choosing of the correct threshold

In section 2.1 will be analyzed the multiple uses of the TC signals and of the ATC parameter, for the sEMG signal.

1.5 Muscle Synergies

Information about the sEMG signals of the muscles that taking part in the same movement, allows extracting muscle synergies. Synergic control is used by the *Central Nervous System* (CNS) to simplify the monitoring of the body's muscles. In this way, during a movement, the CNS controls the muscles in modules instead of individually. Managing these modules allows it to solve the problems of inverse dynamics related to different degrees of freedom in the musculoskeletal system.

Among the different theories on synergistic recruitment, the most widespread is the theory of "hierarchical control". This involves a complex chain of actions that starts from the motor cortex and reaches the spinal interneurons. For example, when a voluntary movement has to be performed, the CNS controls many muscles to perform the action. Each group of muscles has a specific action to define overall spatial directions, the strength, and the speed of the movement. Synergies are therefore strongly linked to the coordination of muscles to generate movement. So it's as if to make a movement the CNS would draw multiple synergies from a sort of base library. The overlap of these describes a complex movement over time.

The fundamental problem in defining these "groups" is the high variability of the EMG. This variability greatly increases in the subsets with muscle abnormalities.

The study of muscle synergies has a twofold purpose: to investigate the abnormal activation of muscles, to use them as a mechanism to simplify the control of movements. With the technique of synergies, it is, therefore, possible to study how the motor system is organized. This information is clinically useful for rehabilitation.

Synergies not only give information about which muscles are grouped but also how they work together. Each muscle has a certain weight in synergy (figure 1.12). Considering the weight and the temporal activation of the synergy it is possible to regain the activity of a single muscle. It is, therefore, possible to define a mathematical model of the following type:

$$\mathbf{m}(t) \simeq \sum_{i=1}^n \mathbf{w}_i \times \mathbf{h}_i \quad (1.1)$$

where $\mathbf{m}(t)$ is the envelope of the muscular activity, \mathbf{w}_i is the i synergies weight values, \mathbf{h}_i represent the time activation pattern and \mathbf{n} is the number of muscle synergies.

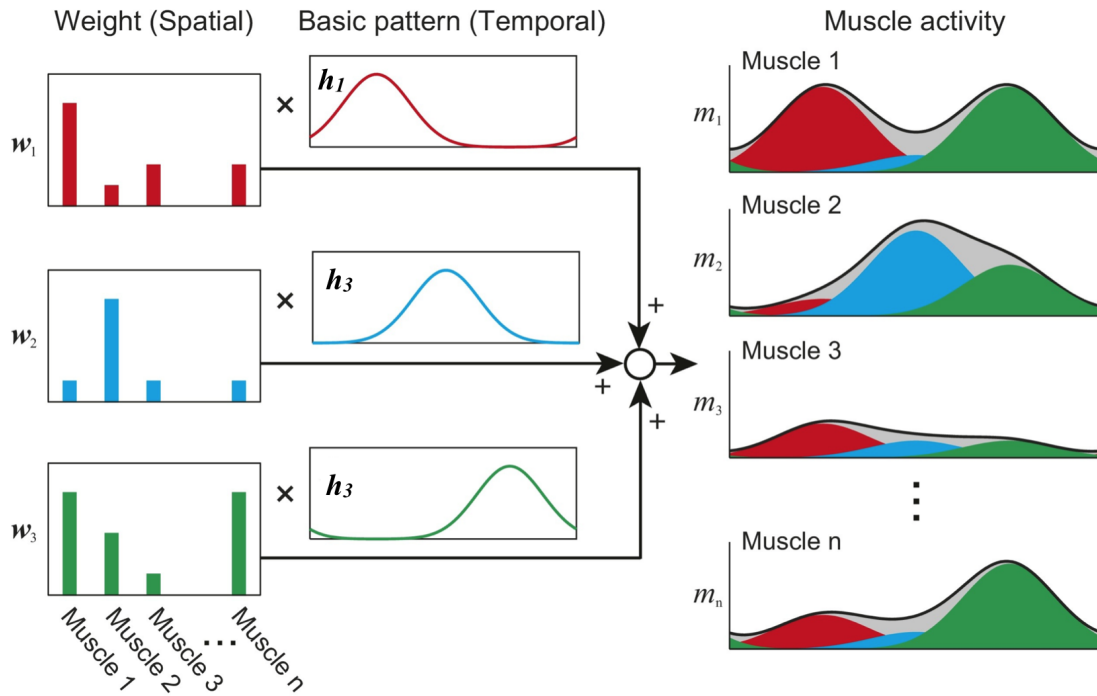


Figure 1.12: Muscle synergies hypothesis: from the sum of the products between the muscle synergies weights (\mathbf{w}_i) and the time activation (\mathbf{h}_i), it's possible define the envelope of the muscular activity (\mathbf{m}).

1.5.1 Extraction and Evaluation of Muscle Synergies

In MATLAB[®], it is possible to extract muscle synergies using the *nnmf* (Non-Negative Matrix Factorization) algorithm. This function to work properly requires the following inputs:

- sEMG envelope: matrix $c \times l$ where c is the number of channels and l is the length of envelopes;
- k : number of synergies.

The outputs of this function are:

- W : matrix $c \times k$ that containing weight vectors for each synergy
- H : matrix $k \times l$ of time activations.

The algorithm selects the W and H factors to minimize the root-mean-squared residual between the matrix of envelopes provided in the input and the reconstruction given by $W \times H$. Factoring uses an iterative method that starts with random values of W and H . This implies that sometimes the algorithm can converge to a local minimum. This implies that the solution rank may be less than k and thus give incorrect results. To avoid this the "replicates" option is activated which allows repeating the factoring several times. According to previous works[11], this value has been set to 1000.

An essential parameter to be given to *nnmf* is the number of synergies that must be defined a priori. To select the appropriate number of synergies, the coefficient of determination (R^2) has been calculated between the original envelopes and the reconstructed muscle activations ($W \times H$). The R^2 values have been calculated for all possible k values(1 to $c-1$). The value of k has been chosen for which the mean R^2 value is greater than 85% and an R^2 greater than 70% for each channel [12].

Similarity Coefficient

to compare and evaluate the similarity between the synergies or the reconstruction of *nnmf* function, three different parameter were used.

- **Coefficient of Determination (R^2)**

The coefficient of determination gives information on the proportion between the variability' of the input data (envelope) and the correctness of the statistical model used (nnmf result: $W \times H$). This coefficient is calculated using

the following formula [13]:

$$R^2 = 1 - \frac{SS_{res}}{SS_{tot}} \quad (1.2)$$

where: SS_{res} is the residual sum of squared and SS_{tot} is the total sum of square that is proportional to the variance of data.

$$SS_{res} = \sum_{i=1}^n (y_i - \hat{y}_i)^2 \quad (1.3)$$

$$SS_{tot} = \sum_{i=1}^n (y_i - \bar{y})^2 \quad (1.4)$$

y_i are the original, \bar{y} is the mean of y_i , and \hat{y}_i is the model estimation data.

R2 has characterized by a maximum value of 1. It means that the model explains the data perfectly.

- **Zero-Lag Cross-Correlation**

The cross-correlation measures the similarity of two signals as a function of a temporal shift applied to one of them. Zero-lag cross-correlation is a particular type of correlation in which the signals are compared with a zero delay. This parameter was calculated using the following MATLAB[®] code:

$$CC = \text{xcorr}(\text{signal1}, \text{signal2}, 0, 'coeff');$$

Where *signal1* and *signal2* are the time signals of synergies [14]. This coefficient compares the signals regardless of their amplitude. The zero-lag cross-correlation verifies if when one signal increases (or decreases) also the other increases (or decreases). For this parameter, however, a signal that always remains at 1 and another that remains at 0 has a very high cross-correlation.

- **Cosine Similarity**

The Cosine similarity allows to compare the similarity between two non zero vectors. This index varies in the range between -1 and 1, but generally is used only in the positive range [0;1] respectively for absence and maximum of similarity. This coefficient was used to compare the weight synergies value [14]. The cosine similarity was calculated by the following formula:

$$CS = \frac{W_i * W'_i}{\|W_i\| * \|W'_i\|} \quad (1.5)$$

Chapter 2

State of Art

2.1 ATC used to sEMG Application

Some studies have combined ATC technology with EMG acquisition devices. In particular, the *Istituto Italiano di Tecnologie* (IIT) has shown that by combining ATC technology with IR-UWB communication technology it is possible to obtain and transmit information on the muscle strength developed.

In a first study [15], a portable wireless device for biomedical applications was built. This system is based on the wireless protocol Impulse Radio - Ultra Wide Band (IR-UWB). This technology consists of the transmission of short pulses of duration to minimize transmission consumption. The system consists of an sEMG acquisition channel and allows to obtain in hardware the ATC signal. In particular, this work demonstrated the correlation between system performance in terms of ATC events (digital pulses) and system performance by looking at the ARV values calculated on the raw sEMG signal in the recognition of force levels. These values have been validated using also the signal of force recorded with a dynamometer during a maximum voluntary contraction.

The results (figure 2.1) show a correlation between ATC and the dynamometer signal of 0.95 ± 0.02 and 0.97 ± 0.02 with the AVR of sEMG.

An improvement of this system was developed by the same research team [10]. This second work concerns the extension of the previous ATC wireless system to a more complex version of multichannel acquisition. Data are transmitted using the AER (Address-Event Representation) approach which uses an encoder to form a packet of data that identifies the input channel and wireless transmitter. The pattern of this prototype is the same as the previous one: starting from the raw signal sEMG is obtained the signal almost-digital (TC) generating pulses for the IR-UWB transmitter that sends data accordingly. The work has determined a confirmation in

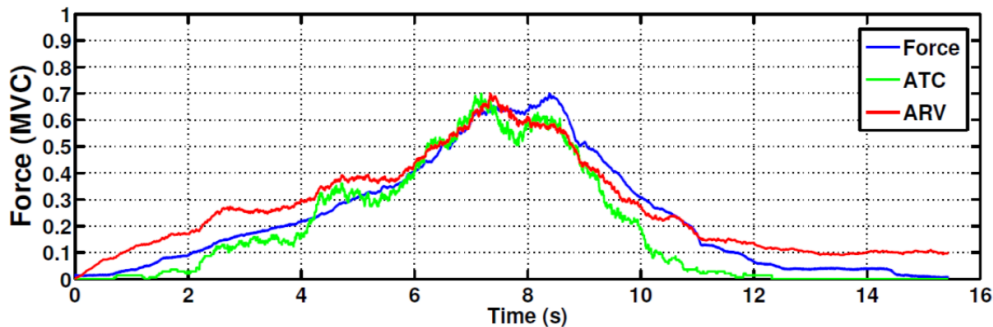


Figure 2.1: ATC, Force, ARV signals in time domain[15].

the reduction of power consumption and the dimensions of the board. This work also aims to evaluate the robustness of the ATC signal by varying the SNR signal, amplifier distortion, saturation and number of lost events. A tolerance of 5-6dB for SNR and 70% for lost events has been demonstrated.

The [8] proposes a prototype for the transmission of wireless muscle force consisting of a wearable PCB. This device contains the sEMG amplification and filtering chain and the IR-UWB transmitter. This prototype shows the possibility to reduce as much as possible the size of the acquisition card and the power consumption. *"In-Vivo"* tests show that the number of TC events increases with the increase in muscle strength produced. The tests were carried out using a series of weights in an isometric and isotonic condition. The system is able to discriminate the state of muscle rest over two levels of strength that differ by at least 6kg, with an error rate of 0% and eliminating the peaks associated with noise.

In [16] a dynamic threshold to generate the TC signal, called D-ATC was introduced. The result of this technique shows greater robustness and a greater correlation with the force level. In further work [17], the prototype of the multi-channel ATC/sEMG card was validated to define the parameters of the ATC (time window, threshold value). In this work, a threshold is fixed to 100mV from the noise on the baseline of the signal. As for the temporal window instead this must be sufficiently large to modulate the muscle activity, but it must not be too large so as not to compromise the temporal resolution. Generally, the values are between 50ms and 200ms [18].

A prototype based on the previous work [17], for the multichannel acquisition of sEMG signals using the ATC approach, was produced in [19]. This work contains tests, performed on biceps and quadriceps muscles, that show how the number of peaks TC increases with the increase in the force produced and therefore how this type of signal is able to describe the muscle activation without the use of any signal

sEMG.

Another work [20] used the acquisition cards designed in [19] in order to control in real-time a functional electrical stimulation (FES) as a therapy used in neuromuscular rehabilitation.

Finally, in the work [11] was used the signal ATC to extract muscle synergies during the analysis of the path. This work the optimal ATC parameters to carry out this type of study has been evaluated. The synergies extracted with the sEMG signal envelope (traditional approach) and those extracted with the ATC parameter have a very high similarity of 95% with a standard deviation of 5%.

2.2 Muscle Synergies Analysis

The number of studies and works on muscle synergies is very large. There are studies such as [21], which compare factor algorithms to extract muscle synergies. The study shows that the best performing algorithms are *factorization algorithm* (FA), *independent component analysis* (ICA) and *non-negative matrix factorization* (NNMF). These provide results without obvious differences and with the same number of synergies extracted. The most commonly used method in literature is the NNMF algorithm.

Other studies such as [22] show a general description of the various application fields of muscle synergies (clinical research, robotics, sports).

D. Rimini's research team has analyzed how the various techniques of preprocessing the sEMG signal can determine the variability of the synergies extracted [23].

In particular, in [24], it is analyzed as changes in standardization techniques (maximum voluntary contraction or maximum signal amplitude), in initial bandpass filtering ([20 – 500Hz] or [50 – 500Hz]) and in the cut-off frequencies of the low-pass filter (0.5Hz, 4Hz, 10Hz, 20Hz) influence the extraction of muscle synergies. The results show that filtering passes band anon causes appreciable changes. Instead, the cut frequency of the low pass filter to get the sEMG signal envelope is the main cause of the variability of the extracted synergies. These changes in terms of both the number of synergies and the contributions of muscle weights. Specifically, it is noted that using too low a frequency (0.5Hz) results in a very blunt signal, which causes an incorrect increase in muscle weight and inter-variability. Frequencies high of 20Hz instead generate an envelope too sensitive to noise that results in a reduction of the number of synergies and variability. For these reasons, an optimal choice is to set an intermediate value like 10Hz.

Various studies analyze the best ways to define the right number of muscle synergies. This value is generally decided by choosing the first condition in which the

variance index, the variance accounted for (VAF) or the coefficient of determination R2, is higher than a certain value. These thresholds are between 90-95% for VAF and 80-85% for R2 or if the parameter does not reach these thresholds when the slope curves in about flat.

In the work of Gelsy Torres-Oviedo and Lena H. Ting [25], the number of synergies is done with the use of a double VAF threshold. The first requires that the VAF for each channel must be $>75\%$ while the second limit refers to the average of the individual VAF ($VAF_{overall}$) which must be $>90\%$. This method of selection was also applied in another work [26].

Other works, however, use the coefficient of determination R2. In [12] the number of synergies is chosen based on the first value that results in a reconstruction of the envelope matrix measured with $R2 >80\%$. While in [27] the number of synergies is determined by assessing when the R2 curve reaches a plateau.

Most research projects study muscle synergies related to walking. It has been shown that based on the number of muscles selected for a path analysis, the number of synergies extracted varies between 4 and 6 [11] [26] [14] .

In [28] the non-negative matrix decomposition algorithm extracted muscle synergies from 6 lower limb muscles, e.g. tibialis anterior (TA), gastrocnemius medialis (GA), rectus femoris (RF), biceps femoris (BF), adductor longus (AL), gluteus medius (GM) and erector spinae (ES). The analysis showed that 4 muscle synergies represent at least 70% and 5 muscle synergies represent at least 90%.

Finally, in the work described in [14], muscle synergies are analyzed considering over 180 gait cycles and 12 healthy subjects. The work showed that all 12 subjects are characterized by 5-7 muscle synergies.

Examining the weights of the synergies W and the temporal coefficients H , have been calculated both the into-similarity of the single subject and the coherence between different subjects. The similarity indices used are cosine similarity (CS) and zero-lag cross-correlation (CC) between the synergy weights W and the temporal coefficients H . The 5 muscle synergies correspond to the main biomechanical functions of locomotion.

2.3 MITOR Project previous versions

The system realized in this thesis is the third prototype of the MITOR system. During the design phase of this new version, the aim was to solve all the problems encountered in the previous prototypes. The first two versions were entirely designed by *Abuduwaili Tuoheti* during his PhD [29].

MITOR System Version 1

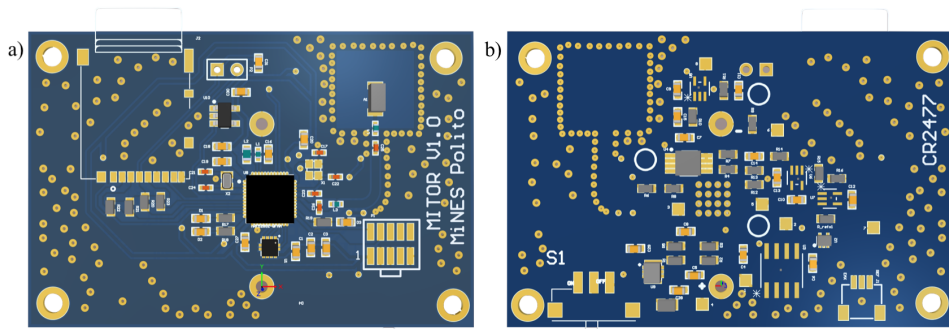


Figure 2.2: PCB Layout MITOR board version 1: a) Top Layer; b) Bottom Layer

The device is a single-layer PCB with dimensions of 58x38x11mm. The sEMG signal is taken using two exploding electrodes and a reference electrode. The acquisition channel has a bandwidth passing between 30Hz-400Hz with a gain of 922 determined by the instrumentation amplifier (INA321). The sEMG signal is input to a microcontroller ADC pin (NORDIC SEMICONDUCTOR® nRF52832). The information on the operating status of the device is given by 3 LEDs of different colors. The boards also have a triaxial accelerometer (LIS2DH12). The device's power supply is set to 3.3V using the XCL210C33 component. In this first version, there is also a switch to enable and disable the power supply of the μ SD card. Radio communication between individual devices is made possible by the use of an antenna chip.

This prototype was used to verify the proper functioning of the acquisition channel, in fact, there are various test points and headers available to connect external components. However, the power regulator was not able to guarantee the correct functioning of the device with all batteries. This was the main reason why no *in-vivo* tests were done with this device.

From a firmware point of view, a custom radio protocol and high synchronization have been implemented.

MITOR System version 2

This new version features a PCB stack architecture on two levels. The final dimensions are 29x27x19mm. The acquisition channel is similar to the previous one but a protection circuit with Zener diodes has been inserted at the beginning of

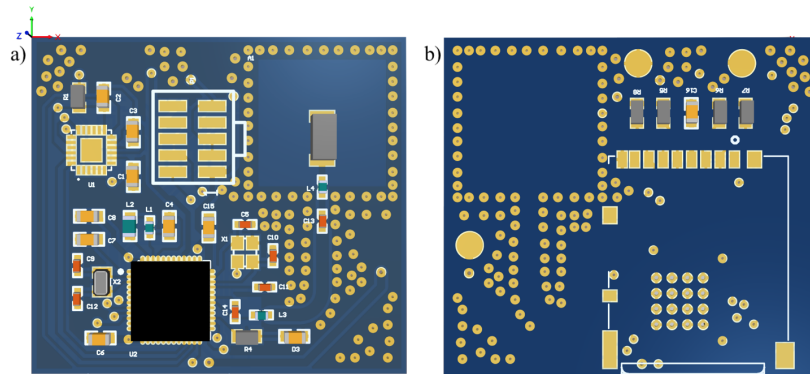


Figure 2.3: PCB Layout MITOR board version 2 (Digital Part): a) Top Layer; b) Bottom Layer

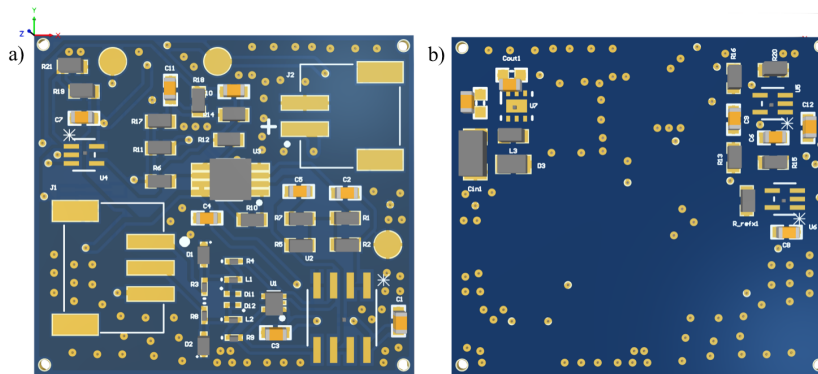


Figure 2.4: PCB Layout MITOR board version 2 (AFE Part): a) Top Layer; b) Bottom Layer

the acquisition chain. The power supply problem has been solved using a boost regulator that sets the 3.6V power supply voltage. In addition, a MEMS Motion-Tracking component (accelerometer and gyroscope) was introduced to replace the old accelerometer.

From the firmware point of view this version allowed to record the sEMG signal in three modes: raw data, envelope, and ATC. ATC is calculated in firmware. A more stable custom radio protocol (ESB) has also been included. The test points of the first version have been removed to reduce space consumption.

This version has been tested during route analysis but the stack structure sometimes presents problems related to mechanical stability. During the tests, it was observed that the acquisition channel was saturated due to the INA.

Chapter 3

Hardware Design

3.1 Design Specification

The MITOR Project aims to develop a wearable, wireless, low-power, multi-channels sEMG signal acquisition system for long-term monitoring of muscle synergies and diagnostic motor rehabilitation. In this thesis, six new boards were developed, and to do it, the same hardware design specification of the previous system was respected. The design specification points to optimize are:

- **Quality of signal**

To obtain a good quality of the signal is required a system insensitive to movement artifacts with a sampling frequency of 1kHz. Moreover, every single channel should be able to filter the recorder signal to obtain the sEMG and also the TC signal.

- **Devices dimension**

The channels should be not so big so as not to restrict the body movement during the exercise.

- **Power consumption**

One of the main tasks of this project is the long-term monitoring of muscle activity. So, for this reason, it is important to optimize power consumption. In line with the other technologies on the market, the device should be work with low power voltage (3 V to 3.6 V). The choice of the component is fundamental to reduce power consumption.

- **Synchronization wireless**

Because of the independence among the channels a wireless communication to synchronize the different boards is need.

- **Data recording**

The system requires a way to storage local recording signals.

- **Reduce component cost**

Whit a view to reducing the cost of the device a good choice is to use no expensive components.

3.1.1 Device Architecture

This third version of the *MITOR* system is composed of six custom slave channels with the same hardware features, and one master board. At present, in line with the type of micro-controller used in the slave boards, a commercial development kit (nRF52840-DK of the NORDIC SEMICONDUCTOR[®]) was chosen as a master (figure 3.1). This board is programmed to communicate and manage wirelessly the slaves.

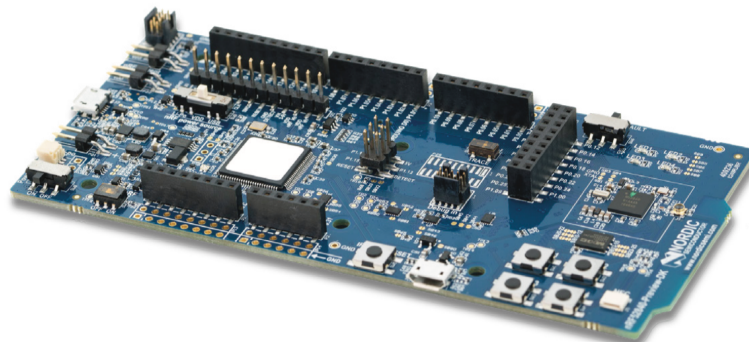


Figure 3.1: nRF52840 Development kit of NORDIC SEMICONDUCTOR[®].

Using the buttons on the development kit it is possible to select the working mode: normal sEMG mode, envelope mode, or the ATC mode. There is a fourth button that is used to start and stop the recording. After pressing the buttons, the master sends a packet containing the start-up information to the slave. Another important task of the master board is to send the synchronization packets with the aim of maintaining a low drift of the sampling frequency between slaves.

The design of the slave boards is shown in figure 3.2 and in section 3.8 the design of this layout will be justified. The *Printed Circuit Board* (PCB) has only 2 layers and all the components are placed strategically to optimize the space occupied. The dimension of the boards is (50.0 x 37.5mm). Each board is supplied by an external battery that given a voltage of 3.6V to all the circuit. To understand if the slaves work correctly or there is a problem, two LED (*Light Emitting Diode*) were

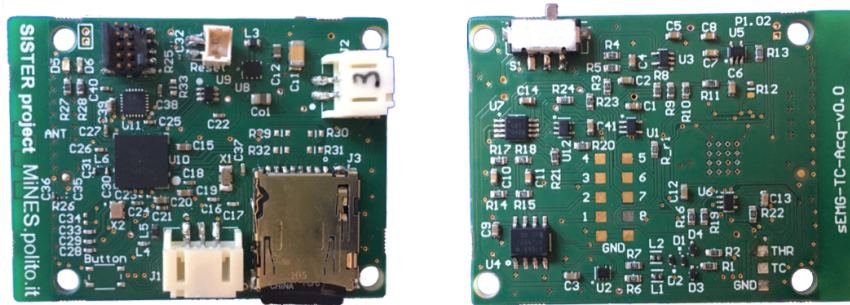


Figure 3.2: PCB slave overview: top layer (*left*), bottom layer (*right*).

added to have visual feedback about the operating state of slave boards. In general, in conditions of corrected operation, after receiving the start command from the master, the slaves start to record the signal (compliance with the selected working mode) in the μ SD card. The storage of the signal continues until a stop command arrives or the supply goes down.

Each slave has a connector that allows connecting to the system an external pressure sensor. The information from this sensor is very useful in the study of muscular activation because, it can be used to discriminate the begin and the end of a cycle of repetition, during for example a gait or grasp analysis.

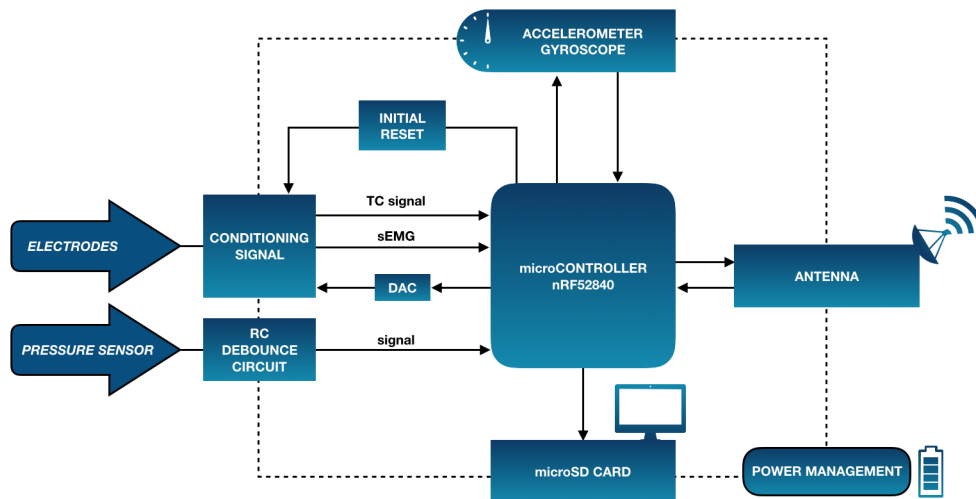


Figure 3.3: Block diagram of the custom slave boards.

In figure 3.3 are show the main blocks that composed the designed slave board.

In the next sections of this chapter, each block will analyze in detail from an electronic point of view and all the design choices will be justified.

3.2 Analog Front-End

The *Analog Front-End* (AFE) is the part of an analog circuit that has the role of making the input signal suitable to be processed by the microprocessor. The AFE is composed by a succession of blocs that generally be *operational amplifier* (op-amp), filter and analog specialized circuit to data acquisition for the sensor. In each slave, there are two different and separate analog front-end: one of them is responsible for the conditioning of sEMG and also of the TC signal[19], the other one, however, management the signal from an external pressure sensor.

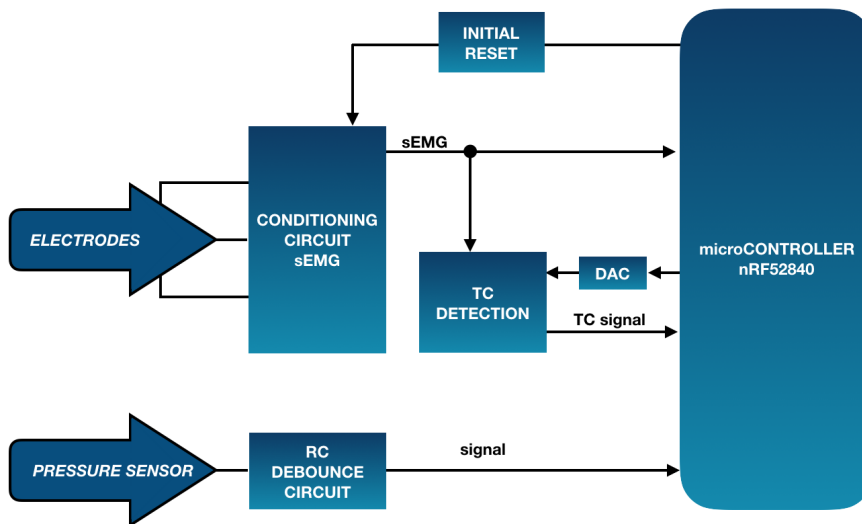


Figure 3.4: Block diagram of analog front-ends.

Figure 3.4 shows which are the interconnection for each AFE. The sEMG's conditioning circuit has four input and three of them are signals from the electrodes. The actual version of the board detects the sEMG in bipolar mode, and it uses a pair of the electrode to record the electrical activity produced by skeletal muscle and one electrode like the reference. Furthermore, the conditioning circuit requires also a signal from the microcontroller to activate the initial reset of the channel, in a way to impose the initial condition of the circuit.

3.2.1 sEMG Acquisition Chain

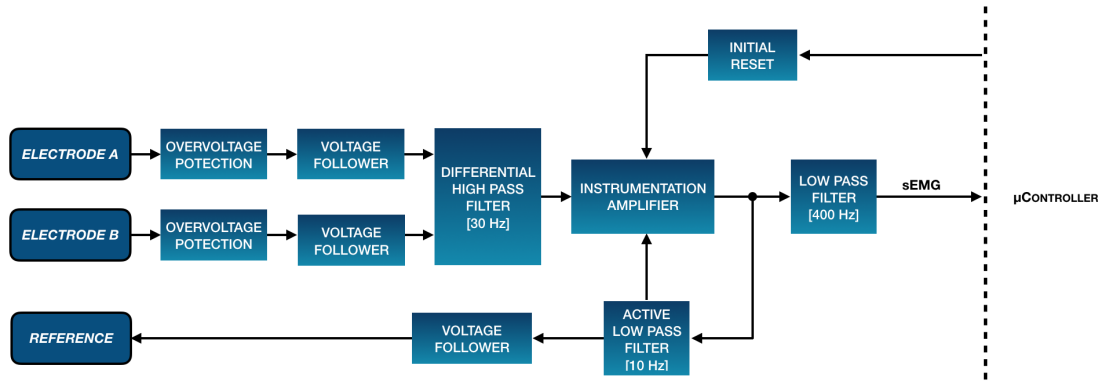


Figure 3.5: Block diagram of EMG conditioning circuit.

Figure 3.5 shows the block diagram of the sEMG acquisition channel. The chain has a total amplification of 922 and a bandwidth from 30Hz to 400Hz. The chain is implemented as a single block (*Instrumentation Amplifier*) and on the whole bandwidth from 30Hz to 400Hz.

The circuit schematic of this acquisition chain is realized to follow the schematic of the previous version of the MITOR system [29]. The complete circuit diagram of the system is in *Appendix A*.

Overvoltage Protection

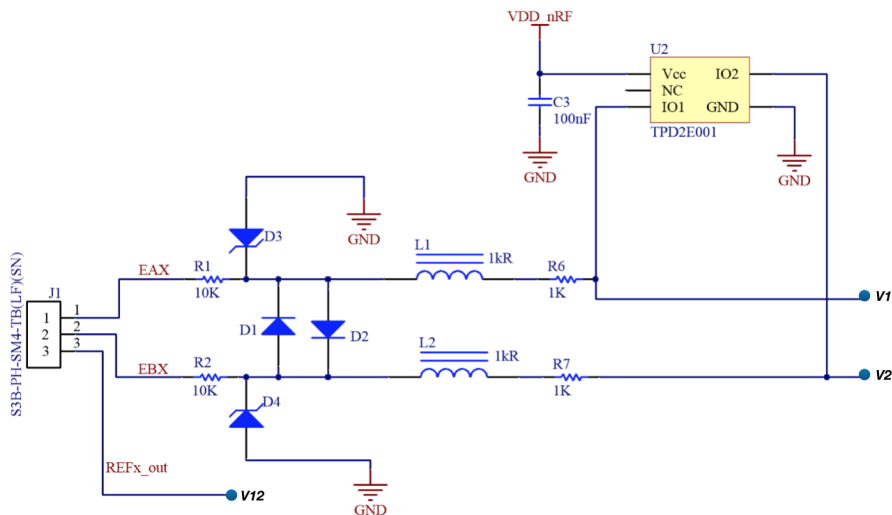


Figure 3.6: Circuit diagram of overvoltage protection.

The overvoltage protection allows preserving the circuit from excessive out-range voltage inputs. In fact, the high or negative voltage could damage all the board because the components have a limited input voltages range. In the design shown in figure 3.6, *Zener diodes* [ESD5Z3.3][30] are used in reverse bias configuration with a breakdown voltage of 3.3V. In this way each time that the input voltage exceeds this value, the diode works as a short circuit and conducts current to ground. This model is chosen because it is characterized by a small dimension, little response time and low leakage current.

The other two *normal diodes* [CMAD6001-TR][31] are added to compensate for the voltage input between the two lines and also the noise. An additional protection is provided by *ferrite chip* [BLM15AG102SN1D][32] and by the *Transient Voltage Suppressor (TVS)* [TPD2E001-DRLR][33] based on two line of Electrostatic Discharge (ESD) protection diode array.

Voltage Follower

A voltage follower is a configuration of the *Operational Amplifier* (Op-Amp) characterized by negative feedback obtained by connecting the inverting input with the output, how shown in figure 3.7a. The features of this configuration are a unity gain and a very high input impedance (hundreds of $M\Omega$) that allow isolation of the output from the signal source. In the developed acquisition channel, a *microPower*, rail-to-rail, low-cost operational amplifier [OPA2347UA][34]. The connection are shown in figure 3.7b. This component is chosen for two reasons. Firstly, because

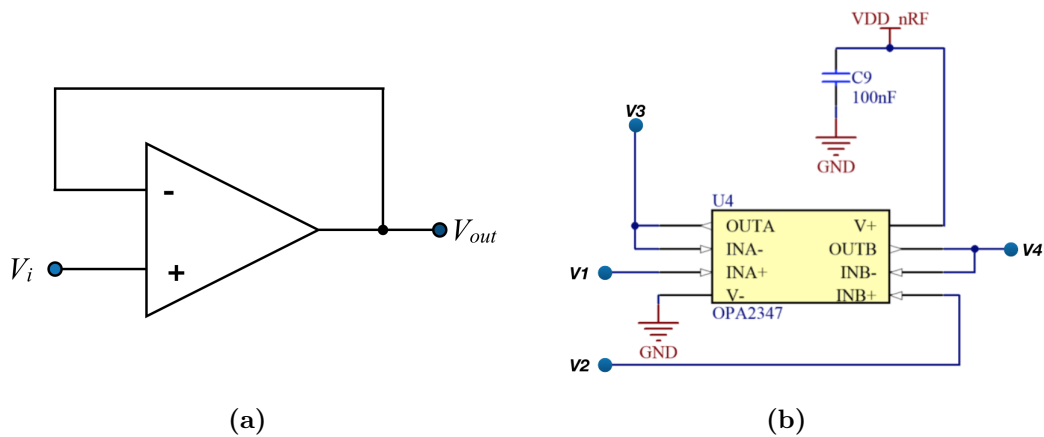


Figure 3.7: a)Op-Amp in voltage follower configuration, b)Circuit diagram voltage follower.

allow a space optimization in which it has inside two separate voltage followers, and secondly because has a very small quiescent current (max 34 μ A);

Differential High Pass Filter

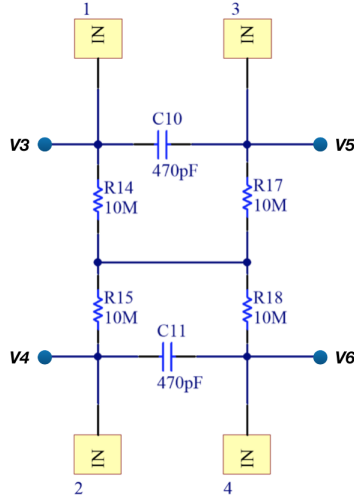


Figure 3.8: Circuit diagram of overvoltage protection.

The filter configuration in figure 3.8, is a second-order passive high-pass filter that allows removing the DC input voltages [35]. The term 'passive' implies that no active component (an op-amp), but only resistors and capacitors are used to implement the filter. The cut frequency can be calculated as:

$$f_{cut} = \frac{1}{2\pi RC} \quad (3.1)$$

According to equation 3.4, the value of R and C are chosen in order to have a cut frequency approximately of 30Hz so be sure to remove the motion artifact from the sEMG signal ([36],[37]). Selecting $R = 10 \text{ M}\Omega$ and $C = 470 \text{ pF}$ the frequency of the filter is set to 33.86Hz.

In figure 3.8, it is possible to note 4 test point that allows monitoring the state of the circuit. These points are placed also in other parts of the front-end because so it is possible to follow the input signal during the several steps of the acquisition channel and in case of incorrect operation, identify the problem and correct it. Moreover, the test points are useful also to provide test signals.

Instrumentation Amplifier

Instrumentation Amplifier is a particular type of op-amp suited for amplifying signals, since it has a stable gain (typically adjusted via one or more resistor outside the chip), very high common-mode and differential mode impedance and low output impedance. Usually, the gain required in an acquisition channel for sEMG is more or less 1000 V/V because the input signal has an amplitude of the signal of few millivolts peak-to-peak.

The instrumentation amplifier chosen for this application is the INA321 [38]. This

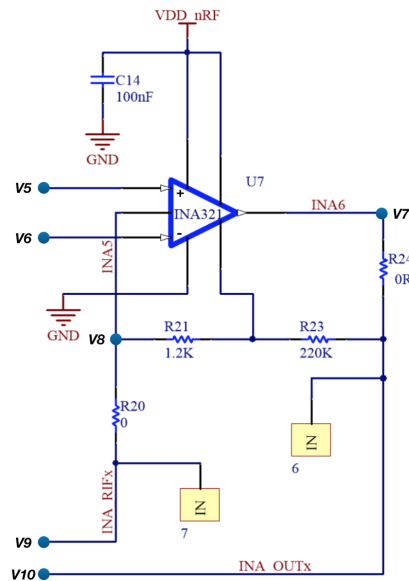


Figure 3.9: Circuit diagram of Instrumentation Amplifier.

chip has a range of gain from 5V/V to 1000V/V and this value depends by the two resistor R21 and R23 (figure 3.9) according to equation:

$$G = 5 + 5\left(\frac{R23}{R21}\right) \quad (3.2)$$

The gain is set exactly to 922V/V, having chosen $R21 = 1.2 \text{ k}\Omega$ and $R23 = 220 \text{ k}\Omega$.

Initial Reset

The previous versions of the MITOR project are characterized by a mistake that causes the saturation of the sEMG acquisition channel. The error is due to INA321 because in some cases, the reference pin (pin 5) raise to voltage supply value and consequently the output (pin 6) falls in zero. The system was unable to get out of this situation. Initially, the reason for this behavior was not clear, but a way to fix

a problem was made, manually, a short circuit between the pin 5 and 6 of INA321. It is like the initial condition of the amplification chain are set from the outside. To avoid the saturation problem, in this third version, an analog switch operated from the microcontroller (MAX4594)[39] is added to the acquisition channel. This component is normally open, and during the initialization phase of the device, the microcontroller changes the state of the control pin (high active) of the switch (pin 4), in the way to link the pin 5 and 6 of the INA321 for a few milliseconds. This

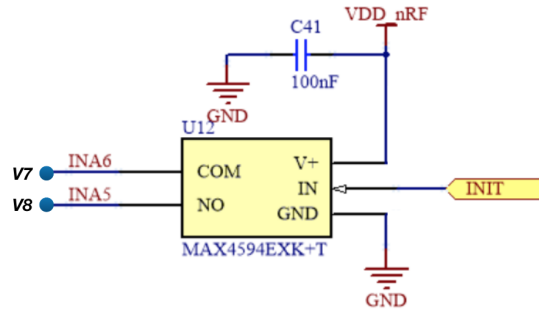


Figure 3.10: Circuit diagram of the switch to initial reset of the INA321 condition.

component is chosen because has a extremely low off-leakage current (0.5 nA max), excellent off-isolation (80 dB), low supply current (1 μ A max) and digital input logic level compatible with the microcontroller chosen.

To decide how much time the switch should be closed and to understand the impact this component has on the rest of the system, the circuit was tested with simulation software (LTSPICE[®]), before it "is printed".

All the acquisition channel is reconstructed with the data of the real components. In figure 3.11 is shown the result of the simulation. The blue and the green waves are two sinusoids with a frequency in the sEMG band that simulate the input signal of the system. The red signal is the output (pin6), and the turquoise is the reference (pin 5) of the INA321. After powering the device on, the reference raises to supply voltage (3.3V in the simulation), instead the output is not able to follow the input signal and so has a slight variation near the zero. The white square is the moment in which the microcontroller turns on the switch for 10 ms. After this event, the INA starts to work properly. As a result of this test, the switch is kept turned on for 10ms, during the initialization of the system. In this way, the problem was averted in the third version of the MITOR.

After the realization of the PCB, the cause of this problem was found during the working test of the device. The source of the problem is the limited voltage input of the reference pin of the INA321, in fact on page 10 of the datasheet [38] is given: "The output is referred to the reference terminal, which must be at least 1.2V below

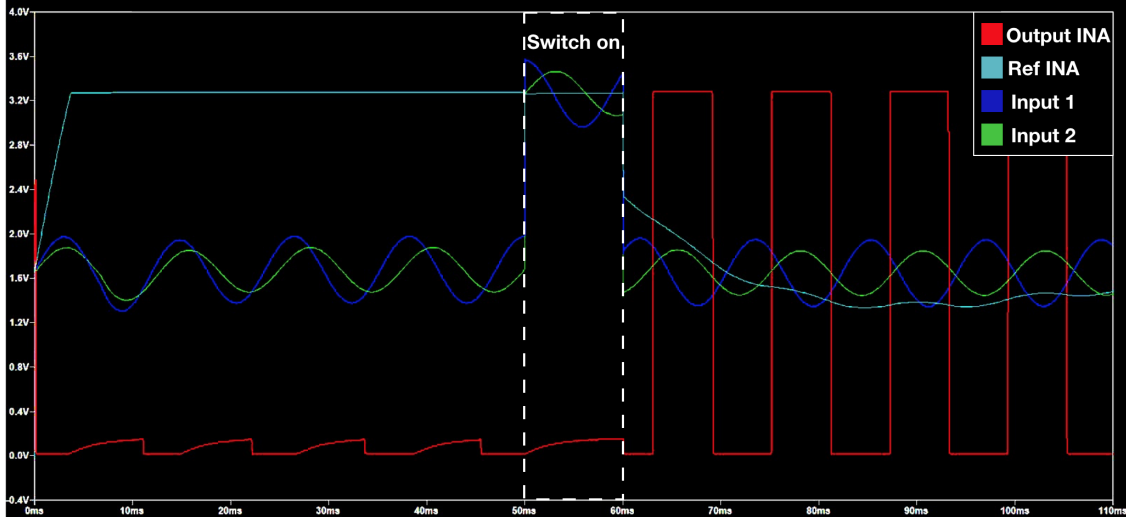


Figure 3.11: The picture shows the impact that the switch has on the circuit when the channel goes in saturation. On LTSPICE® the saturation condition are recreated thought the two input signal. The INA reference is blocked to the supply voltage and for this reason, the INA output is about zero. So the switch is activated. In this way, the short circuit between the output and reference of INA can allow the channel exit from saturation condition.

the positive supply rail.". So to solve the problem the reference pin should not be allowed to reach the power supply value, so a simple Zener Diode with a breakdown voltage of at least 1.2V, could be included between pin 5 and pin 6 to comply with the condition found on the datasheet.

Active Low Pass Filter (Feedback)

The filter, shown in figure 3.12, has a multiple-feedback architecture that takes advantage of the higher open-loop gain. This filter is active because is composed also by an op-amp is used to provide negative feedback to reference voltage of the INA321 and allow to remove the low-frequency component introduced by the INA. The cut of the frequency of this filter is about 10 Hz, calculated as:

$$f_{cut} = \frac{1}{2\pi\sqrt{R4 \times R5 \times C2 \times C4}} \quad (3.3)$$

with $R4 = 150 \text{ k}\Omega$, $R5 = 33 \text{ k}\Omega$, $C2 = 470 \text{ nF}$ and $C4 = 100 \text{ nF}$.

This type of filter is defined as "active" because it is composed not only by resistor and capacitor (passive component) but also by an op-amp. Moreover, this filter is of the second order this means that the transfer function has two poles.

The operational amplifier chosen for this application is OPA333 [40] because has

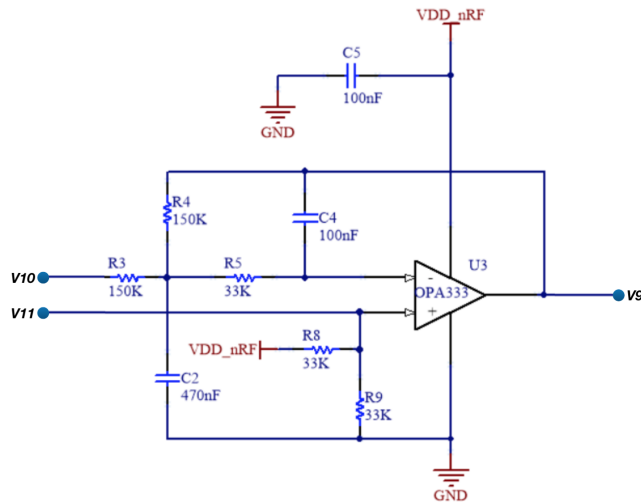


Figure 3.12: Circuit diagram of the active low pass filter for the reference-output INA321 feedback.

minimum *Common Mode Rejection Ratio* (CMRR) of 106dB and a very low quiescent current ($10\ \mu\text{A}$).

In this filter block, the reference electrode voltage is generated by a resistive divider on voltage supply ($R8$ and $R9$). This voltage is not directly connected to the electrode but passes through a voltage follower in order to isolate input and output as in figure 3.13.

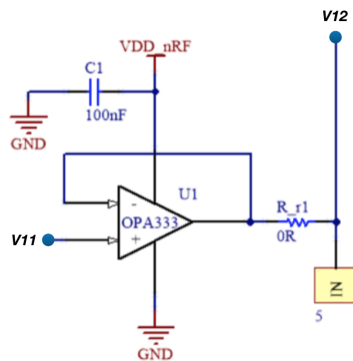


Figure 3.13: Circuit diagram of voltage follower to the reference electrode voltage.

Active Low Pass Filter (Sallen-Key)

Figure 3.14 is the last stadium of the sEMG signal acquisition channel. Also, this (like the filter in figure 3.12) is an active low pass filter of the second order but

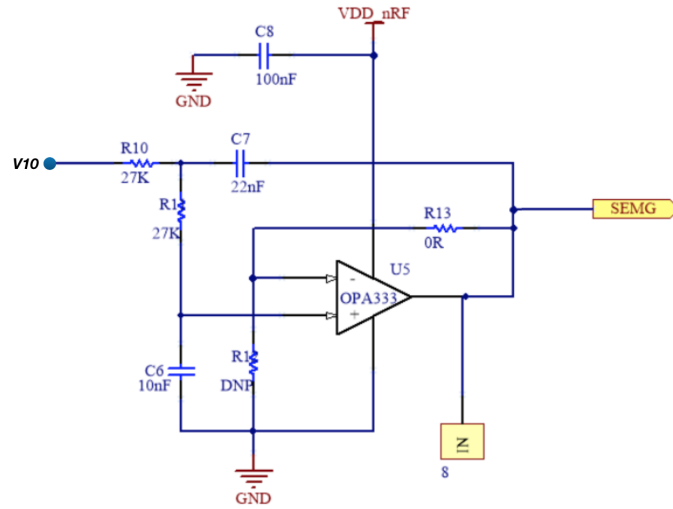


Figure 3.14: Circuit diagram of the active low pass filter with architecture Sallen-Key.

it has a different architecture called *Sallen-Key*. This filter is characterized by a unitary gain and the cut-off frequency is 397Hz given by the following formula:

$$f_{cut} = \frac{1}{2\pi\sqrt{R10 \times R11 \times C6 \times C7}} \quad (3.4)$$

The output of this filter (sEMG signal) is connected to the ADC input of the microcontroller (*nRF52840* provide by NORDIC SEMICONDUCTOR®).

3.2.2 TC Events Detection

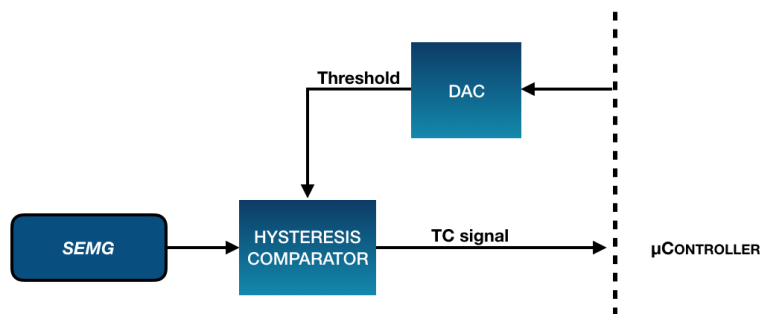


Figure 3.15: Block diagram of TC events detection.

The block diagram (figure 3.15) shows the additional components necessary to generate the TC signal from the sEMG signal.

Hysteresis Comparator

A comparator is an electronic circuit made by an op-amp, that can provide in output only two continuous levels near, respectively, to the negative and positive supply voltage. In particular, if the non-inverted input voltage is more than inverted input, the output is about positive supply (V_{OH}). Instead in the opposite case, the output is V_{OL} (about negative supply voltage).

The hysteresis is a feature of a system to react to sollicitation depending on its previous state. To obtain a hysteresis comparator (or *Smith Trigger*) is required to add non-inverted feedback to the op-amp. This circuit is very important because it is able to remove quick commutation caused by electronic noise. The V_a and V_b

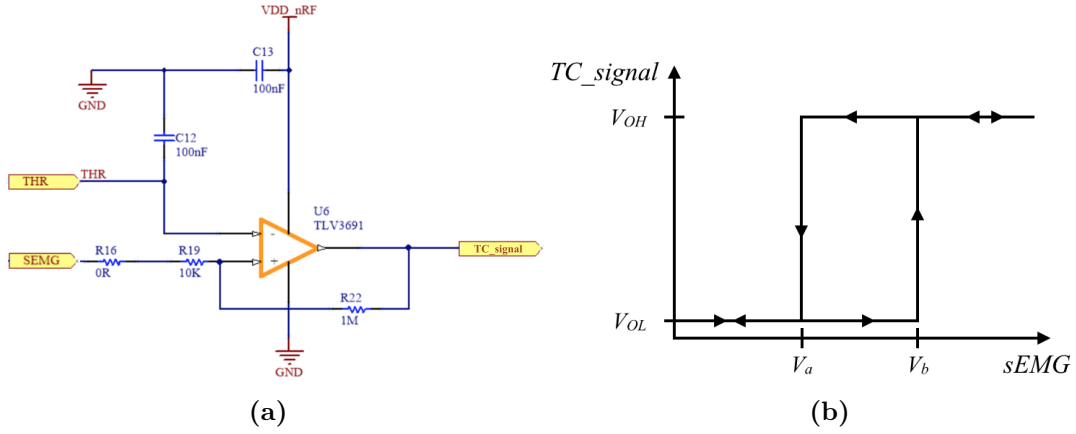


Figure 3.16: a)Hysteresis comparator configuration, b)Hysteresis output.

values depending by THR , $R19$ and $R22$ according to the following equation:

$$V_a = R19 \frac{THR}{R22} + THR \quad (3.5)$$

$$V_b = \frac{THR(R19 + R22) - V_{DD}R19}{R22} \quad (3.6)$$

$$\Delta V_{HYS} = V_{DD} \frac{R19}{R22} \quad (3.7)$$

In particular, equation 3.7 allows to calculate the hysteresis width, that means which is the noise oscillations that the circuit can stand without changing state. Have a big width makes the system slow to react more slowly. With the value of resistor chosen ($R19 = 10\text{ k}\Omega$ and $R22 = 1\text{ M}\Omega$) and the voltage supply of 3.6 V , the hysteresis is about 36 mV .

The comparator chosen for the developed circuit is TLV3691 [41], because has a

low quiescent current (150nA maximum) and extremely small packages. The output of the comparator is a *quasi-digital signal* so it can be connected to any input of the microcontroller because is not required the ADC.

Digital Analog Converter (DAC)

To get the threshold reference (THR) for the hysteresis comparator handled by the microcontroller, an external DAC is required, that is because the nRF52840 does not have an internal DAC.

To choose the best component for this circuit, the features considered are the number of bits, operating current, shutdown current, accuracy, type and dimension of the package. The DAC chosen is the AD5621[42], the characteristics of which are given in table 3.1.

The DAC is connected to microcontroller in *Serial Peripheral Interface*(SPI) way.

Table 3.1: DAC AD5621 characteristics

Bit Resolution	12
Operating Current	60 μ A
Shutdown Current	0.2 μ A
Accuracy	± 0.5 LSB
Package	SC70 (6 pins)
Dimension	$2.2 \times 2.4 \times 1$ mm

In this case, with this protocol the communication the Master (microcontroller) send to the Slave (DAC) a command of *Chip Select* (or also Sync) with which the master enable the slave, the *Serial Clock* (SCLK) to synchronize the communication, and the *Serial Data Output* (SDIN). Each line is unidirectional. Figure 3.17 shows the connection of the DAC. The pin SYNC is denied and it means that this input pin is active low. The input signal of the DAC is binary coded. Each bit is saved in a 16-bit shift register on the falling edge of the SCLK signal. Only when the internal register is full the output (VOOUT) is available.

The ideal output voltage is given by:

$$V_{OUT} = V_{DD} \times \left(\frac{D}{2^n}\right) \quad (3.8)$$

where D is the decimal equivalent of the binary code loaded to the DAC register, n is the bit resolution, and V_{DD} is the voltage supply. The maximum output voltage settling time is 10 μ s.

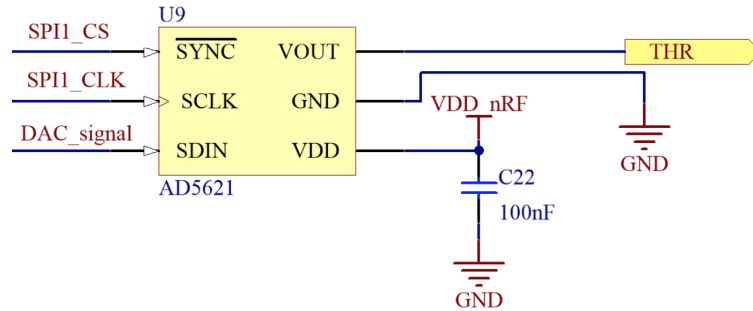


Figure 3.17: Circuit diagram of the DAC connections.

3.2.3 RC Debounce Circuit

The RC debounce circuit is used as a conditioning circuit to connect a Reset button or, as in this case, a *Force Sensing Resistor* (FSR) to the microcontroller. In the developed system, this type of sensor is used as a pressure button, to detect the phases of body movements, during grasp or gait analysis.

An FSR is a sensor made by a polymer thick film that changes resistance when external stress (force, pressure) is applied. The structure of a generic force-sensing resistor is shown in figure 3.18. This sensor is very thin, chip and easy to integrate.

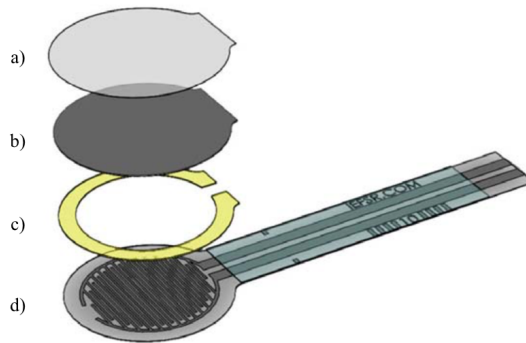


Figure 3.18: Basic FSR construction[43]: a)Flexible substrate, b)Printed semiconductor (PTF), c)Spacer adhesive, d) Flexible substrate with printed interdigitating electrodes

These sensors are characterized by high impedance (tens of $M\Omega$) that go down to few Ω when the sensor is pressed. Its operation is like a button and for this reason a conditioning circuit, like the one shown in figure 3.19, is required.

This circuit neutralizes the non-ideal behavior of the contacts that creates multiple electrical transitions for a single input. The RC circuit delay filters out the

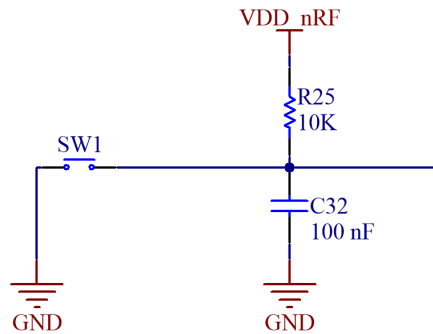


Figure 3.19: Circuit diagram of the RC Debounce Circuit.

rapid changes in switch output in order that the microcontroller sees a clear single transition. Essentially the capacitor quickly charges and discharges over every voltage spike, smoothing out the button bounce. Depending on how quickly the capacitor can charge, the button bounce should be mitigated. The time constant of the circuit ($\tau = R25 \times C32$) is 1ms.

With this circuit when the FSR has not stressed the output is high logic level, instead, the output goes down when the FSR is pressed.

3.3 Power Supply Unit

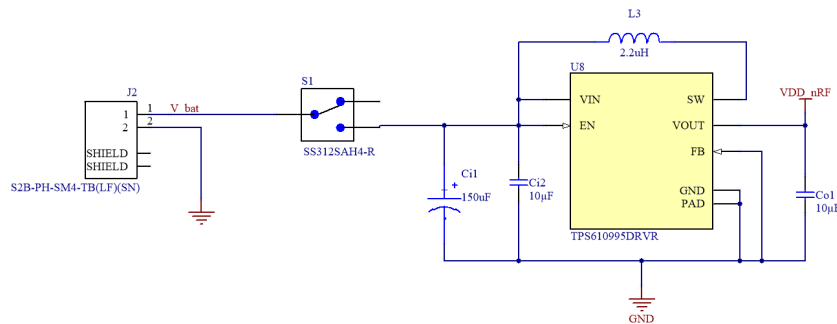


Figure 3.20: Circuit diagram of the power supply.

The system can be supplied by an external lithium battery, with a voltage from 3V to 3.6V. That is made possible by a boost voltage regulator that uses a hysteretic control to ensure power supply of 3.6V to the whole system. The component chosen is the TPS610995 [44] that has a ultra-low quiescent current (10 μ A). According to the datasheet the application circuit is shown in figure 3.20.

An on-off switch to enable the supply is added between the battery holder and the voltage regulator.

3.4 Antenna

A planar meander line PCB antenna 2.4GHz is added to the system to allow wireless communication with the master board. The layout of the antenna is exactly the same of the *nRF52840 Dongle* of the NORDIC SEMICONDUCTOR®, downloadable from the official web site[45]. The antenna layout is illustrated in figure 3.21.

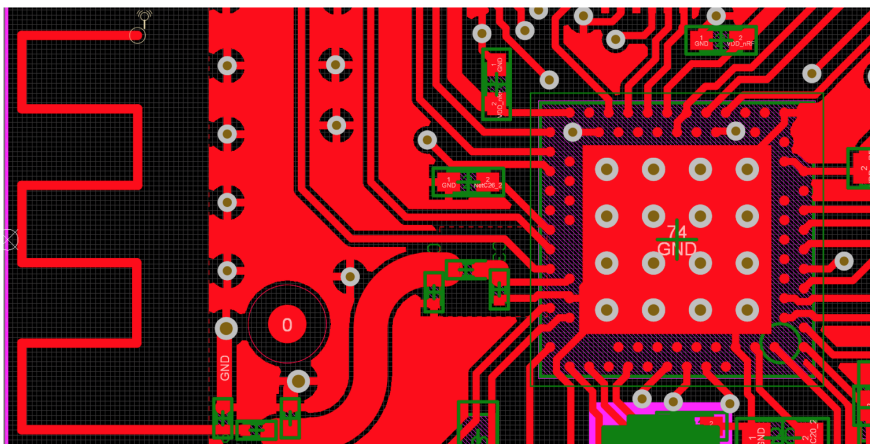


Figure 3.21: Antenna layout of the developed board.

3.5 Local Storage Unit

The local storage unit allows saving the data locally. For this reason a *microSD* (μ SD) card slot is added in the design. This type of memory is the smallest and easiest to use, as all PCs have a microSD reader and so that the measurement data can be fetched easily. For this project, the *Kingstone micro SDCS 16GB class 10* memory cards are used. The system works also with a different type of μ SD card. The circuit diagram to connect the memory slot is very easy and it is shown in figure 3.23. Four resistor pads are predisposed if a pull-up resistor should be necessary. Also for this peripheral, an SPI protocol is used to interface with the microcontroller. In this case, in contrast to DAC interconnection, there is also a *MISO* (Master Input Slave Output) wave. This is an output line for the memory slot but an input for the microcontroller. This pin allows to peripheral to communicate its

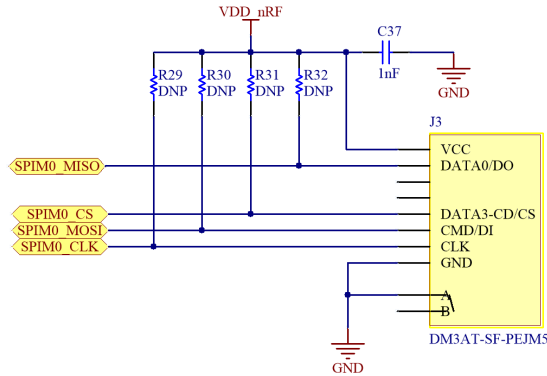


Figure 3.22: Circuit diagram of the μ SD card slot.

status to master. The other 3 lines are the same as the DAC connection, except by name of the input data that here is called *MOSI* (Master Output Slave Input).

3.6 Accelerometer and Gyroscope

A 6-axis MEMS (*Micro Electro-Mechanical Systems*) MotionTracking™ Device (ICM-20649)[46] is added to the system because have information about acceleration and angular velocity is very important during the study of the body movement. This component is added for future application, in fact, in this thesis, the Motion-Tracking™ is not tested and programmed in the firmware.

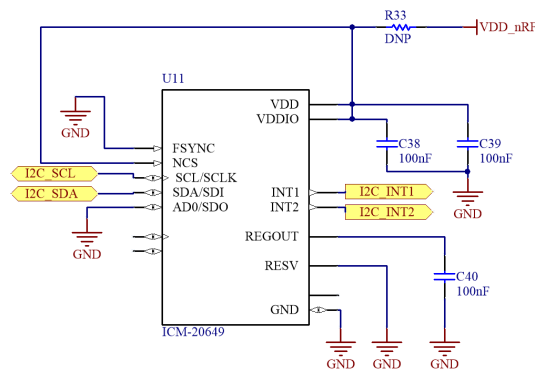


Figure 3.23: Circuit diagram of the MotionTracking™ Device.

The protocol used to connect this component to the microcontroller is I2C (*Inter Integrated Circuit*). As opposed to SPI, in the I2C there are only 2 lines: one for the data (bidirectional) and the other one for the Serial Clock. This type of transmission is slower than SPI but it requires a less number of interconnection.

3.7 Microcontroller

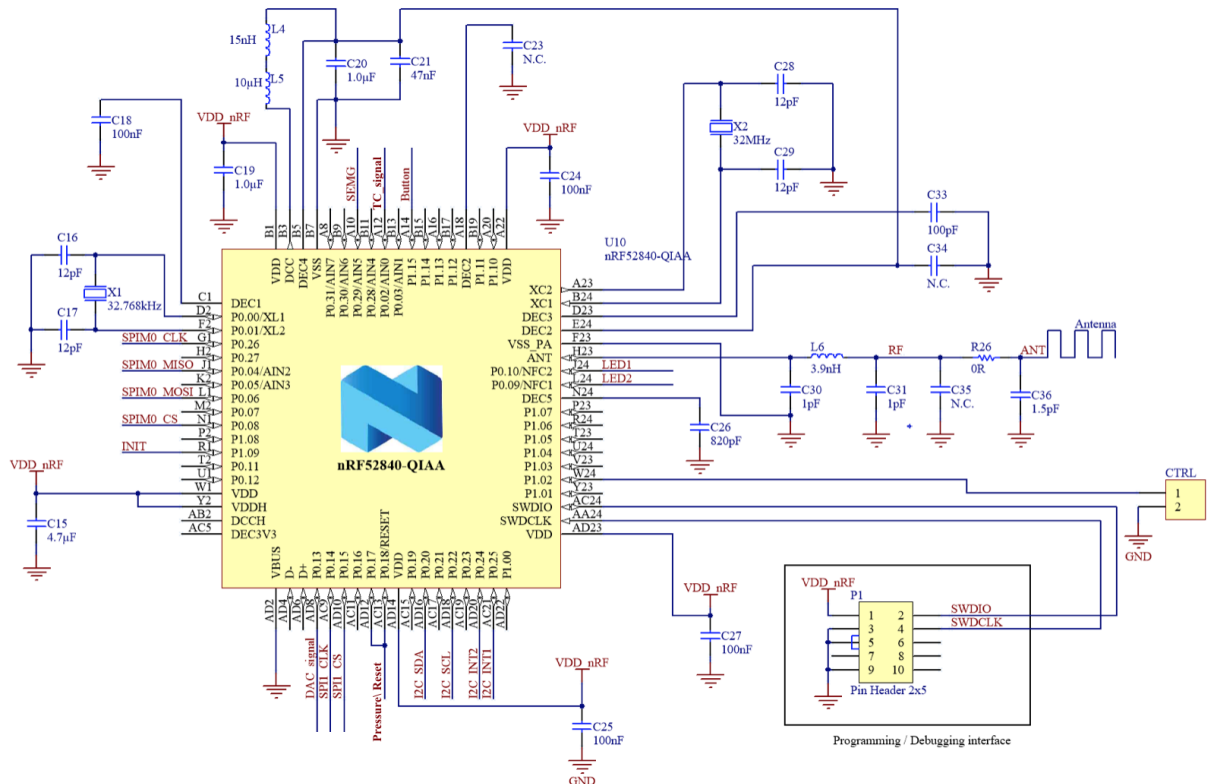


Figure 3.24: Circuit diagram of microcontroller setup.

The nRF52840 by NORDIC SEMICONDUCTOR[®] is an ultra-low-power multiprotocol SoC microcontroller (μ C) suited, in a particular way, to wireless application. Its core is an ARM Cortex-M4F processor with both flash (1MB) and RAM memory (256kB).

The circuit configuration, in figure 3.25, is chosen as a result of a careful analysis of the microcontroller datasheet [47]. With configuration enables only the internal DCDC converter but the other possible features as a USB connection, NFC and external supply (EXTSUPPLY) are disabled.

3.7.1 Other component

Many components surround the microcontroller and these are useful to ensure its proper functioning or to understand the effective operation of the μC .

Programming/Debugging Interface

A *Joint Test Action Group* (JTAG) 10-pin header is added in order to debug and program the μC . The *J-Link EDU Mini* by SEGGER® is used as debug probes.



Figure 3.25: a) J-Link EDU Mini SEGGER®, b) Connection of the J-Link EDU Mini followed to implement the electronic interconnection to JTAG port [48].

Control Pins

Two pins (P1.02 and P1.15) are connected to a header in such a way that they can be used to make available on output internal signals of the microcontroller. This is a handy feature in the firmware design phase. These pins can be also used to give digital input to the system.

LEDs

Two LEDs are added to the board to discriminate with a light signal, the several states of the system. Figure 3.26 shows the simple way in which the LEDs are connected to the μC . A resistor of 750Ω is placed in series of each diode LED, as protection. D5 is the green LED and D6 is orange, with a current test of 2mA and 1mA respectively.

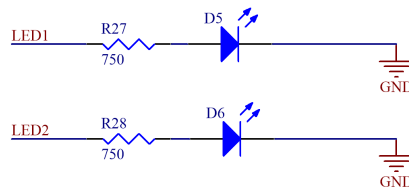


Figure 3.26: Circuit diagram of LEDs connection.

3.7.2 nRF52840 Vs nRF52832

In this third version of the MITOR system, the microcontroller is updated to have a component up-to-date characterized by ultra-low power consumption. In table 3.2, there is a comparison between the main features of the actual microcontroller and the previous one (nRF52832 by NORDIC SEMICONDUCTOR®).

Table 3.2: Comparison between features of nRF52840 and nRF52832 [49].

	nRF52840	nRF52832
Processor	32-bit ARM® Cortex®-M4F @64MHz	32-bit ARM® Cortex®-M4 @64MHz
RAM	256KB	32/64KB
FLASH	1MB	256/512KB
TX Current	13.6mA @8dBm DC- DC 7.3mA @4dBm DC-DC 5.3mA @0dBm DC-DC (3V)	7.5mA @4dBm DC-DC 5.3mA @0dBm DC-DC (3V)
RX Current	5.4mA @3V DC-DC	9.7mA @3V DC-DC
Serial Interface	2x I2C master/slave 4x SPI master/slave 1x QSPI 2x UART CTS/ RTS 1x I2S 1x PDM 1x QDEC	2x I2C master/slave 3x SPI master/slave 1x UART CTS/ RTS 1x I2S 1x PDM 1x QDEC
GPIO Pins	48	32
Package	7 × 7mm AQFN-73	6 × 6mm AQFN-48
Supply Voltage	1.7-5.5V	1.7-3.6V

3.8 Device Development

To implement the circuits and realize the PCB ALTIVUM DESIGNER® 18 is used. This software is user-friendly and only 3 steps are required to have a PCB "ready for printing".

Step1: Library generation

The first step consists of the software realization of all the component that is necessary to make the circuit. For each component, a schematic symbol and the PCB footprint are designed. The symbol is drawn with the help of line or shape generator tool available. In this phase, it is good practice to check the correct number of pins and the right symbol representation of all the components.

A particular toolbox (*IPC[®] Compliant Footprint Wizard*) allows to generate the footprint. This is semi-automatic tools, in fact, the user has to select the family of components, define the overall dimension of the packaging and the dimension of the pin. All this information is available in the last pages of all the datasheets. It is possible to include also the 3D reconstruction of the component in the library. Figure 3.27 shows an example of setting parameter on IPC[®] Compliant Footprint Wizard.

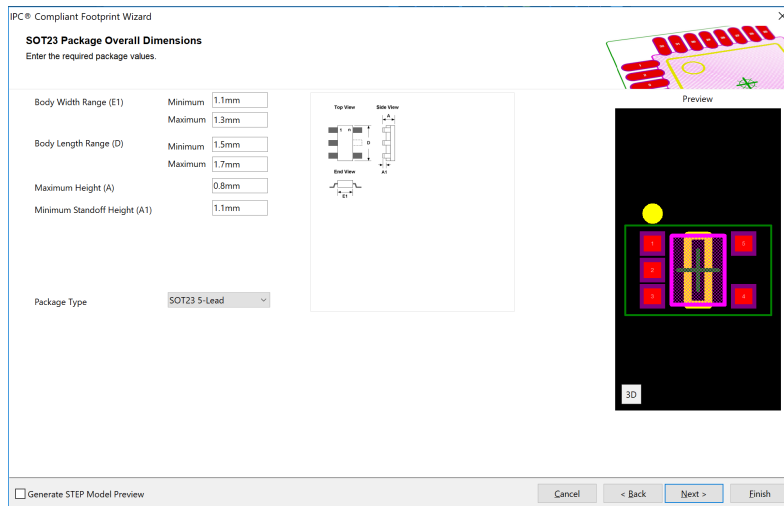


Figure 3.27: Setting parameter on IPC[®] Compliant Footprint Wizard.

Step2: Schematic editing

In this second step, the schematics of the circuits are drawing. In this phase, the schematic symbols created in step 1 correctly link so that design the complete electric circuit.

In addition to that explained in previous sections *bypass capacitors* are placed between the supply line and each active component in order to de-couple the noise. Another important aspect analyzed in this phase is the choice of header, connector that is useful for the board.

In figure 3.28 a screen capture of ALTIUM DESIGNER® 18 during the schematic editing phase is chosen.

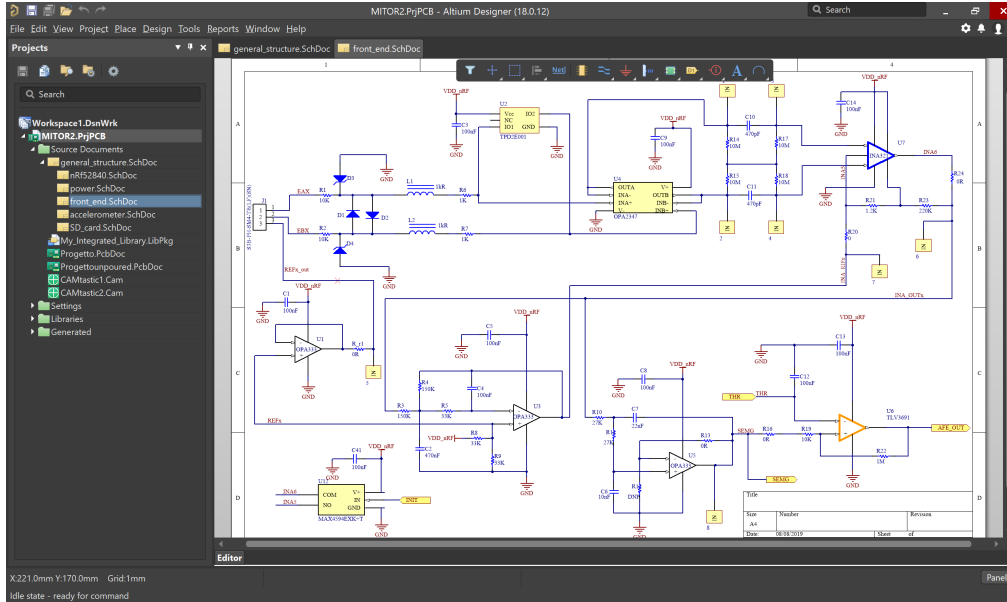


Figure 3.28: Schematic editing screen capture.

Step3: PCB layout

In this phase, all the component are placed with the aim of optimizing the PCB dimensions and the track to interconnect the component are draw. To do this, it is necessary to follow particular *PCB layout design rules* that are different between every company that prints circuits. These rules are guidelines to minimize errors during manufacture. For example set a limit on the minimum and maximum size of the link track, on vias dimensions (track intra-layer that allow going through from one layer to the other), on the minimum distance between the mechanical layer or on legend print size. For this project, as a result of cost analysis, EURO CIRCUITS® is chosen to print the devices, and so the rules class 8D are followed [50].

An important aspect is the position of each component. Some components or circuit parts may interfere with each other or have special needs about the position. For example, the antenna and battery, supply have to be placed in the opposite part of the board. The antenna requires an empty space without a ground plane and other components to work in a proper way.

In this phase, it is also necessary to think how will be the physical device and in which position is more user-friendly place the battery holder, the connector for the

electrode waves, μ SD card slot and the on-off switch.

The layout of the top and of the bottom layers is shown in figure 3.29. In the bottom layer, all the components of the analog front end and the powered switch are placed. The top layer contains all the other components.

Four mechanical holes are designed on the edges board to allow that the board can be attached to a package with plastic screws (3.2mm).

The final step is the generation of the *Gerber file*. It is used by printed circuit board (PCB) industry software to describe the print the PCBs.

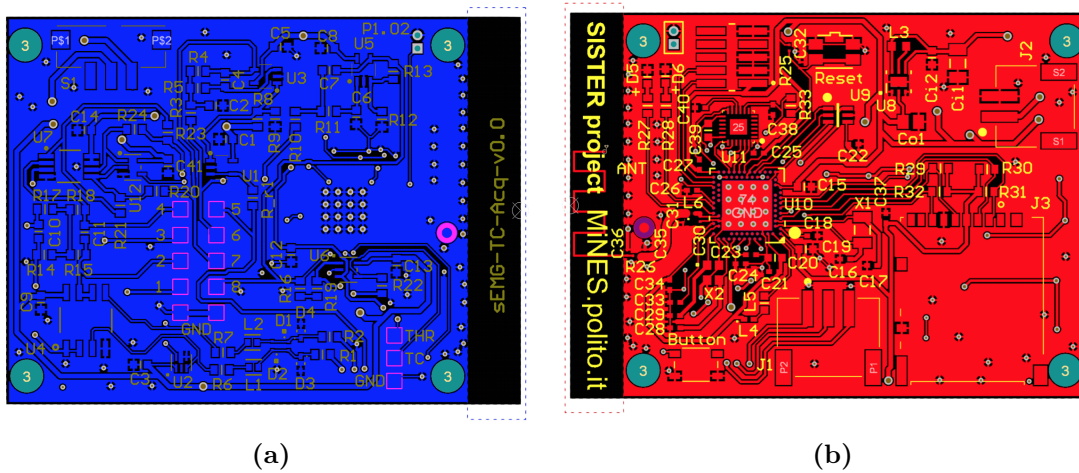


Figure 3.29: PCB layout: a)Bottom layer, b)Top layer.

Soldering Process

In the developed board some components are characterized by a QFN package. This component is very difficult to place manually and so for this reason, they were soldered by the company chosen to print the PCBs (EUROCIRCUITS®). All the other components were soldered manually or with the use of a pick-and-place machine.

3.8.1 Case Design

A case for the PCB is realized with SOLIDWORKS® (figure 3.30).

This package has two openings in the side that allow integrating an elastic band to fix the board on the body. The back part is characterized by a circular shape to hold a coin battery to supply the board. The case is made with a 3D printer at Politecnico di Torino. Transparent resin is used to print it so that the led light

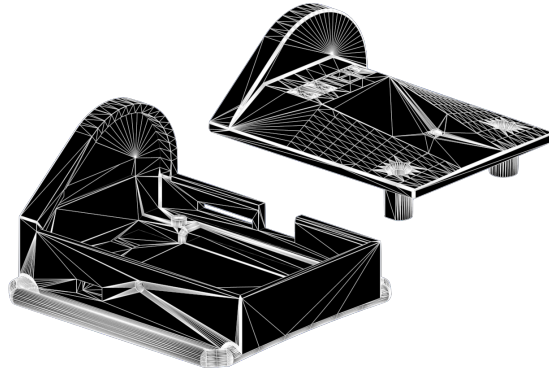


Figure 3.30: 3D virtual design of the PCB case.

is visible. All apertures are predisposed to guarantee easy access to the connector and on-off switch.

Chapter 4

Firmware Design

4.1 Overview

The firmware of the developed system is achieved by making changes and integration to the firmware of the previous version. First of all, the project set-up is changed to upgrade the microcontroller and new functions are made to manage the components added.

The firmware is written in a mix of C and C++ languages. To debug and program the board the software IAR EMBEDDED WORKBENCH IDE FOR ARM®.

There is two different firmware one for the master and the other for the slaves.

4.2 Slave Firmware

The flowchart, in figure 4.1, describes the high-level operation of slaves' firmware. The first phase of the firmware is the initialization of all the variables, timers, protocols that the devices required to work properly. After this, the slave put the antenna in received mode (RX mode) and it is in these conditions until the slave receives from master the work mode and the start command. From this moment a routine is repeated until the reception of the stop command. The routine consists to check if there is a synchronization event, sampling the input signal with the ADC and storage the data. In the case in which there is a synchronization event, the slave receives the clock information from the master board at which each slave shall calculate the offset with its clock. This offset is useful to adjust the ADC time sampling.

In the next subsection the most important part of the firmware will be analyzed in detail.

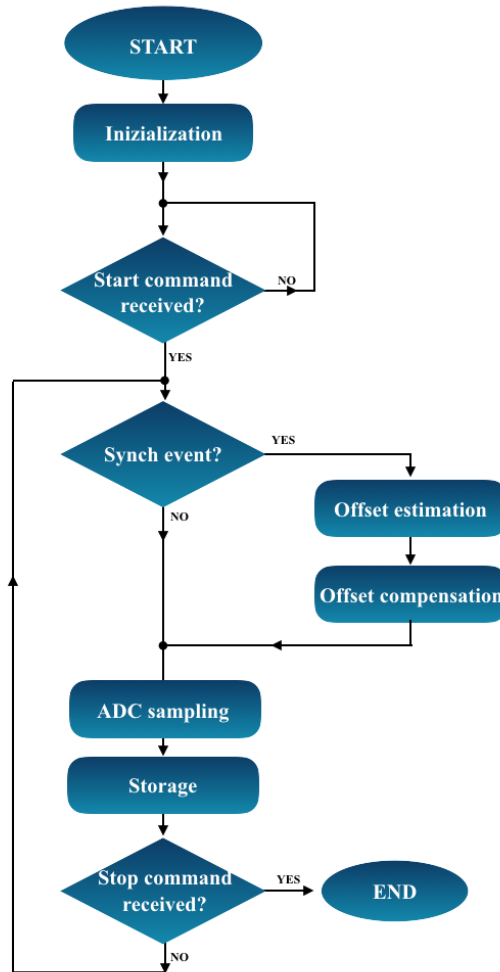


Figure 4.1: Main high level flowchart of slave boards.

4.2.1 Initialization: General

The initialization is the first part of the firmware, in which all used structure are defined.

- **Pins Mapping**

SPI ports and in general GPIO pins are set to respect the connection of the circuit diagram.

- **Peripheral Programmable Interconnect**

The PPI enables interconnections between peripherals using tasks and events independent of the CPU. In this way, the CPU activity is reduced. This method is also useful to manage the *Capture&Capture registers*. Each time

that there is an interrupt from one of this timer the PPI perform a different command. This register is named CC[x], in which x represents the number of channels. In this firmware CC[0] and CC[1] manage the radio communication, CC[3] enables the sampling of each 1 ms, CC[2] is used during the synchronization to reset and adjust the sampling timer.

- **Timers**

Three different clocks are required from the firmware: two high-frequency timers (16MHz) and on *Real-Time Counter* (RTC) with a frequency of 32.768KHz. The radio communication requires a 16MHz clock, instead, the other one is used for the synchronization (synchronization timer). The RTC timer has multiple uses.

- **Initial Reset Switch**

The reset switch is the component connected to the pin 5 and 6 of the INA321 and avoid that the channel goes in saturation. The part of the code to manage this component is very easy in which the microcontroller set high the pin of control of the switch, only for 10ms.

- **µSD card**

The storage is based on FatFS library of nRF52840 provided by NORDIC SEMICONDUCTOR®. The firmware structure of the data storing is a FIFO (*First Input First Output*) structure with 7 blocks. In this way, the phase of sampling and storage can be independent in the event of delays during the saving in µSD card.

- **Power Management**

In this phase of initialization, the internal DCDC converter is enabled to optimize power consumption.

- **Radio Protocol**

In this system, a custom wireless radio protocol 2.4GHz *Enhanced ShockBurst* (ESB) is used. This protocol supporting two-way data communication and automatic retransmission in the case in which a packet is lost or in general if the *Primary Receiver* doesn't receive the feedback within 30ms. It is a low power consumption protocol and it is characterized also by a small code easy to modify. These are the principal reason because this protocol is preferred to the Bluetooth® communication. For example, ESB allows to connect more than 8 devices with a simple change in the code: add extended address into the data payload in order to identify each node.

4.2.2 Initialization: ATC

This part of the initialization manages all firmware components that the ATC mode requires to work properly.

GPIO Rising Edge Sensitive

In section 1.4 the TC signal was analyzed and also the way to detect this signal it was explained. The output of the comparator (figure 3.15) is a quasi-digital signal and the information of this signal is in the rising edges because of these meaning that the signal crosses the threshold. To identify the rising edge, the ADC is not required. In fact with the function `NRFX_GPIOTE_CONFIG_IN_SENSE_LOTOHI` of NORDIC® it's possible make a pin (**P0.2** in this case) sensitive to rising edge in with the aim of generate an interrupt for each rising edge. In this way, the ATC parameter is calculated by counting the number of an interrupt from **P0.2** in a time window. According to a previous study [51], about the detection of muscle force with ATC parameters, a value of 130ms was set as an initial time window.

Threshold Calibration

Another important step on the ATC initialization is the definition of the threshold. How shown in section 2.1 the value of the threshold is very important. The optimal threshold should be sufficiently high to avoid the baseline noise, but at the same time, very close to this in order to quickly discriminate the muscle activation from the noise. For these reasons, a robust but simple algorithm was implemented. In figure 4.2 the flowchart of *Threshold Definition Algorithm* is given.

The aim of the algorithm is to identify the top end of base line noise. To Hardware specifications, the signal is developed around 1.8V, because this is the theoretic value of the reference. In the reality application not all the board have the same base line level, so to be sure that the algorithm start from a value that is definitely higher than the base line level a value of 2100mV is chosen.

The first part of this code is really fast. The *THR* (threshold value) decreased by 10mV and only when an event from P0.2 (*TC_events*) is detect, the code can proceed in its second part. In this moment, the algorithm found something, but it may be or the real base line noise or an anomalous pick of voltage. In the second part of the algorithm there is a close monitoring of *TC_event* in order to be sure that the base line noise was detected if not the code fixes the error.

At the beginning of second part there is the initialization of 2 variables:

- **flag_window**: This variable is managed by the algorithm and also from the

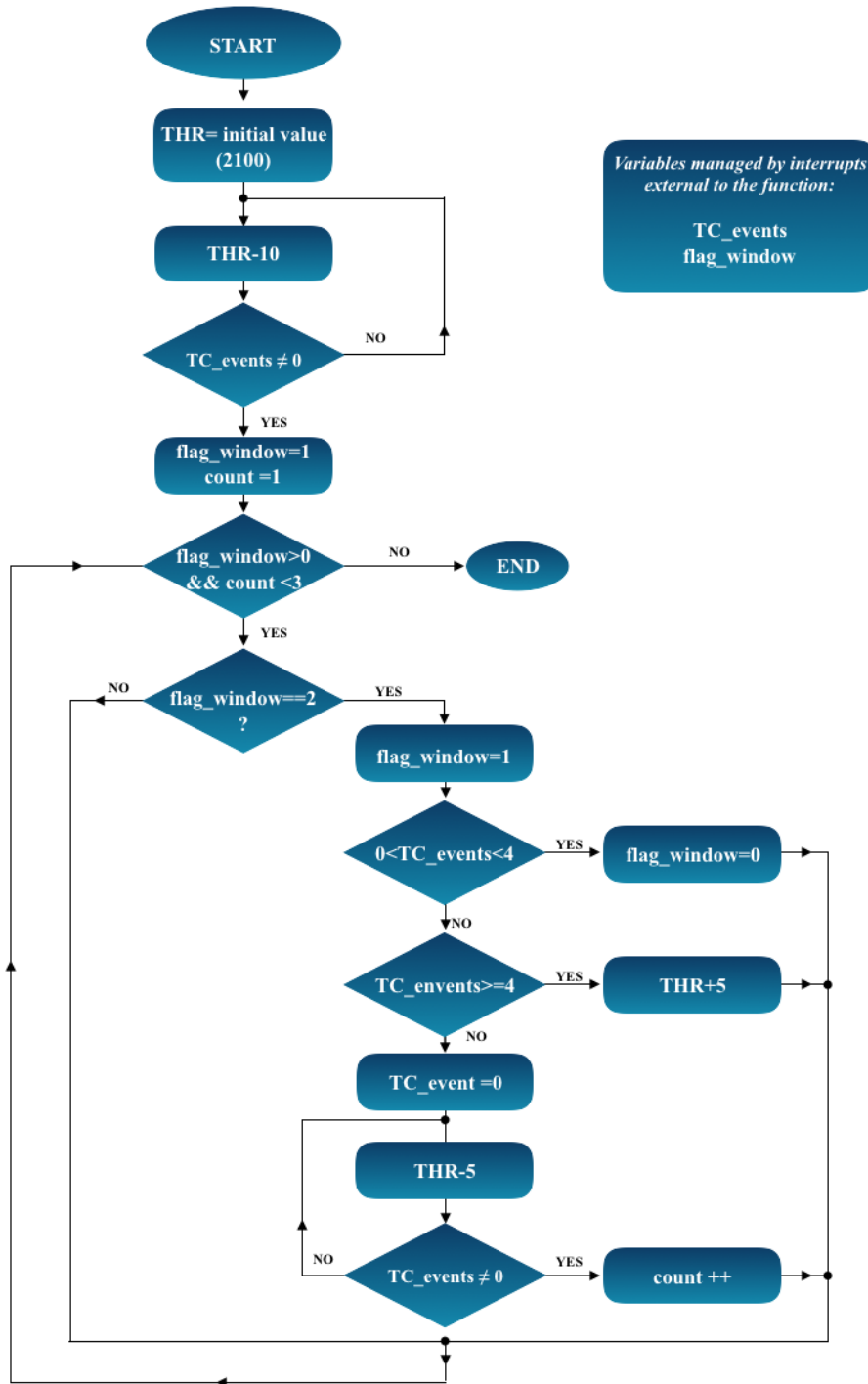


Figure 4.2: Threshold Calibration flowchart of slave boards.

RTC timer. This timer, using PPI, produces an interrupt each 1ms. In particular, when *flag_window* is 1 the RTC timer activates a variable that is increased each 1ms. All the time that this value counts 2 times the time window (260), RTC routine set *flag_window=2* and reset the counting variable. The value of 260ms is double of the normal windows that the system uses to calculate the ATC parameter. During part 1, *flag_window* is set to 0. During the second part the condition *flag_window==0* is useful to end the routine.

- **count:** This variable is a way to be sure that the algorithm does not block inside a while cycle. This variable is increased if THR does not allow to detect an adequate number of events. If *count* is 3 the algorithm ends. The case in which *count* becomes 3 only happens when THR oscillates between the conditions $THR+5$ and $THR-5$. The position of the block *count++* causes that in bounce case the result is $THR-5$.

In the second part of the algorithm each 260ms, *flag_window* is set to 1 (in order to ensure that this routine will be carried out only after other 260ms) and *TC_events* value is compared with 3 limit values. These values are chosen as results of analyses of the amount of TC events related to different values of threshold. In the case in which the threshold is put inside the band line noise the minimum number of events in a window of 130ms, generated by noise is at least 3. So to be sure that the selected threshold is out the band line noise the maximum number of TC events (in 130ms) should be less than this value. A more restrictive condition is implemented in the firmware, in fact, the better solution for the algorithm is when *TC_events* is between 1 or 3 (in 260ms). When that happens *flag_window* is set to 0 to end the algorithm. If the amount of TC events is more than 3, it means that *THR* is low and so THR is increased of 5mV and after 260ms the new *TC_events* is check. Instead, if there are 0 events, it means that *THR* is too high. This could happen if the first part of the algorithm converges in an anomalous pick of voltage. In this case, there is a quick decrease, with a step of 5mV, that finishes only when a TC event is detected and only in this case the variable *count* is increased. Each time that the threshold value is updated in the algorithm, *THR* is sent to DAC that converts it at a voltage level. This algorithm is very robust and few sensitive to noise. The results are shown in section 5.3.3.

DAC Programming

To convert the digital values of *THR* calculated in the calibration threshold algorithm, it is necessary to program the AD5621 (DAC). The microcontroller's pins that manage the DAC are initialized as SPI port.

The AD5621 has a resolution of 12 bit, and the input register to define the value is composed of 16 bit how shown in figure 4.3. Considering that communication between microcontroller and DAC use "words" of 1 byte (8 bit), to program the AD5621, two different bytes are required.

In the firmware $PD1$ and $PD0$ are set to 0 (Normal operation) as also the last

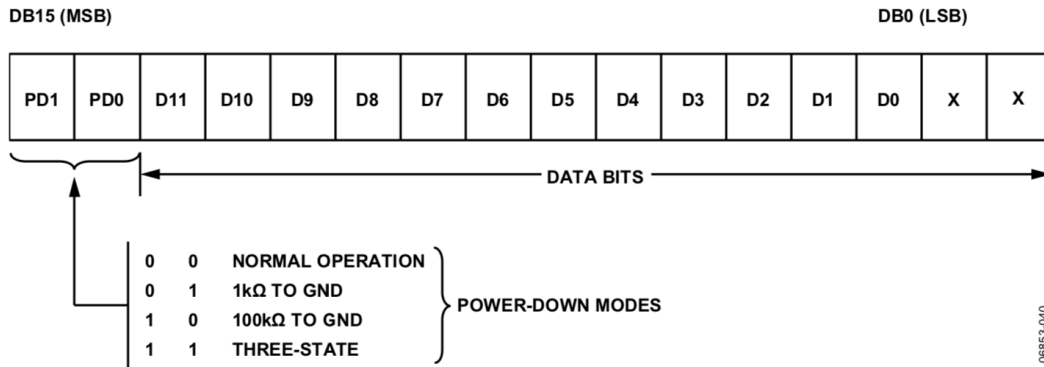


Figure 4.3: AD5621 Input Register Contents [42].

2 low significant bits (do not have relevance). The code between D11 and D0 is the binary code equivalent to the decimal value of D . This value is calculated by equation 4.2, and allows to set the threshold to THR value with a define power supply (V_{DD}).

$$D = THR \times \left(\frac{2^n}{V_{DD}} \right) \quad (4.1)$$

To obtain from D the two word two simple operations are made:

- $D/2^6$ to obtain the 6 most significant bit that makes up the first word;
- $(D \% 2^6) \times 2^2$ with the operation in brackets (rest of division) the 6 less significant bit is found, but an operation of a shift to the left is required to add the two 0 that corresponds to the not relevance bits of the input register.

The output resolution of the DAC, with $V_{DD}=3600\text{mV}$, $D=1$ and $n=1$ is:

$$Resolution = D \times \left(\frac{V_{DD}}{2^n} \right) = 1 \times \left(\frac{3600\text{mV}}{4096} \right) = 878.9 \mu\text{V} \quad (4.2)$$

4.2.3 Synchronization routine

A good synchronization is one of the principal aspects of a system composed of many boards. This makes sure that the different slaves start to sampling at the same moment and also keeps the synchronous condition for an indefinite time. The

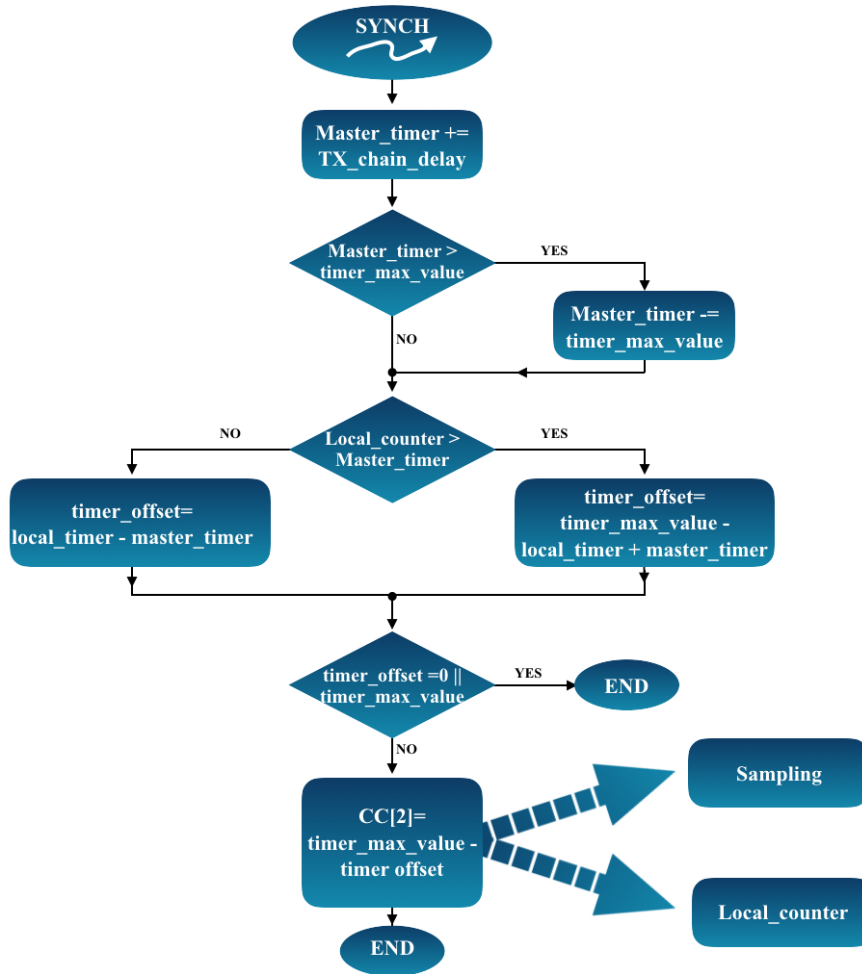


Figure 4.4: Synchronization routine flowchart.

flowchart of the interrupt routine of the synchronization is shown in figure 4.4. This routine is repeated each a fixed time called *synchronization time* after that the start command is received by the slaves. In fact master board, at the beginnings, with the start command send also the synchronization package to guarantee that all the slaves start together. If the master does not receive the feedback from all the slaves, it waits the synchronization time and re-send the start command until all the slave answer. So biggest is the synchronization timer, higher is the amount of time required to start the system. At the same time, however, this time should not be too low in order to optimize power consumption. An acceptable value is in the 5s-20s range.

Each synchronization time the slave set the antenna in receive mode and if a

synchronization packet is received an interrupt allows the start of the synchronization routine. When the slave receive the master clock information, firstly there is the compensation of the transmission delay (according to *ESB* protocol). The next step is to check if the mister timer is in overflow and in case adjust the value. After that there is the comparison between the timers of master and slave. If the clock of the slave (*local_timer*) is higher than *master_timer* means that the slave is faster, on the contrary if the slave is slower than master, the *master_timer* value is bigger. If the two values are exactly the same, the routine ends because the board are already synchronize. Otherwise, the difference of the timers of the master and of the slave is load in the register *Capture&Compare 2*. In this way when the internal counter arrive to the value saved in *CC[2]*, an interrupt is generated in order to clear and restart the counter. In this way master and slave start again to sampling in the same time with an accuracy of 62.5 ns. Furthermore another value that is modified by synchronization routine is the *Local_counter*. This variable count the number of sample. It has a value in 0-999 range. In fact after the synchronization, slave *Local_counter* is update in order than all the salve re-start from the same number of sample. So the synchronization acts to fix not only the delay between master and slave, but also to eliminate the misalignment, due to missing synch event, between the signal recorder form the different slaves.

In section 5.2, the results of the synchronization are analyzed, and all the features of the synchronization routine will be shown in detail.

4.2.4 ADC Management

Each 1ms, *CC[3]* generates an interrupt that starts the *ADC routine*. In figure 4.5a the high level flowchart of this routine is chosen. The ADC interrupt is composed of three subroutines one for each working mode of the system. In all the case there is the same initial initialization. All the data are saved in a buffer of 500 (*data_length*) spaces and only when this is complete the board storage the data in the μ SD card. The ADC has a resolution of 12 bit, and a sampling frequency of 1kHz. The voltage resolution is fixed to 1 mV.

After the initialization block, there is a switch structure based on the value of *work_mode*. For simplicity in the organization of the firmware and also to guarantee the same synchronization condition for all the working mode, the *ATC routine* is inside the ADC interrupt. When ATC mode is selected the ADC routine is used not for sampling but only like a timer to count, in a synchronous way, the difference between the time windows required from the ATC technique.

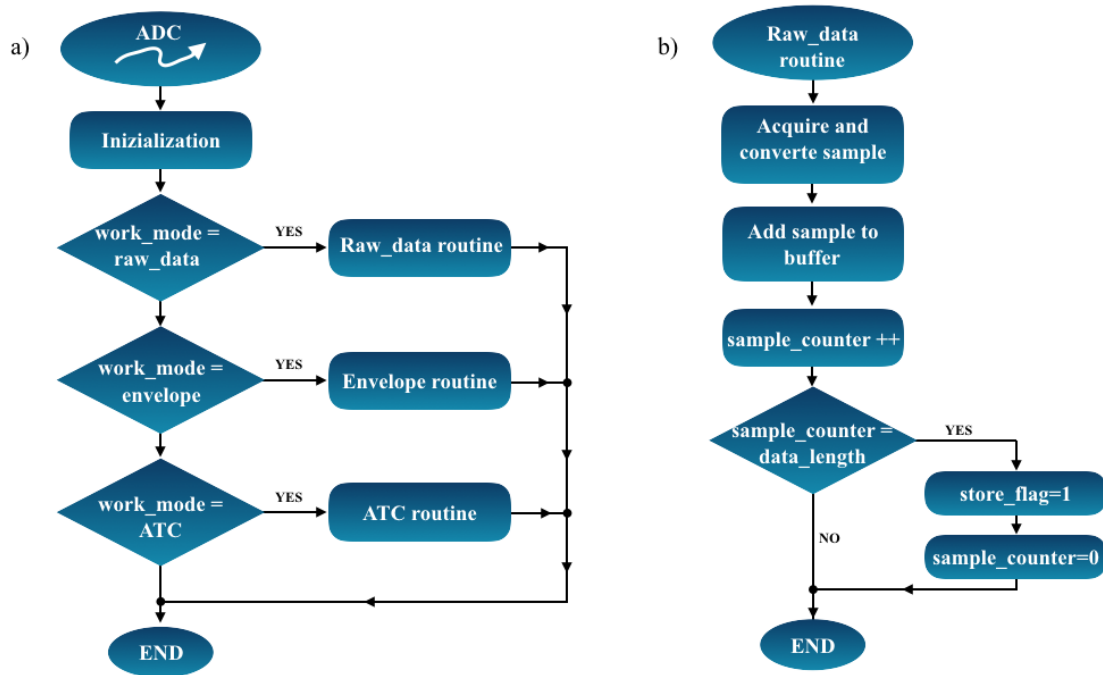


Figure 4.5: Flowchart: (a)high level ADC and sampling routine, (b)raw_data (classic sEMG) routine.

Raw_data (Classic sEMG) Routine

This routine (figure 4.5b) is very simple. The ADC acquires and converts a sample and each 500ms the flag for the storage in the external memory is enabled.

Envelope Routine

This routine shows in figure 4.6a, starts with the acquisition and the conversion from ADC. A 2^{nd} -order *Butterworth high pass* filter is implemented to remove the DC component from the input signal. After that, the absolute value is calculated. At this point, a 4^{th} -order *Chebyshev low pass* filter with a cut off frequency of 10Hz, is applied to extract the final envelope. In this case, the storage of the data is each 10s because the sampling period of the envelope is 20ms.

ATC Routine

When the ATC mode is set, the ADC interrupt is used only as a timer. So each determinate time (windows time), the number of TC event is saved in the buffer. In this case, the storage of data, with a window size of 130ms, is each 65s.

$ATC_counter$ is the variable that counts the number of interrupts generate from the pin **P0.2** (the GPIO rising edge sensitive for the TC detection). The routine is shown in figure 4.6b.

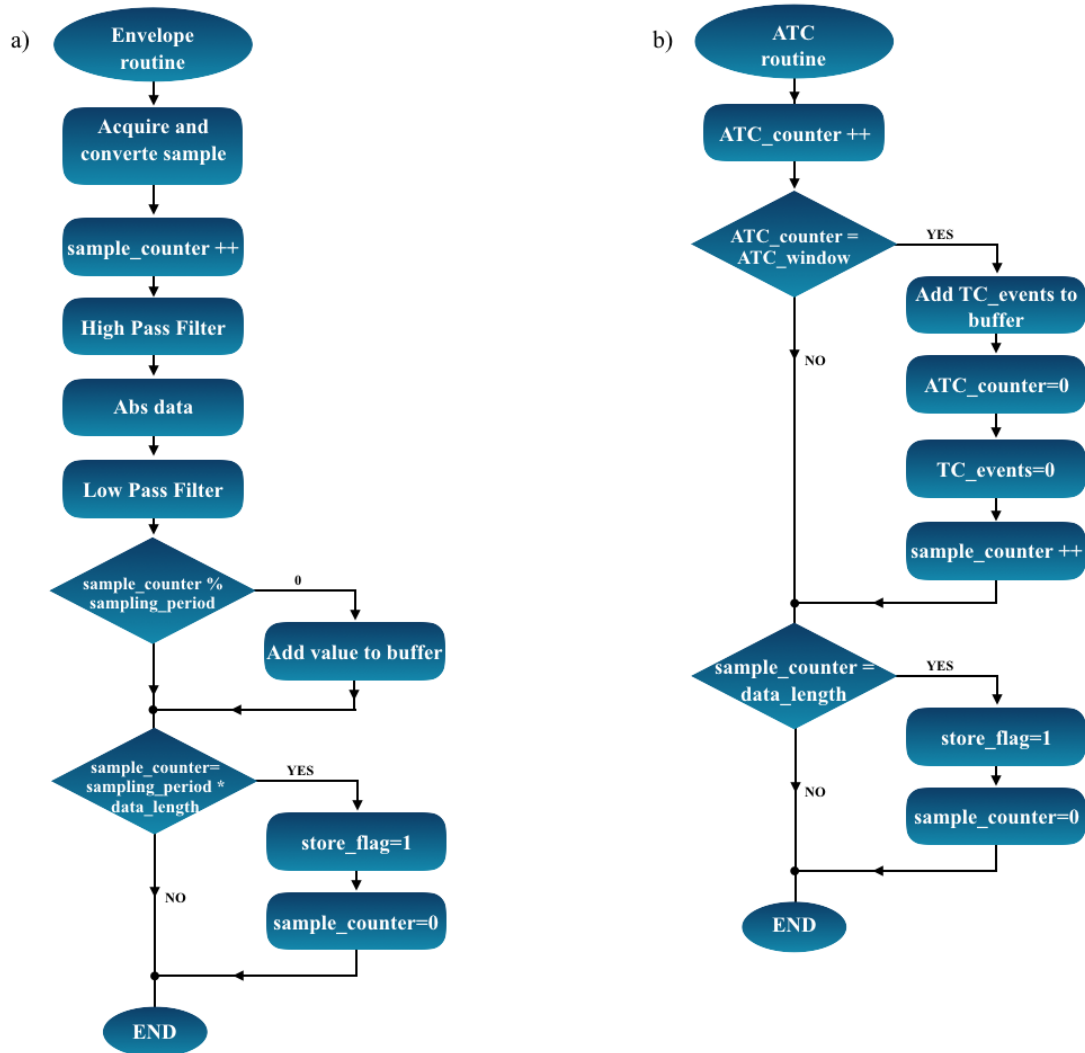


Figure 4.6: Flowchart: (a)envelope routine, (b)ATC routine.

4.3 Master Firmware

The flowchart, in figure 4.7, describes the high-level operation of master's firmware. As slave's firmware, in the initialization phase all the flag, variable, pins are initialized in order to enable all the necessary functions. Unlike the slave, in the master algorithm, there is not the initialization of DAC, memory, ADC and in general of

all these functions useful to manage the signal from the electrodes.

Extra initial setup is needed to control the four buttons on the board in order to generate a different interrupt when one of these is pressed. The second step of the master firmware is check if one of *Button1* (*raw_dat*), *Button2* (*envelope*) or *Button3* (*ATC*) is pressed to set the work mode. Only if the work mode is selected the *Button4*, to start the system, is enabled.

At this point, the firmware each synchronization period sends its clock information to the slaves. The firmware ends only when *Button3* is pressed again to send the stop command.

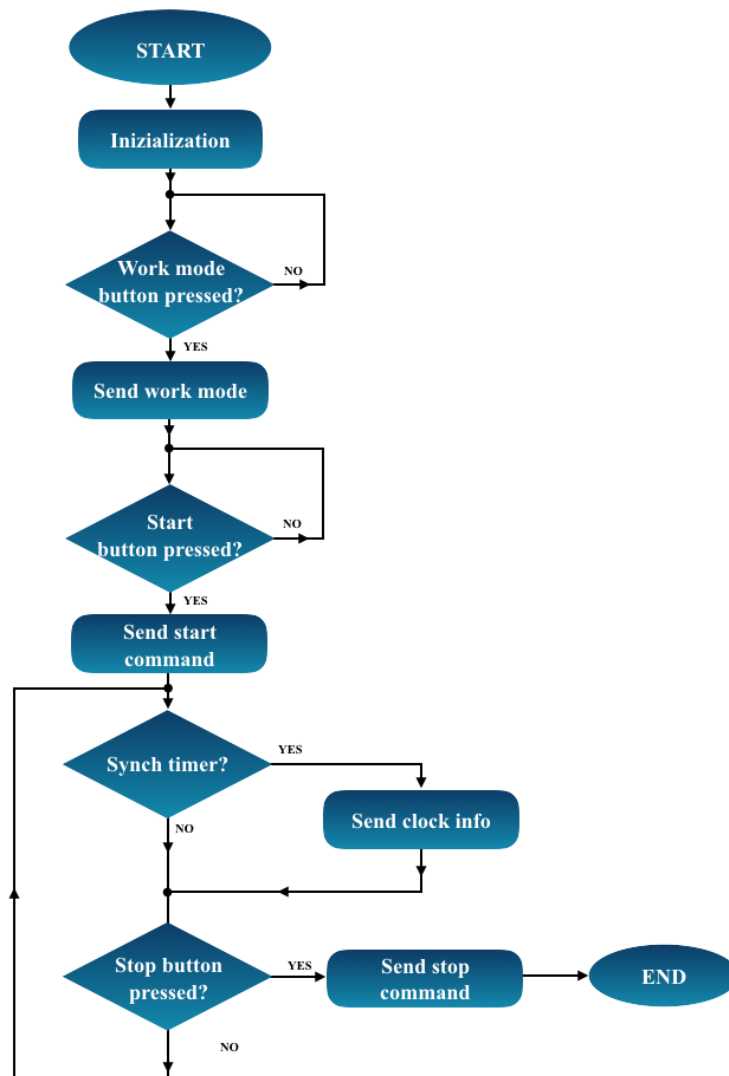


Figure 4.7: Main high level flowchart of master board.

Chapter 5

Operation Testing

5.1 Electrical test

Most of the components were soldered manually or with the use of a pick-and-place machine. Once the components were set, the electrical connections were checked with a multimeter to check if there were unintentional short circuits. After that, a simple firmware was loaded on the board to test the proper functioning.

5.2 Synchronization Test

The main feature of the firmware is wireless synchronization between the different MITOR boards. This is the crucial element that needed to be tested to guarantee long-term analysis. The synchronization is aimed to minimize the delay between the board. In this way, it is possible to guarantee, also after many hours, that the signals stored by different boards have a maximum delay that does not compromise the muscular analysis.

The delay depends on the drift of the timer of the different boards. This varies due to the external quartz use in the microcontroller electrical layout. The oscillation of quartz can change according to PCB features like the soldering of the quartz chip or of the two capacitors close to the crystal used to balance it. Other external features like temperature and humidity may affect the behavior of the oscillator.

The figure 5.1 shows what happens in terms of the average delay between two different boards without synchronization. The test was made using several couple combinations of boards and in diverse environments. The tests have been 5 hours and 30 minutes. Each couple of board has like input an FSR that it was pressed every 30 minutes to generate an impulse. At the end, the recorded signals were

compared to evaluate the delay. Considering the rectification wave, the boards are

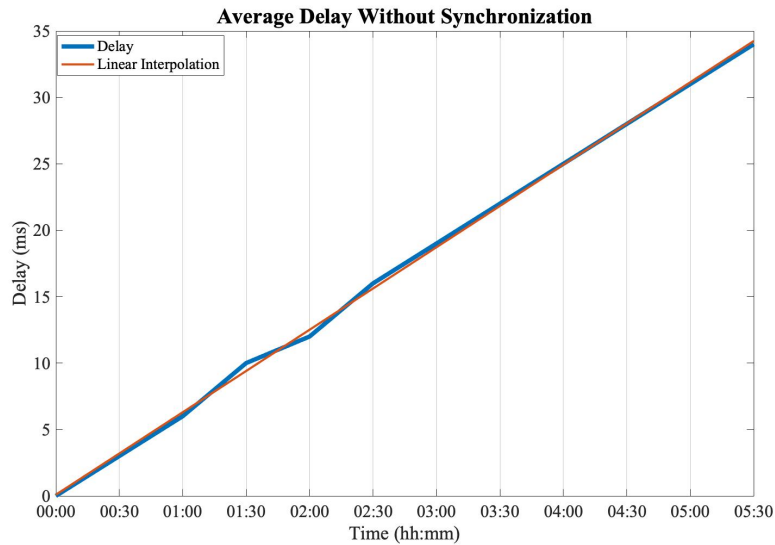


Figure 5.1: Test average delay without synchronization.

characterized by a delay of approximately 1ms every 10 minutes of recording. This result shows

This result demonstrates the need to have synchronization for a long-term analysis of the sEMG. Without this, after two hours of recording, the system may have accumulated a delay high enough to invalidate the analysis.

Another test on the average delay between the boards was done, this time using synchronization. This measure was performed under the same conditions as the previous test. The synchronization time window has been set to 5s. The start time of the whole system, as explained in the *Synchronization Routine* section 4.2.3, depends on this window value. For this reason, a good time range was set between 5s or 20s. The choice of 5s will be justified in section 7.1 about the power consumption analysis also.

The results show in figure 5.2 highlight the delay inside the windows of 5 s. The average value is about 10 μ s. This value coincides with the normal mean drift of the boards without synchronization after 5s. If for a wireless communication problem, one or more, synchronization packages are miss, the graph shows that, in any case, the maximum delay is below a 1ms. The synchronization routine makes changes to both the ADC timer (to correct clock delay) and the local counter (to correct misalignment). So when a sync event isn't received, the boards are delayed and also misaligned temporally with the others.

Tests with 3 boards have been performed to show what happens when a board

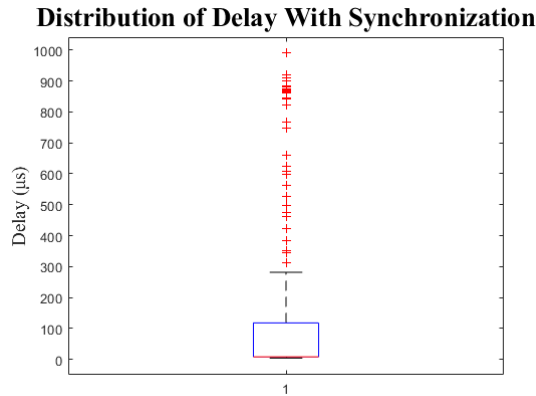


Figure 5.2: Test average delay with synchronization.

does not receive or receives the synchronization trigger. The boards have as input a triangular wave, obtained from wave generator, with amplitude 1.6Vpp, d.c. an offset of 0.4V and duty cycle different from 50%.

Figure 5.3 shows the case where two boards receive the synchronization event and another not. It is possible to notice that the third board (purple line) is misaligned

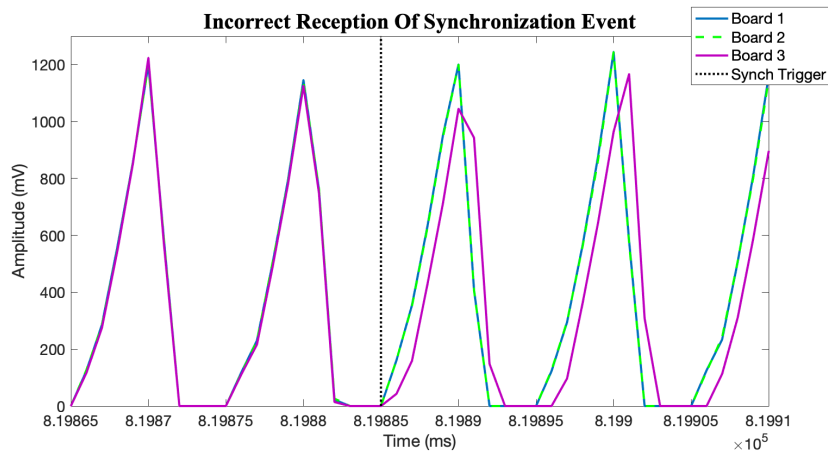


Figure 5.3: The plot shows what happens when a board miss a synchronization event.

with the others and it is easy to understand that the boards sample at different times (see the reconstruction of the peak). In this case, the misalignment can easily be corrected in a pre-processing phase before continuing with signal processing.

The synchronization routine can synchronize the boards, even when these are misaligned and delayed following a previous missing event. The figure 5.4 shows in detail how the misalignment is corrected by updating the local counter. This value

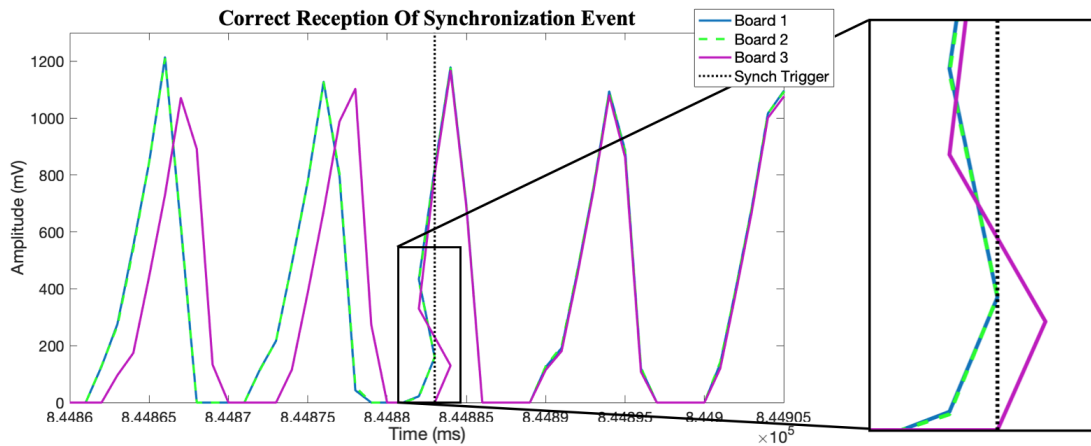


Figure 5.4: The plot shows what happens when all the boards received correctly the synchronization event.

goes back. From the reconstruction of the peaks, it is possible to notice that the board restart to sample at the same time.

5.2.1 Data Pre-Processing

Data pre-processing is necessary to make effective changes made by the synchronization routine. This step follows the following flowchart (figure 5.5).

First, a common time axis for all recorded signals must be defined. The local

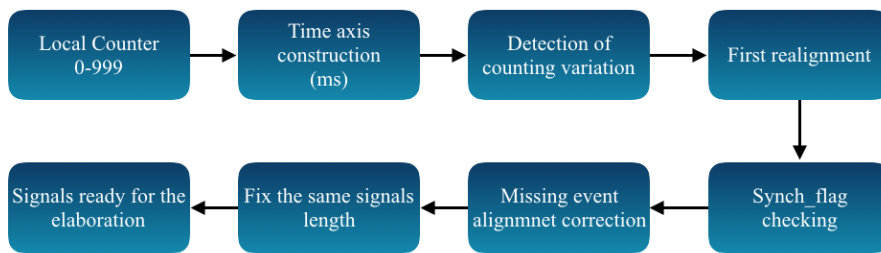


Figure 5.5: Data Pre-processing Flowchart.

counter (in the range: 0 - 999) is practically translated into a vector from zero to the recording length. The new time axis has jumped back or forward each time that the synchronization routine has changed the local counter. This is a problem because in a plot each signal must be compared point by point with the value of the time axis, which must be unique. So in the first realignment, these jumps are corrected by removing the duplication values.

The misalignment due to not receiving the synchronization event is corrected checking *Synch_flag*. This flag gives information on whether or not the boards received the synchronization package. If some boards are not synchronized, they are corrected by adjusting the time axis according to the other properly synchronous boards.

All the signals are cut in order to have the same length. In fact, the signal change length, as a result of the previous pre-processing steps. After this, the signals are synchronized and ready for the next steps of processing.

5.3 Recording Data Analysis

In this section, the three different working mode was tested to assess their proper functioning.

5.3.1 sEMG Signal

Figure 5.6 show an example of recorded sEMG signal.

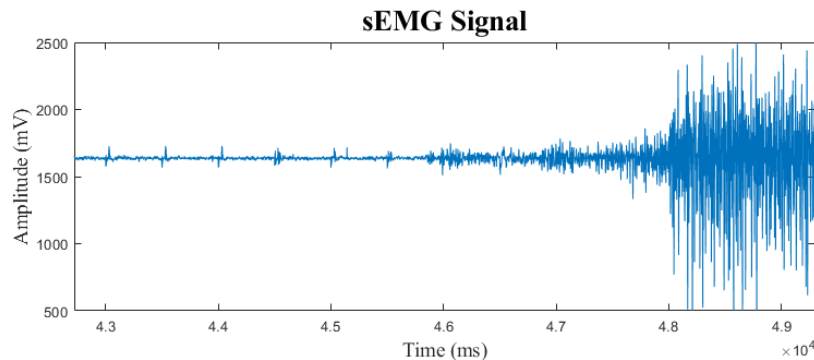


Figure 5.6: Example of a recorded sEMG signal.

In the baseline, there are strange peaks every 500ms. These peaks are due to the change in the voltage of the reference electrode. This voltage depends directly on that of the board. The timing of these peaks suggests that these peaks are due to the inrush current required by the μ SD card during writing. First of all, we tried to solve the problem through software filtering. The artifact was isolated and studied the *power spectral density* (PSD). It has been observed that these peaks present themselves with strong harmonic components in the same band for the study of the sEMG. It is however chosen to filter between 50-300Hz with an order 10, Butterworth bandpass filter.

As shown in the figure 5.7, the peaks have been attenuated but not eliminated.

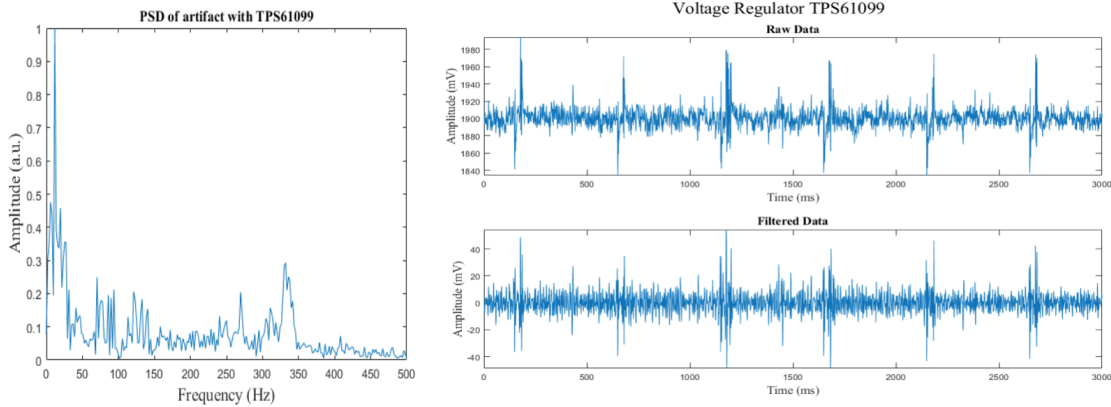


Figure 5.7: Power Spectral Density (left), sEMG signal before and after filtering (right) with designed voltage regulator TPS61099.

The peaks are not repeatable in time and shape enough to use subtraction filtering methods like those used to remove ECG from EMG.

Initially, it occurred if the problem was the voltage regulator. The TPS61099 perhaps is not optimal for this application. It is characterized by a wide voltage drop in cases a high output current is required. The graph of the datasheet is shown in figure 5.8a.

An external development card of SPARKFUN (COM-152085)[53], with a Buck-

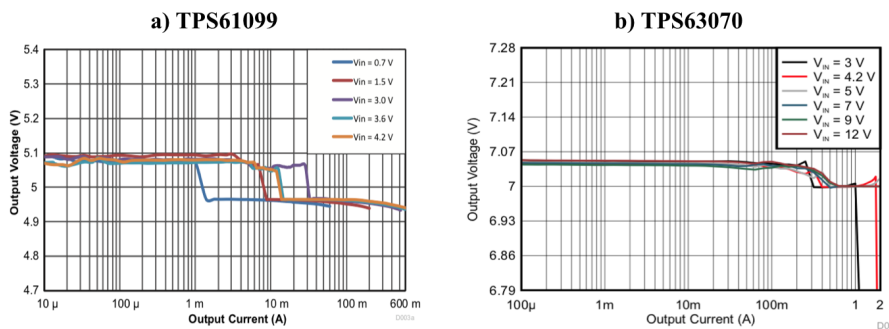


Figure 5.8: a)TPS61099 Load regulation[44], b)TPS63070 Load regulation[52]

boost regulator TPS63070, was tested. From the datasheet, this new regulator can provide more current if required by the load, as shown in the figure 5.8b. This external kit was soldered on a MITOR board. The sEMG signal test reports the following results. The peaks as seen in the figure 5.9 have decreased further.

Mistakenly, at the design stage, a capacitor of 1nF (too small for these applica-

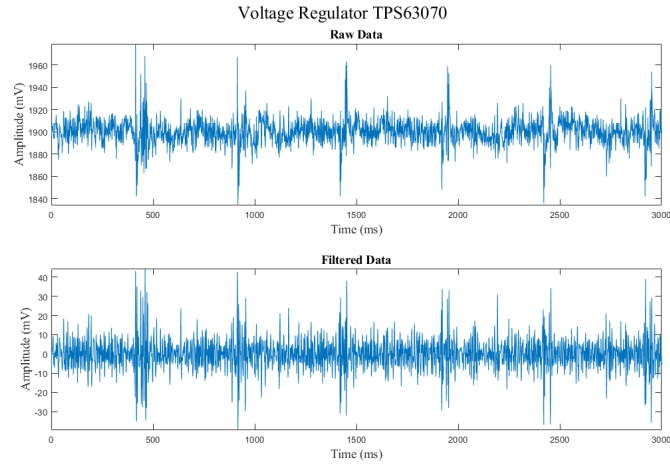


Figure 5.9: sEMG signal before and after filtering with designed voltage regulator TPS63030.

tions) was chosen as a bypass capacitor for the μ SD card.

So another hardware modification that has been tested, was to create a larger bypass capacity ($20\mu\text{F}$). In this way, the frequency component has changed (figure 5.12 and the peaks have decreased in amplitude (figure 5.10).

Figure 5.12 show how change the PSD of the peak artifact during the three different steps. In the last case (TPS63070 + capacitor) most of the frequency components of the peaks are outside the useful range. So for this reason the filtering is more effective.

The table 5.1 shows the values of peak amplitude in the three cases tested. These

Table 5.1: Comparison of Peak Artifact Amplitude in the three different hardware test

Test	Amplitude (mVpp)	
	<i>Raw Data</i>	<i>Filtered Data</i>
sEMG	160	103
Envelope	147	84
ATC	134	78

tests show that the peaks are caused by a mix of factors (voltage regulator, μ SD conditioning circuit). One idea might be to enter into the design phase more bypass capabilities for the μ SD circuit. Moreover, some inductive effects directly generated by PCB or the features of the supply tracks, cannot be excluded as causes of peaks. These factors are difficult to test if not by redesigning the PCB. To conclude the

peaks have been however attenuated, so as not to create problems for the extraction of muscle synergies.

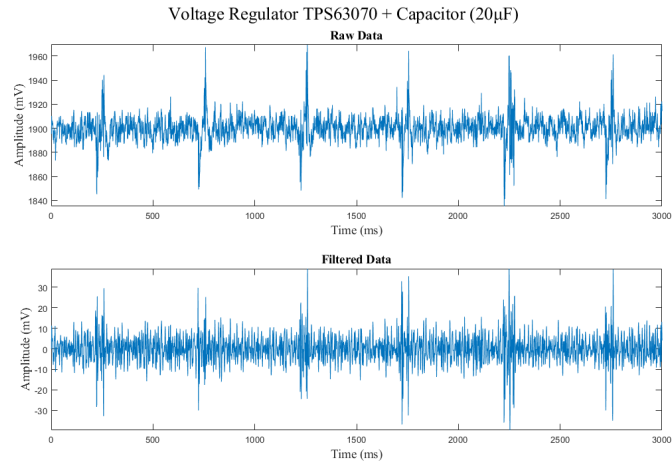


Figure 5.10: sEMG signal before and after filtering with designed voltage regulator TPS63070 and 20 μ F bypass Capacitor.

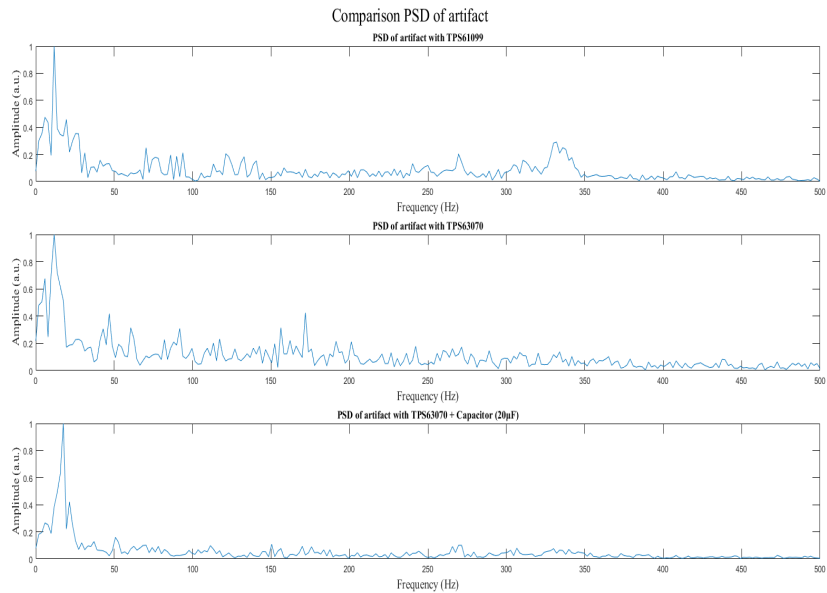


Figure 5.11: PSD comparison between the three different test.

5.3.2 sEMG Envelope

In envelope mode, the board saves the value of the envelope and also the value of the sEMG signal. The figure shows an example of the envelope mode recording. The envelope mode was extensively discussed in the previous version of the system.

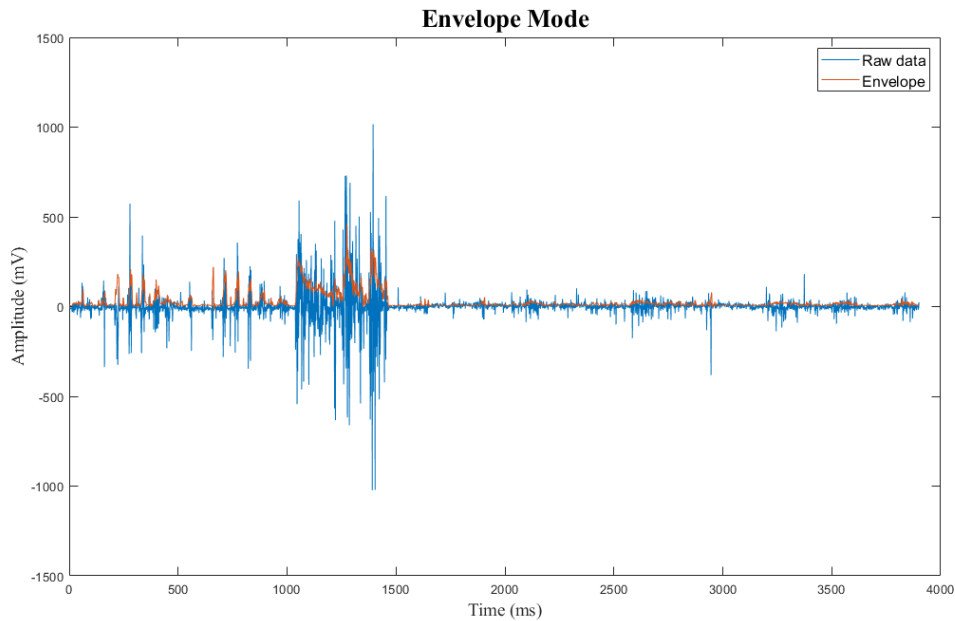


Figure 5.12: Example of a recorded sEMG envelope.

No changes were made and for this reason, only the final result was shown.

5.3.3 ATC Parameters

The ATC parameter has been tested to evaluate the threshold selection algorithm with a time window of 130ms. Several tests have shown that the algorithm selects an acceptable threshold *4 times of 5*. The figure 5.13 shows an sEMG signal with its detected threshold considering the hysteresis generated by the comparator in the hardware. The threshold value is very close to the baseline. This makes the TC signal also sensitive to small activations but at the same time also to noise peaks.

To validate the ATC values recorded by the boards, a MATLAB[®] function has been realized. This function requires as input, the sEMG signal (recorded at the same time as the ATC signal for this test), the window time on which to evaluate the TC signal and the threshold. In software also hardware hysteresis has been

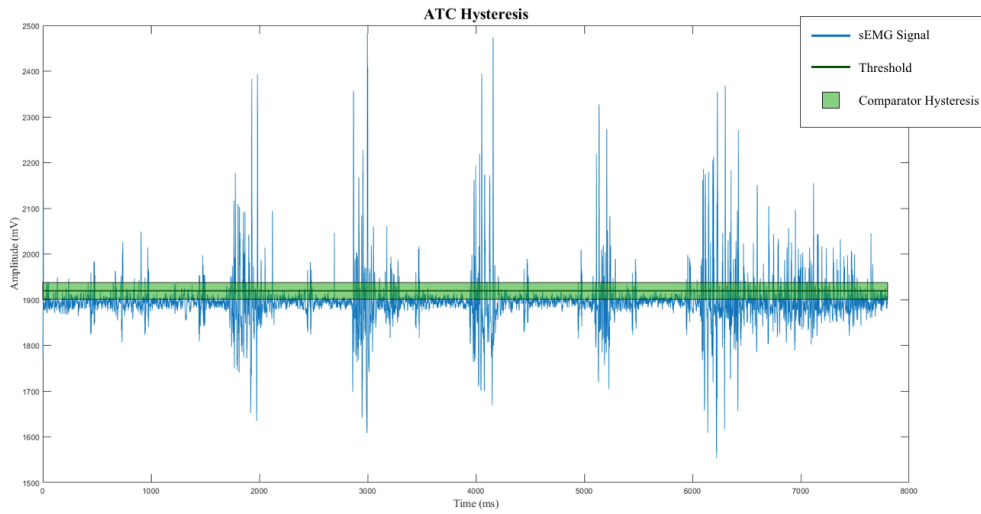


Figure 5.13: Example of a selected threshold for ATC mode.

implemented.

The results are shown in the figure 5.14. The measured values are almost equal

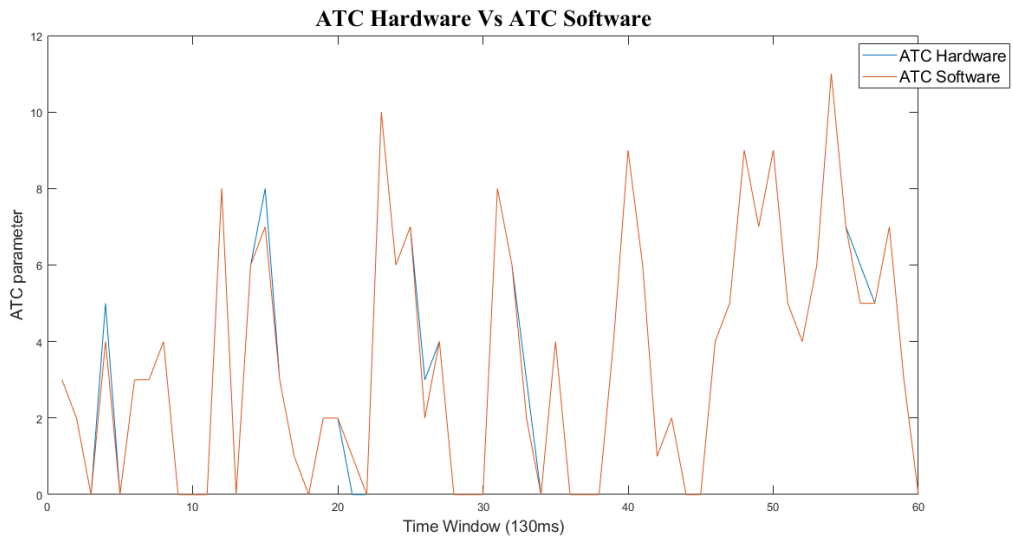


Figure 5.14: Comparison between the ATC parameter recorded in Hardware and in PC Software.

with an error of more or less 1. This difference is caused by the different nature of the two compared signals. During the recording, the board compares a "continuous" signal with a "continuous" threshold. Both can be subject to small variations caused by the tolerance of the components. In software instead, the signal is composed of

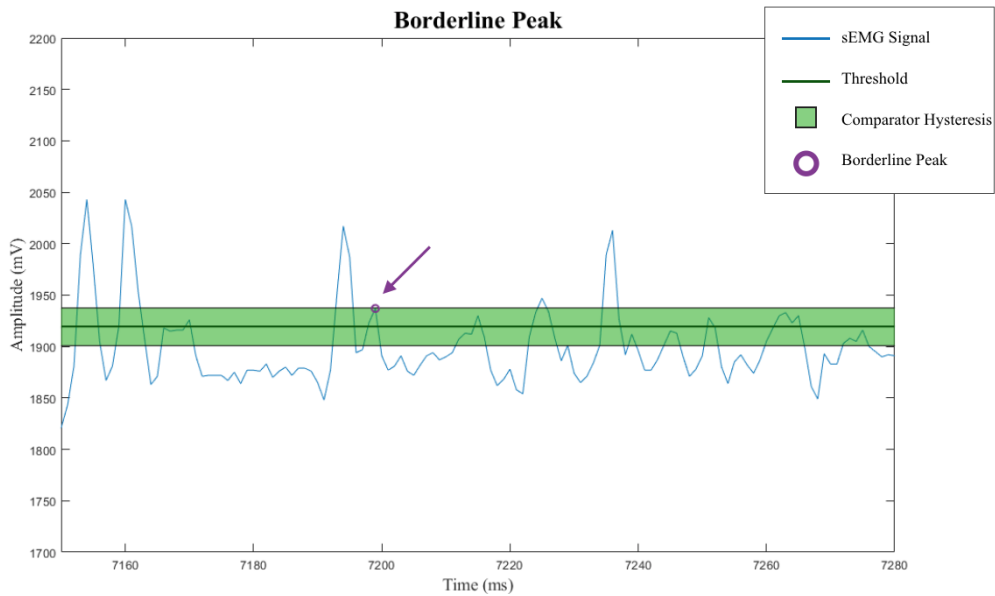


Figure 5.15: Borderline peaks that can create different ATC counts between Hardware and Software

discrete data with 1mv resolution and the threshold has a constant value as well as hysteresis.

This difference in signals can generate different results in borderline cases where a peak is very close to the upper threshold of hysteresis. Figure 5.15 shows what happens in signal *window 54*. The software calculates 5 events while the hardware records 6. The borderline peak marked in the figure is the possible cause of the difference counting. The discrete value of the peak in software is close to the upper threshold of hysteresis but does not exceed it. Possibly comparing the real values, the peak exceeds the threshold. This difference is therefore generated due to the different resolutions between hardware and software. In fact, in the software, the resolution is 1mV (defined by ADC), while in hardware the resolution (in terms of the threshold) equal to 0.879mV (defined by the DAC).

To validate the results the ATC signal has also been tested with a simpler waveform. The test was done using a square wave with a frequency of 200Hz, amplitude of 2.2V, duty cycle of 50% and with a threshold set at 1.902V. The test lasted 30 minutes. The data recorded in hardware coincide with the results obtained in software showing a constant value of 26.

Chapter 6

System Validation

6.1 Methods and Materials

6.1.1 Motion Lab Systems

The MA-300 EMG System, provide by *Motion Lab System*[®] (MLS), was used to validate the sEMG signal quality of the MITOR system. The MA-300 consists of two units (a desktop unit in figure 6.1a and backpack in figure6.1b) with a single thin coaxial connecting cable. The subject carries the backpack, attached to a belt or vest. The system support 16 EMG pre-amplifier probes and up to 8 event switches. Each EMG channel have an adjustable gain. The EMG, event switch are

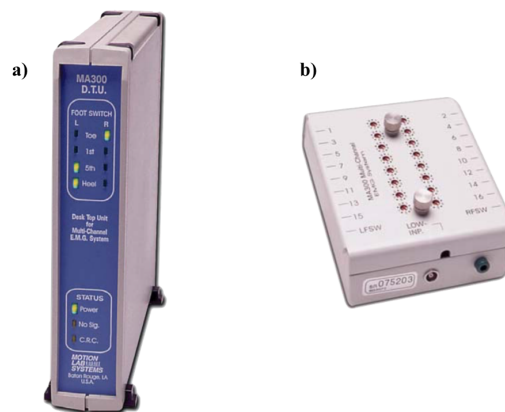


Figure 6.1: MA-300 EMG System, Motion Lab System: a)desktop unit, b)backpack device.[54]

digitized and processed within the backpack and transmitted as digital information

to the desktop unit over the coaxial cable. The table ?? show an overview of system specifications.

Table 6.1: MA-300 EMG System, Motion Lab System, System Specification [54]

<i>Number of EMG channels</i>	16
<i>EMG signal output level</i>	$\pm 5V$ (Full Scale)
<i>Standard EMG Bandwidth</i>	20 to 2000Hz at -3dB
<i>Built in Low Pass Filter</i>	-3dB at 350, 500, 750, 1000, 1250, 1500, 1750 and 2000Hz. Set by user.
<i>Number of foot switches</i>	8
<i>Unit Gain Range</i>	10 to 500

6.1.2 Test Protocol

Validation aims to demonstrate that the boards of the MITOR system have a good noise signal ratio (SNR) and record the signals promptly on time.

As far as signal quality is concerned, this has been assessed, recording the maximum muscle contraction of the Biceps Long Head and Triceps Brachii Lateral. These arms muscles were chosen because they are superficial and easy to pick up. To validate the timing of muscle activation instead of the muscle activity of the Gastrocnemius Medialis during the walk has been recorded.

The tests include the recording of the electrical activity of the muscle, both with the Motion Lab System and with a MITOR board. For the Motion Lab System (MLS) the MA-411 preamplifier probe (figure 6.2a) has been used. These probes



Figure 6.2: a) Motion Lab System probes MA-411, b) Covidien Mini Electrode for MITOR board.

are fast binding to the surface of the muscle. They do not require the use of gel. Between the two exploding electrodes is a ground reference electrode. The probe characteristics are shown in the table.

Table 6.2: MA-411 EMG Preamplifier probe Specification [55]

<i>Sensor Contact</i>	2 12mm disks
<i>Reference Contact</i>	13 x 3mm bar separating the sensors
<i>Inter-electrode distance</i>	20mm
<i>Signal Bandwidth</i>	20Hz to 3,500Hz (-3dB)
<i>Input Protection</i>	ESD protected
<i>Gain</i>	at 1 kHz x20 ±1%

For the MITOR system, *Covidien*[®] mini electrodes (figure 6.2b) with a sensor contact diameter of 1.4mm were selected. The probe and electrodes were placed in the same place and ensuring the same (or almost) inter-electrode distance. For both systems the sEMG signal was recorded with a frequency of 1kHz (1 sample per ms).

6.2 Validation Results

SNR Comparison

The quality of the sEMG signal recorded by the board of the MITOR system was compared with that recorded by the Motion Lab System using SNR. This value gives quantitative information on the reliability and clarity of the recording signal. Depending on the type of signal and noise SNR is calculated in different ways. When signal and noise are processes, the SNR is calculated by the following formula:

$$SNR = \frac{P_s}{P_n} \Rightarrow SNR_{dB} = 10 \times \log_{10}\left(\frac{P_s}{P_n}\right) \quad (6.1)$$

P_s is the power of the signal and P_n is the power of the noise.

In the case of EMG, it is not possible to separate the signal from the noise, as both are random processes with similar characteristics. In this case, it is necessary to distinguish a part in which there is only noise and in which there is muscle activation + noise. The SNR is then calculated as follows:

$$SNR_{dB} = 10 \times \log_{10}\left(\frac{\sigma_1^2}{\sigma_2^2}\right) \quad (6.2)$$

σ_1^2 and σ_2^2 are the standard deviation are the standard deviations of the signal + noise and only noise respectively.

The SNR was calculated on the sEMG signal generated by the maximum voluntary contraction of two arms muscles (Biceps Long Head and Triceps Brachii Lateral). The following figures 6.3 show the sEMG signals recorded with the two systems for the two muscles. The SNR values obtained are shown in the table 6.3.

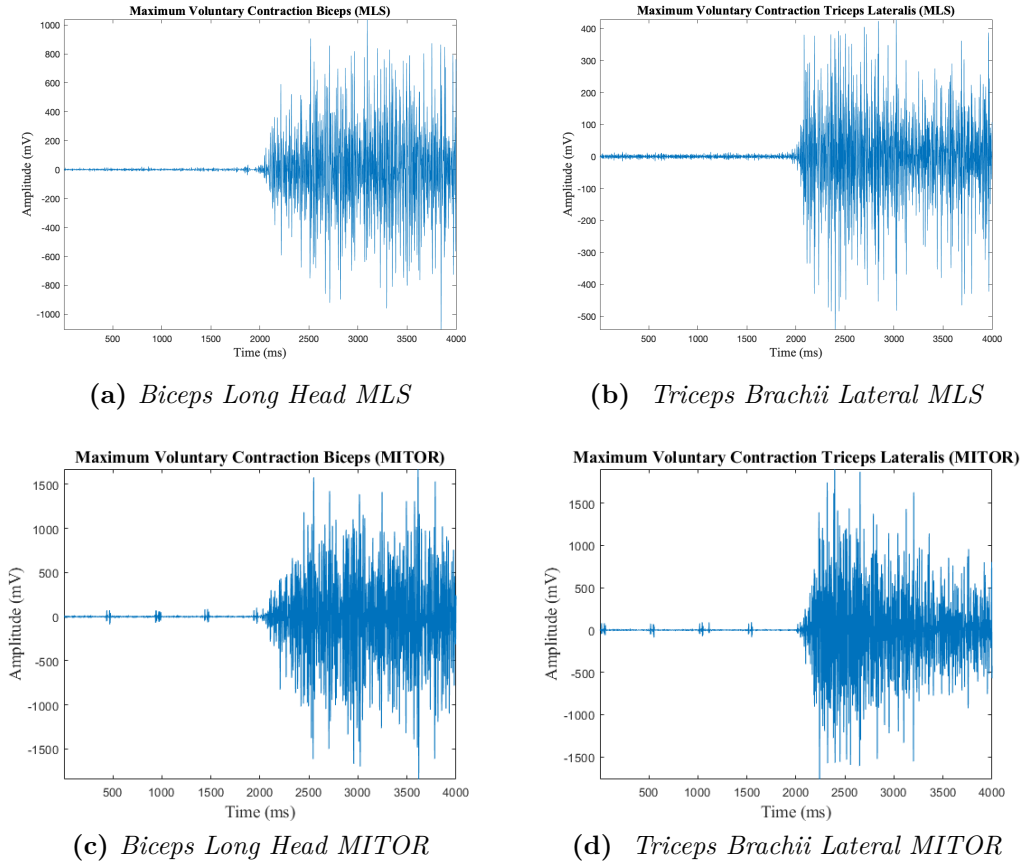


Figure 6.3: Signal recorded during maximum voluntary contraction of: a)Biceps Long Head by Motion Lab System; b)Triceps Brachii Lateral by Motion Lab System; c)Biceps Long Head by MITOR system; d)Triceps Brachii Lateral by MITOR system

Table 6.3: SNR values calculated in maximum voluntary contraction of muscles of Upper Limbs recorded by Motion Lab System and MITOR system

Muscles	SNR (dB)	
	<i>MLS</i>	<i>MITOR</i>
Biceps Long Head	33.77	32.82
Triceps Brachii Lateral	32.34	30.27

The calculated SNR values show that the MITOR system are able to record a signal with competitive quality.

Time Activation

The timing sensitivity of the MITOR system has been compared with that of the Motion Lab System. For this test, the Gastrocnemius Medialis activity was measured during the gait. An insole equipped with an FSR was used to identify the beginning and end of each step. This makes it easier to determine whether the two systems are recording activation at the same time. Moreover, this test is useful to understand if the two systems record coherent signals between them. The two signals were compared by calculating the zero-lag cross-correlation between the envelopes of the signals recorded with the two systems. Considering 10 different steps a cross-correlation of $98.63\% \pm 0.82\%$ has been obtained. Figure show an example of signal recorded by the two different system.

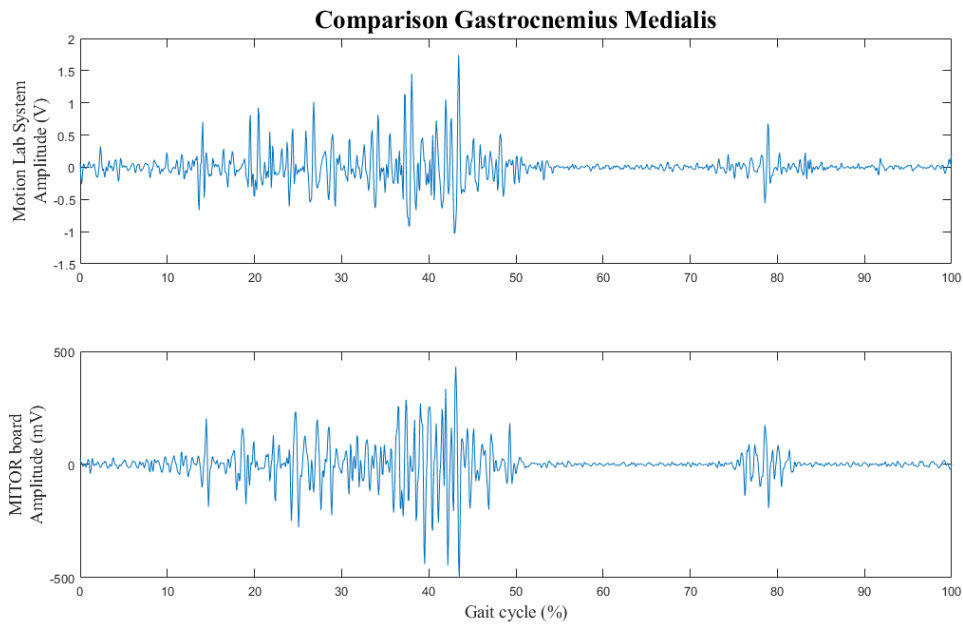


Figure 6.4: Comparison between the sEMG signal from Gastrocnemius Medialis recorded by Motion Lab System and by MITOR system during the gait.

Chapter 7

Electrical Characterization

7.1 Power Consumption

The power consumption of the developed device is tested measuring the input current that flows from the supply battery to the input of the PCB. To calculate this current, the best option would be using a current probe but unfortunately, that on the lab has a resolution of 100mV/1A that is not appropriate to analyze current of a few dozen mA. For this reason, the supply current is performed indirectly, by measuring of the voltage drop of a test resistor set in series on the supply line. The smallest resistor available ($1.2\Omega \pm 5\%$) is chosen so that the voltage drop is not too big for the rest of the board. To measure this voltage drop on the test resistor, an oscilloscope (TEKTRONIX[®] *MSO3034*) is connected in parallel as shown in figure 7.1.

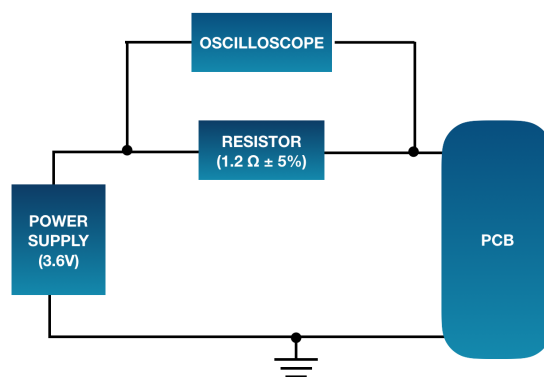


Figure 7.1: Block diagram of the power consumption test connection.

During the test, the board is supplied by an external voltage generator at 3.6V

and the power consumption is tested on the three different working modes that the developed board offers: sEMG, Envelope, ATC.

Moreover, the software TEKVISA[®] (TEKTRONIX[®]) is used in order to retrieve on PC, the measured data by oscilloscope. The data is saved in a file *.svg* in which there is all the information available on the oscilloscope screen (vertical and horizontal scale, offset, source, probe attenuation. . .). The software saves the data to guarantee a fixed number of the sample (10^6) and so it uses a sampling frequency of $10^6 / (10 \times \text{horizontal scale})$. In the denominator, there is 10 because this is the number of time-division on the oscilloscope.

MATLAB[®] is used to convert the voltage information in supply current that the boards need to work correctly. To do this, the law's Ohm is applied using the real resistance value.

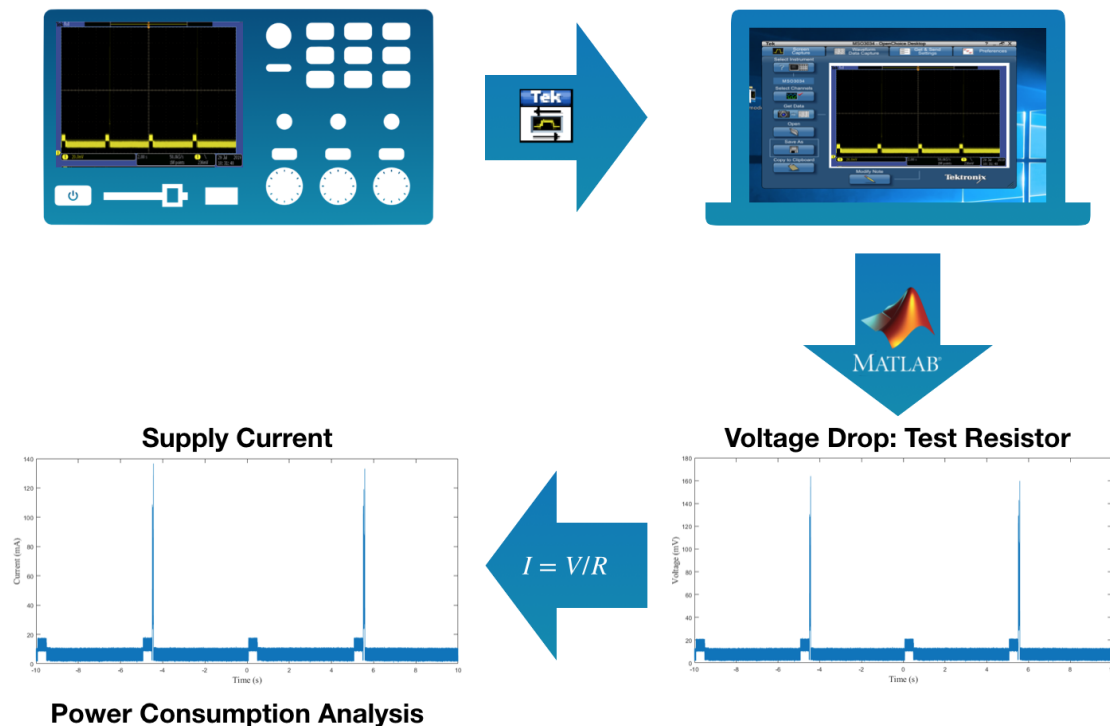


Figure 7.2: The scheme shows the necessary steps to obtain current information from the detection of voltage drop by oscilloscope.

In figure 7.3 are shown the results about the current supply required by the board in three different working mode, during the recording of real data. The board's firmware is set to have a synchronization period of 5s, so for this reason, in the graphs, there are little variations on the baseline that defining when the

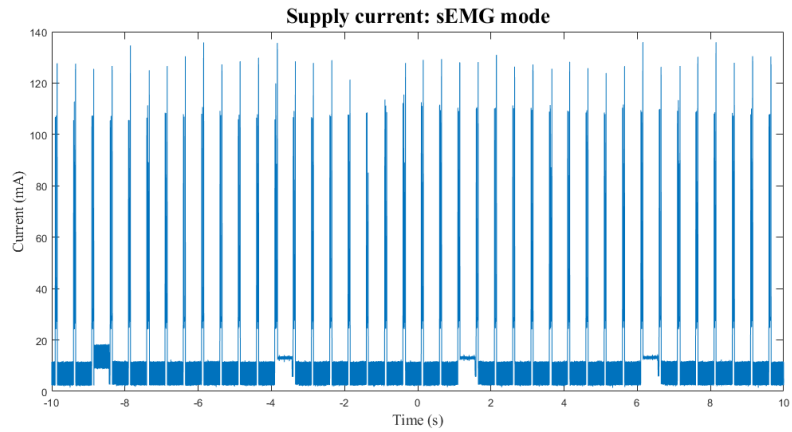
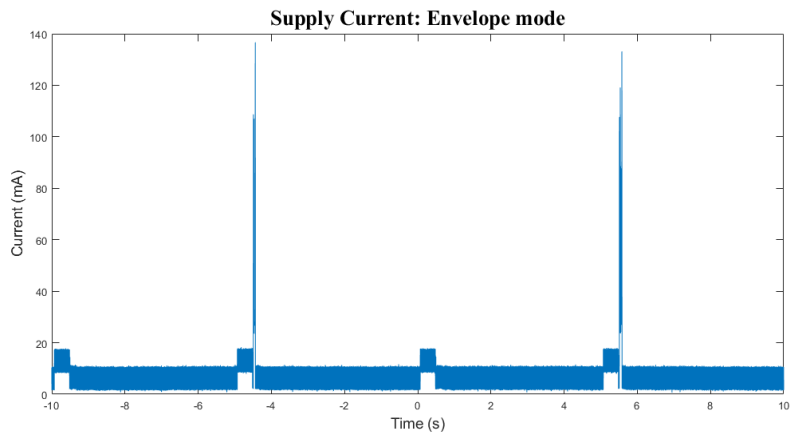
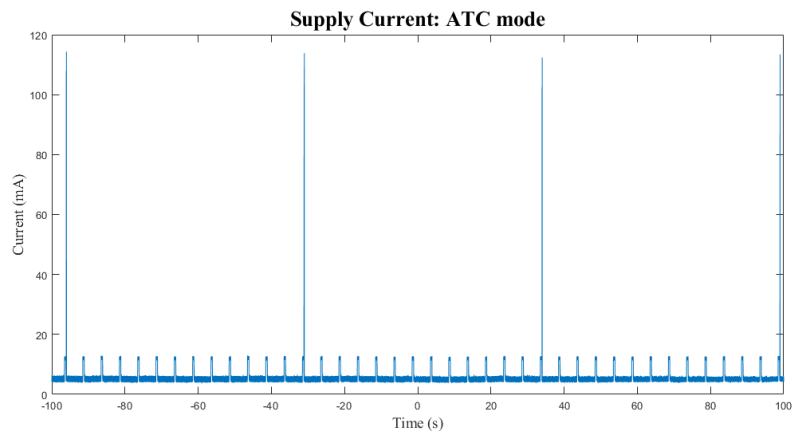
(a) *sEMG*(b) *Envelope*(c) *ATC*

Figure 7.3: The figures shown the current supply required by the PCB, in cooperatively condition, during three different working mode: a) sEMG signal, b) Envelope of sEMG, c) ATC parameter.

Antenna switches to RX mode to wait for the synchronization trigger. The synchronization period has a little impact on consumption, in fact, if this time change from 5s to 25s, there is a saving, in term of consumption of $< 3\%$.

Instead, the main cause of power consumption is the high picks of currents that correspond to the storage in the μ SD card. Two features were analyzed to understand the consumption of the data storage: the height of picks and the frequency. Regarding frequency, the board has a buffer length 500, and only when this buffer is full the data are saved. The voltage picks are much more common in n sEMG mode because the board adds one sample to the buffer each 1ms (ADC sampling of 1kHz), and so, for this reason, there is a pick each 500ms. Instead in envelope mode, the data are saved each 5s due to firmware filter operation to obtain the signal. The ATC mode is the lowest power consumption mode because the storage is each 65s (with an ATC window of 130ms because of $length\ buffer \times windows\ size = 500 \times 130ms$) and also this technique does not require the conversion of the ADC. Moreover, the height of the picks depends on the amount of bit 1 that is written in the μ SD card, because in flash memory (like the SD card family) saving 1 is more expansive, from the required current point of view, than bit 0. For this reason, the amplitude of the picks is different from one storage and the other also in the same working mode.

In table 7.1, the mean value of the current supply required by the board are given. This value is essential to choose the correct battery to supply the system.

Table 7.1: Current consumption test on three working modes

Working mode	Current Consumption (mA)
sEMG	10.56
Envelope	6.48
ATC	5.65

7.1.1 Comparison With Other Devices

Usually, a commercially available device uses a battery with a capacity of 150-450mA/h and it allows a continuous recording of 8-12 hours of sEMG signal. The developed device, with a battery of 150mA/h, can store data for more than 14 hours and more than 42 hours with a battery of 450mA/h. So from a power consumption point of view, the MITOR device V3 is competitive with the other device in commerce, especially if used in ATC mode too long term analysis (>26 hours with a battery of 150mA/h or >79 hours with 450mA/h).

In table 7.2, a comparison of consumption on the three different working mode between the developed version and the previous (MITOR version 2 [29]) are given. So this new board, in terms of consumption, consume more than 20% less compared to the previous version.

Table 7.2: Current consumption comparison with previous version

Working mode	Current Consumption (mA)	
	<i>Previous Version</i>	<i>Actual Version</i>
sEMG	14.0	10.56
Envelope	7.9	6.48
ATC	7.3	5.65

7.1.2 ATC consumption: Hardware VS Firmware

Table 7.3: Current supply comparison between the two different way to detect the TC signal

Working mode	Current Consumption (μA)
Hardware	210
Firmware	300

How amply discussed in the previous chapter, this third new version of the MITOR system is catheterized by the detection of the TC signal by the hardware component. This choice allows to have a simply firmware to manager the TC signal but requires the other two additional components in the acquisition channel compare to the previous version. The current consumption is analyzed to understand if this new way to detect the TC leads to an increase in consumption. To do this test, the firmware is modified in order to obtain the TC signal both directly like the output of the acquisition channel as like results of the comparison between the ADC conversion of the sEMG and a software threshold. For each mode, 5 sessions of 2 minutes of the recording are done and the mean current consumption is compared. The result is that the part of firmware that use the ADC and compare the sample with a value to understand if the signal is above or below the threshold add a power consumption of 300 μA . This value is greater of the maximum current consumption caused by the two additional hardware components, calculated from the components' datasheet. So even if only a little, the new way to detect the

ATC involves also a reduction of power consumption. Table 7.3 shows the additional current supply required to implement the TC signal detection in hardware or firmware.

7.2 Impedance Measurements

Table 7.4: Measured impedance of line of the acquisition channel and of supply track

	Impedance (Ω)
Acquisition channel	14×10^6
Supply track	0.9

Table 7.4 shows two impedance values measured thanks to the use of a multimeter. The acquisition channel impedance has been measured by connecting one probe of the multimeter to an exploding electrode and the other to the reference electrode. The measured value is consistent with the expected value (given the presence of the instrumentation amplifier on the channel).

The impedance on the power line was measured downstream of the generator. This was measured to verify the presence of possible voltage drops on the supply track. This value should be as small as possible. The average current required by the circuit varies between the range 5.6mA - 10.6mA (according to the results in the table 7.1 (section 7.1)). Considering these values, in the supply line, there is a drop of 5mV - 9.5mV. This range of values does not cause problems to the power supply of the circuit components.

7.3 Potential Risk

The technical specification IEC 60-479-1 "Effect of Current on human being and livestock" [56] provides basic guidance on the effects of shock current on human beings and livestock, for use in the establishment of electrical safety requirements. It is necessary to check if the developed device can release enough current on the body to cause damage. As shown by the figure the danger of the current depends not only on the intensity of the current but also on its time of application. The graph is composed of 4 areas of increasing danger proceeding from left to right.

- **Zone AC-1:** Total safety;
- **Zone AC-2:** Perceptible but without physiologically dangerous effects;

- **Zone AC-3:** Reversible effects: muscle reaction;
- **Zone AC-4:** It is divided into 4 zones where the probability of irreversible effects changes (ventricular fibrillation).

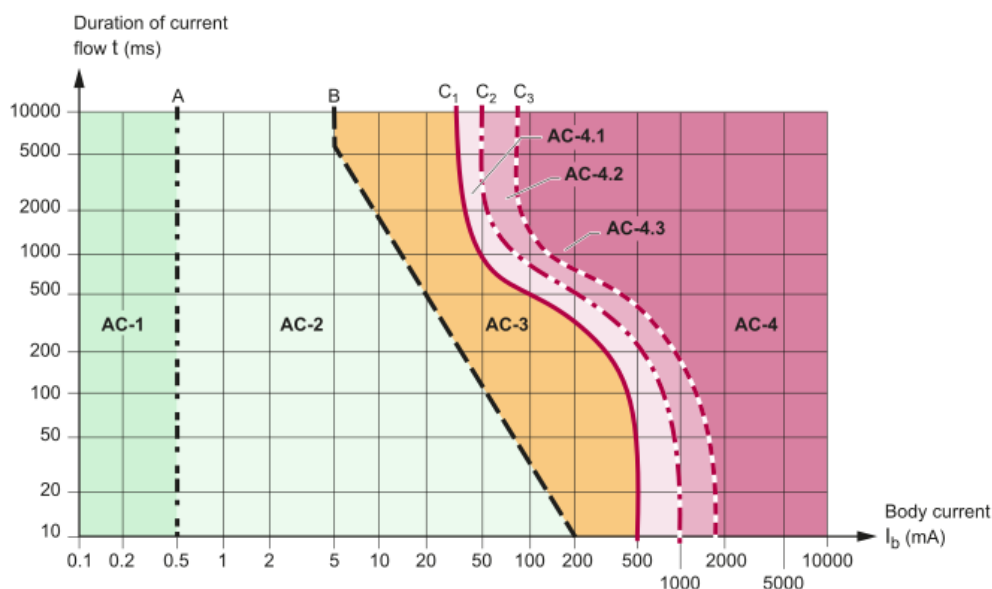


Figure 7.4: Zone time/current of AC current on human body (hand-hand).

The threshold values shown on the graph refer to a hand-hand (or hand-foot) path of the current. There are multiplying constants that are used to adapt this graph to other possible current paths.

To establish protection against electric shocks, it is necessary to limit the touch tension. This depends on the impedance of the body which varies greatly depending on many conditions (skin wetness, contact surface size, current path, etc).

For the designed device, the supply voltage is 3.6V. The device is connected by two electrodes to the body of the human subject. Assume electrodes with a not very high impedance (worst case) of 220Ω. During the tests, the skin is clean with alcohol so it has a reasonable impedance value of 10kΩ. This value drops drastically if the skin is wet or sweaty (1kΩ). The total skin impedance is 1440Ω, in the worst cases. Considering only purely resistive components the maximum current that can flow is equal to 2.5mA. This value, referring to the figure, corresponds to the beginning part of zone AC-2. In a state of normal operation, the current would be in zone AC-1.

Chapter 8

Muscles Synergies Analysis

8.1 Gait Analysis

The gait is the shortest task repeatable during human locomotion. The gait analysis is performed by monitoring and measuring body movements, body mechanics and skeletal muscle activity. The study of the EMG signal allows evaluating the health status of each muscle. It is, therefore, possible to evaluate which conditions affect the ability to walk, particularly for subjects suffering from neuromuscular disorders. The physiological gait cycle (also called stride) is the timing between two different steps. Each cycle is composed by two phase: *Stance* and *Swing*. The stance phase is the period in which the foot is, whole or in part, in contact with the ground. The swing phase begins with the toe-off and is the air phase that allows the body advancement. Figure 8.1 shows all the several phases that compose a single gait cycle. The stance phase is approximately the 60% of the gait cycle, however, the

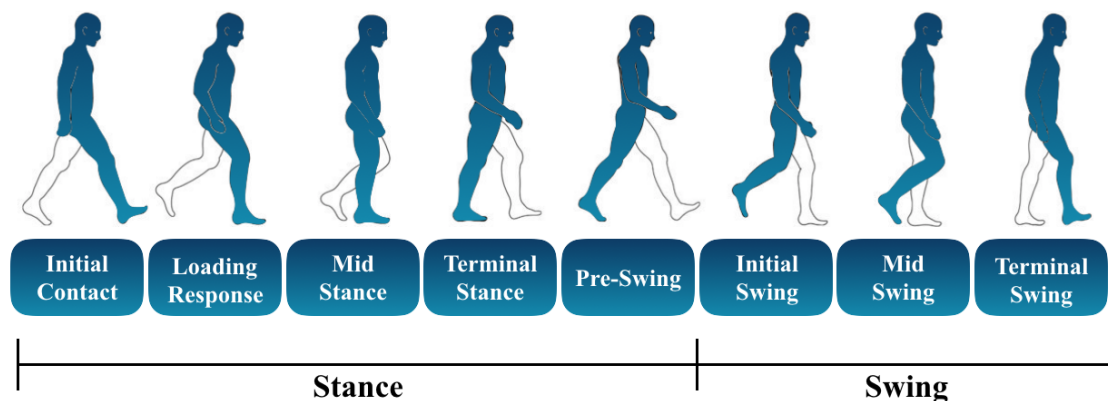


Figure 8.1: Mains phases during gait cycle.

swing phase is the other 40%. Only the 20% of gait cycle (Initial Contact and Pre-swing) is a double support. This means that both the lower limb touch the floor. All the other phases are a single support.

Moreover the terminal stance and the pre-swing take also the name of push off phase.

During the gait, the limb achieve three main task (*Weight Acceptance*, *Single Limb Support* and *Limb Advancement*)[57].

Weight acceptance

- **Initial Contact**

This phase 1 happens in the 0-2% of the gait cycle. It begins when the heel touches the floor, occurs hip flexion and knee extension.

- **Loading Response**

This phase is at the 2-12% of the gait cycle. This phase 2 ends when the other foot is in swing phase. During this movement all the weight is transferred to the forward lower limb. The hip is fixed to increase the stability and the knee is in shock absorption position.

Single Limb Support

- **Mid Stance**

In this phase 3, at 12-31% of the interval of the gait cycle the body stability increase.

- **Terminal Stance**

The phase 4 (31-50% of gait cycle) is the moment of body progression beyond the supporting foot. This

Limb Advancement

- **Pre-Swing**

This phase 5 takes place in the range 50-62% of gait cycle. In this position This position is characterized by toe off.

- **Terminal Stance**

In the phase 6 (62-75% of gait cycle) the foot does not touch the floor and hip flexion helps to advance the limb. This is the begin of the acceleration part.

- **Mid-Swing**

In 75-85% of gait cycle the limb advance. This movement is accomplished by hip flexion and knee extension in response to the gravity.

- **Terminal Stance**

This is the last part of the gait cycle (87-100%). This is a deceleration phase in which the limb advancement finishes by the knee extension

8.2 Materials And Methods

8.2.1 Muscle Selection

The final aim of the 'in-vivo' test is extract and study the muscle synergies during the gait. To do this, 10 muscle (distal and proximal) of the lower limb were selected with the help of a physician. The figure 8.2 shows which muscles were selected and how the electrodes were placed. For each selected muscle, the description of

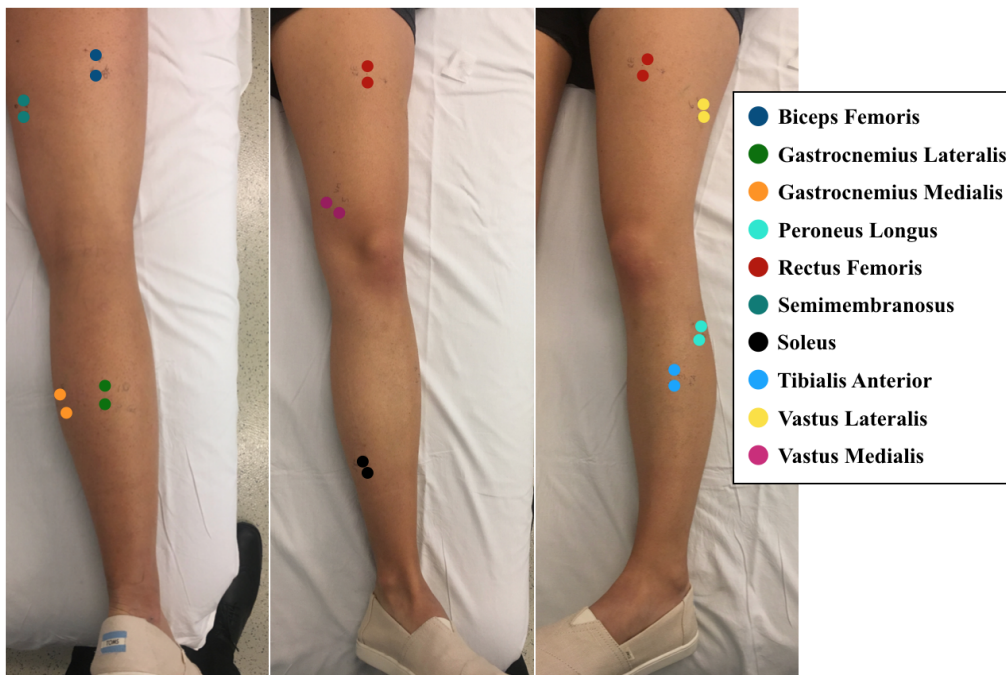


Figure 8.2: Bipolar electrodes placement scheme (lower limb).

muscle activity [57], the correct position, and orientation of the electrodes have been analyzed.

Biceps Femoris (BF)

- **Activation:** The BF is part of the lateral hamstring. These muscles are activated in the second half of the swing phase. Their function is to decelerate hip flexion and knee extension. Also, there is an activation at the beginning of the step (first half of the position phase) as an antagonist of rectus femoris.
- **Location:** Electrodes need to be placed at 1/2 on the line between the ischial tuberosity and the lateral epicondyle of the tibia.
- **Orientation:** In the direction of the line between the ischial tuberosity and the lateral epicondyle of the tibia.

Gastrocnemius Lateralis (GL)

- **Activation:** The Gastrocnemius is a knee flexor distal muscles. The contraction of this muscle begin at the initial contact and finish with the end of the Stace phase.
- **Location:** Electrodes need to be placed 1/3 of the line between the head of the fibula and the heel.
- **Orientation:** In the direction of the line between the head of the fibula and the heel.

Gastrocnemius Medialis (GM)

- **Activation:** The GM has the same activation pattern of the Gastrocnemius Medialis.
- **Location:** Electrodes need to be placed on the most prominent bulge of the muscle.
- **Orientation:** In the direction of the leg.

Peroneus Longus (PL)

- **Activation:** The PL is a Ankle plantar flexor muscle. The muscle activation starts after the Gastrocnemius and it ends in the terminal Stace.
- **Location:** Electrodes need to be placed at 1/4 on the line between the tip of the head of the fibula to the tip of the lateral malleolus.
- **Orientation:** In the direction of the line between the tip of the head of the fibula to the tip of the lateral malleolus.

Rectus Femoris (RF)

- **Activation:** This muscles has as an activation among the end of pre-swing and the begin of the initial Swing. In this pattern the RF have a double task: Knee Extensor and Hip Flexor. Moreover at the begin and at the end of the gait cycle the RF is active to stabilize the knee.
- **Location:** Electrodes need to be placed at 1/2 on the line from the anterior spina iliaca superior to the superior part of the patella.
- **Orientation:** In the direction of the line from the anterior spina iliaca superior to the superior part of the patella.

Semimembranosus (SM)

- **Activation:** This muscle, as the Biceps Femoris, is an Hamstring.
- **Location:** Electrodes need to be placed at 1/5 on the line between the ischial tuberosity and the popliteal fossa.
- **Orientation:** In the direction of the line between the ischial tuberosity and the popliteal fossa.

Soleus (SO)

- **Activation:** The SO is a ankle plantar flexor muscle with the same pattern of the Gastrocnemius.
- **Location:** Electrodes need to be placed 2/3 of the line between the medial condylis of the femur and the medial malleolus.
- **Orientation:** In the direction of the line between the medial condylis to the medial malleolus.

Tibialis Anterior (TA)

- **Activation:** Its Activity starts at the toe off and continue during all the swing phase. Also at the begin of the stance phase there is a TA activation due to hell strike. This activation ends when the foot is entirely in contact with the ground.
- **Location:** Electrodes need to be placed at 1/3 on the line between the tip of the fibula and the tip of the medial malleolus.

- **Orientation:** In the direction of the line between the tip of the fibula and the tip of the medial malleolus.

Vastus Lateralis (VL)

- **Activation:** In general the Vasti is Knee extensor muscle. For this reason the activation of the VL starts during the terminal swing and it reaches its maximum at the begin of the gait cycle.
- **Location:** Electrodes need to be placed at 2/3 on the line from the anterior spina iliaca superior to the lateral side of the patella.
- **Orientation:** In the direction of the muscle fibers.

Vastus Medialis (VM)

- **Activation:** The VM has the same pattern of VM.
- **Location:** Electrodes need to be placed at 4/5 on the line between the anterior spina iliaca superior and the joint space in front of the anterior border of the medial ligament.
- **Orientation:** Almost perpendicular to the line between the anterior spina iliaca superior and the joint space in front of the anterior border of the medial ligament.

Figure 8.3 shows the main activation patterns of the selected muscles.

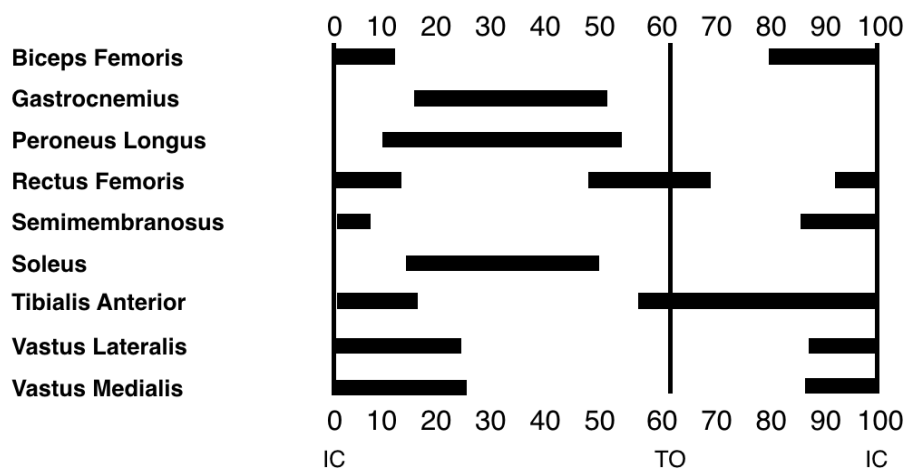


Figure 8.3: Timing of muscle activity during normal gait (draw up by [58]).

8.2.2 Data Collection Protocol

For collect the data during a normal gait, a health subject (Female, 23 years old, 58Kg) has been recruited. The data collection has been done at the Motion Analysis Laboratory at Spaulding Rehabilitation Hospital, Harvard Medical School.

Both legs of the subject were analyzed but with two different setups. The sEMG signals of the left leg muscles were recorded using the Motion Labs System. For the right leg instead, the boards designed were used to record 6 muscles (BF, GM, RF, SM, SO and TA), and to complete the setup the other available channels of the MLS were integrated. During the gait is important to understand the moment in which a new gait cycle begins and ends. So for this reason, two pressure sensors (one for limb) were added to the setup. The right pressure sensor was common to both the system (MITOR and MSL) and was used to synchronize the two systems. The FSRs were fixed on the insoles of the shoes.

In addition to connecting probes and sampler electrodes, MITOR board reference electrodes have also been placed in predominantly bony parts such as the ankle, knee or iliac crest. After the placement of the probe, the legs were wrapped to prevent detaching of the electrodes. This bandage was made in such a way as not to affect the gait.

6 different recordings were made each consisting of at least 10 useful steps (the first and last steps were excluded). For each recording session, the sEMG signals of both legs were measured.

During the data collection, the subject was asked to walk straight, keeping a regular and steady pace.

8.2.3 Initial processing

Both the systems are a sampling frequency of 1kHz. A pre-processing is necessary for two reasons: to synchronize the two systems in the right leg and to filter the signals so that they have the same frequency components. In the figure 8.4 is shown the block diagram of the preprocessing operations. The MSL during the data collection recorded 14 sEMG channels (10 for the left leg and 4 for the right leg), FSRl (left foot pressure sensor) and FSRr (right foot pressure sensor). The MITOR system, made up of 6 boards, recorded 6 sEMG signals and the FSRr signal.

In the section on synchronization (subsection 5.2.1), the need for pre-processing was introduced to synchronize MITOR boards. This is, in fact, the first step of pre-processing for MITOR signals. To synchronize the two systems the common signal FSRr has been used. While the FSRr signal recorded by the MITOR device takes

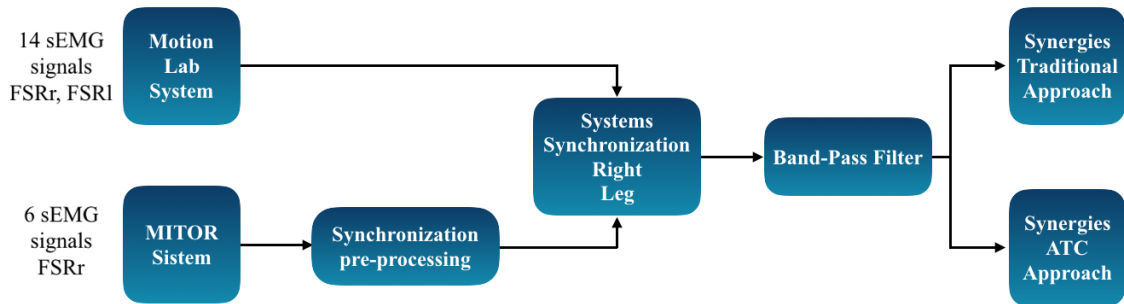


Figure 8.4: Data collection signals pre-processing flowchart.

0 or 1 values, the one acquired by the MSL is a converted signal with ADC (range $\pm 5V$). To compare the two signals the MAL FSRr has been quantized by setting a threshold equal to its mean value. The value 1 was assigned to the above-threshold signal (sensor pressed), 0 to the below-threshold signal (sensor not pressed). The choice of these logical levels is the same as that used by MITOR boards. In this way, the systems are synchronized with maximum misalignments of 2 samples.

Using the FSRr signal, the sEMG signals have been cut and have been rearranged (the first signal of the right leg corresponds to the signal of the same muscle in the left leg). The last step of pre-processing was to filter all the signals (to have the same frequency band). The two systems have different acquisition channels with different filters, so in order to have the same spectral frequency component, the sEMG signals of both systems have been filtered with a Butterworth filter of order 10 with a band passing between 30Hz and 300Hz according to a typical sEMG power spectral density.

At this point, it is possible to proceed with the extraction of muscle synergies in two possible approaches. The classic approach involves the use of the sEMG signal development, while the ATC approach requires the use of the average envelope of ATC signals.

8.3 Traditional Approach

The traditional approach to extract muscle synergies involves following the steps shown in the figure 8.5.

With the use of FSR signals, each channel is segmented. The first and last steps have been removed as they are not descriptive of the gait cycle. Also, abnormal steps for muscle activation or incorrect functioning of the pressure sensor (remained active even during the swing phase) were eliminated. Made this skimming of the

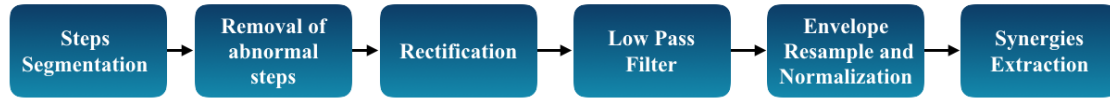


Figure 8.5: Block diagram of traditional synergies extraction method.

data, the residual sEMG signal has been rectified. To get the envelope a low pass Chebyshev filter at 10Hz was used. Each envelope has been resampled to 1000 samples, to have all the steps with the same time length. In addition, each envelope has been normalized to its maximum value. The envelope matrix has been created and given as input to the *nnmf* function of MATLAB[®].

This operation was performed for both the 10 signals of the right leg and those of the left leg. Synergies were extracted from both legs to show that replacing part of the MSL channels with MITOR boards does not change the results. This can also be considered as an additional validation test of the MITOR system.

As mentioned in subsection 1.5.1, the *nnmf* function requires as input the envelopes and the number of synergies to be extracted. For both legs, the smallest k value is chosen, with an R^2 mean $>85\%$ and an R^2 for each channel $>70\%$. In both cases, the optimal value was 4. This result is consistent with the number of channels and the type of muscles taken. Figure 8.6 show the R^2 values obtained with a number of 4 synergies for both the legs. In general, in literature, there is a number of

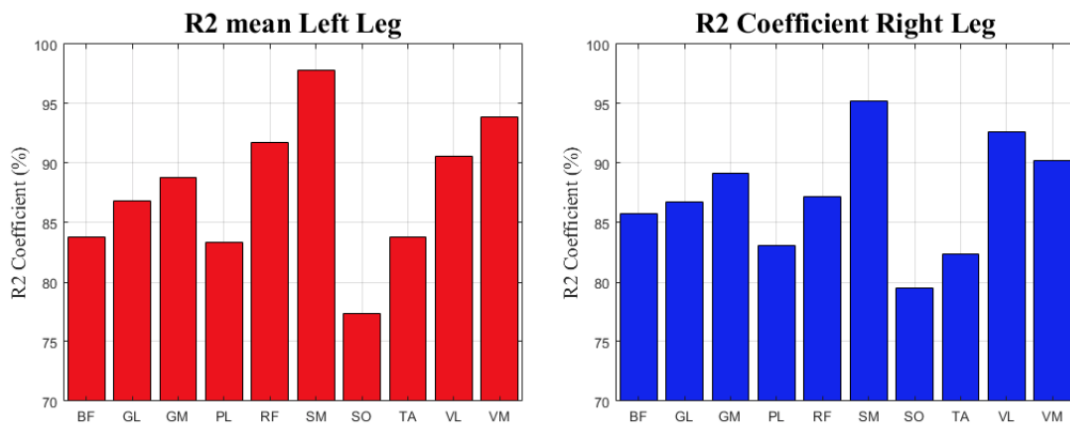


Figure 8.6: Comparison between original envelope and *nnmf* reconstructed envelope (using R^2).

synergies between 4-6 ([11] [14] [26]).

The figure 8.7 shows the outputs of *nnmf* function obtained from the left leg (only

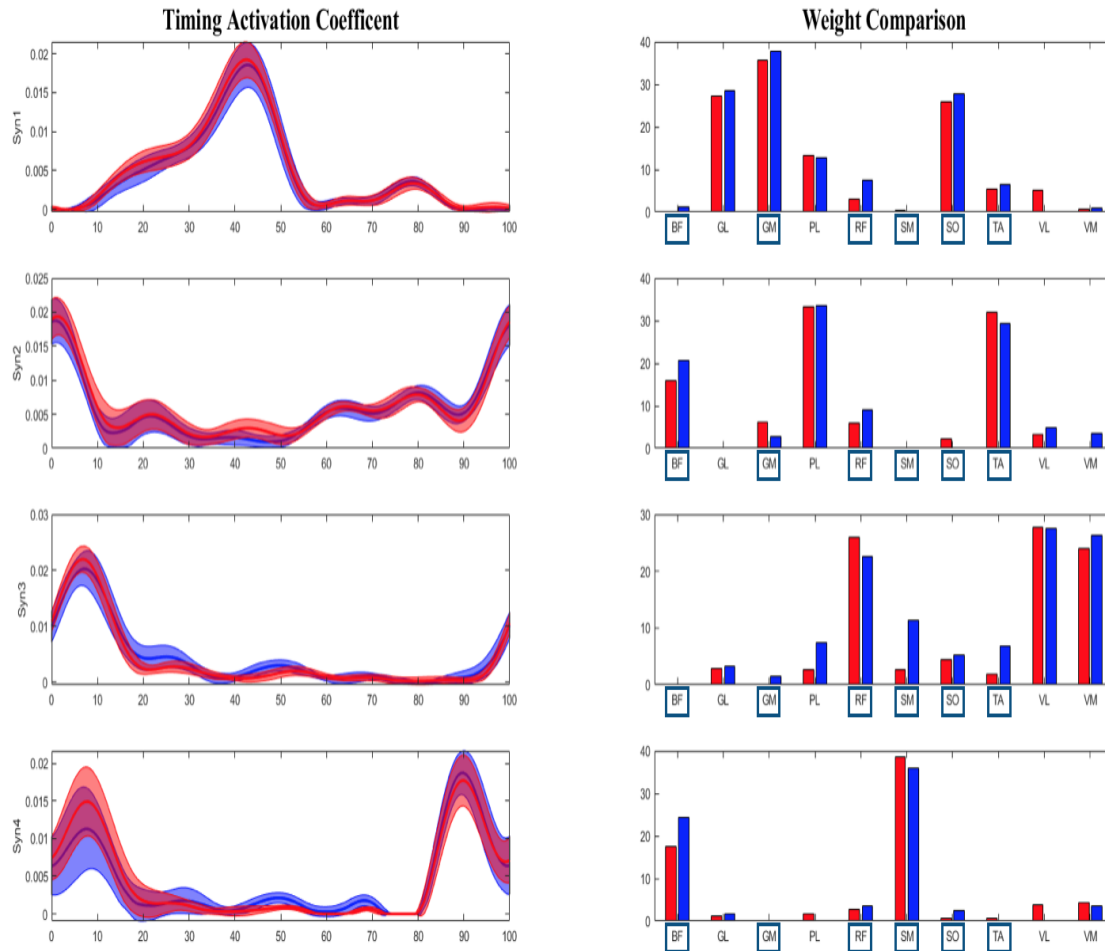


Figure 8.7: Extracted Synergies during the gait Left leg (red: MSL) Vs Right leg (blue: MITOR+MSL).

MSL in blue) and the right leg (MSL and MITOR in red).

The H matrix obtained from the *nnmf* presented the temporal activation of all the steps analyzed (20) in series. The graph was obtained by calculating the mean and the standard deviation of the multiple-step cycles.

The results visually are very similar. This result shows that replacing the Motion Lab System channels with MITOR boards does not alter the results of synergies. Besides, to obtain quantitative information on the similarity between the two results, *zero-lag cross-correlation* was calculated between the average patterns of time activations. To compare weights was used the *cosine similarity*. Results are shown in figure 8.8.

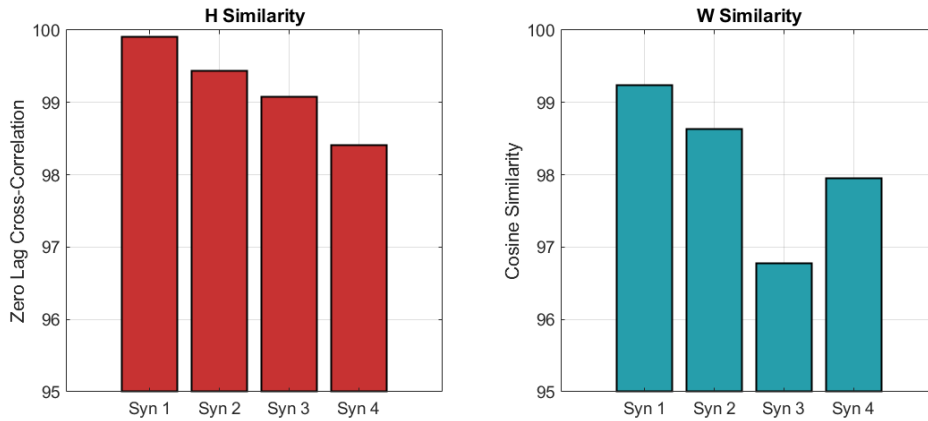


Figure 8.8: *left*) Zero-Lag Cross-Correlation between the time activation of the four synergies of right and left leg; *right*) Cosine Similarity of the synergies weight of the muscles of right and left leg.

The reason why the coefficients are not 100% is due both to the normal variability of the step and to the positioning of the electrodes on the two legs. Doing measurements even with only MLS on both legs is natural not to have two perfectly equal results.

8.4 ATC Approach

The ATC approach to extracting synergies requires a different processing show in figure 8.9.

This technique focuses heavily on enhancing the repeatability of movements. So



Figure 8.9: Block diagram of ATC synergies extraction method.

first, we segment the sEMG signal using the foot pressure sensor. At this point for each gait cycle, the ATC signal is calculated. MITOR boards allow this signal to be obtained directly, while the Motion Lab system does not. So to unify the processing it was decided to calculate the ATC in software. For each signal, the threshold has been calculated using the same algorithm used by MITOR boards (see paragraph 4.2.2). As a time window, according to previous work [11], a window of 50ms has

been fixed. After having obtained the ATC signals of each step these have been re-sampled to have all the same length (20 values) and then mediated to obtain a sort of average envelope calculated on the ATC signal. Before creating the matrix with ATC envelopes, this was normalized. Again the choice of the number of synergies was made in the same way as the traditional approach (using R^2 coefficient). Before proceeding with the extraction of muscle synergies was also analyzed how the average envelope obtained with the ATC is similar to the average traditional envelope of the sEMG signal. These two signals were initially compared using zero-lag cross-correlation. These results are very high, implying that the trends of the two signals are similar. To obtain information also considering the amplitude the R^2 coefficient has been calculated.

In the figure 8.10, it can be seen that all channels have a similarity of more than 75%. For the criteria laid down, this value represents a good reconstruction. Going into detail, the figure shows the example of the comparison of the mean ATC signals and the mean sEMG envelope in the best (SM) and worst (RF) case (figure 8.11). By analyzing the SM signal the classic envelope has the same trend and

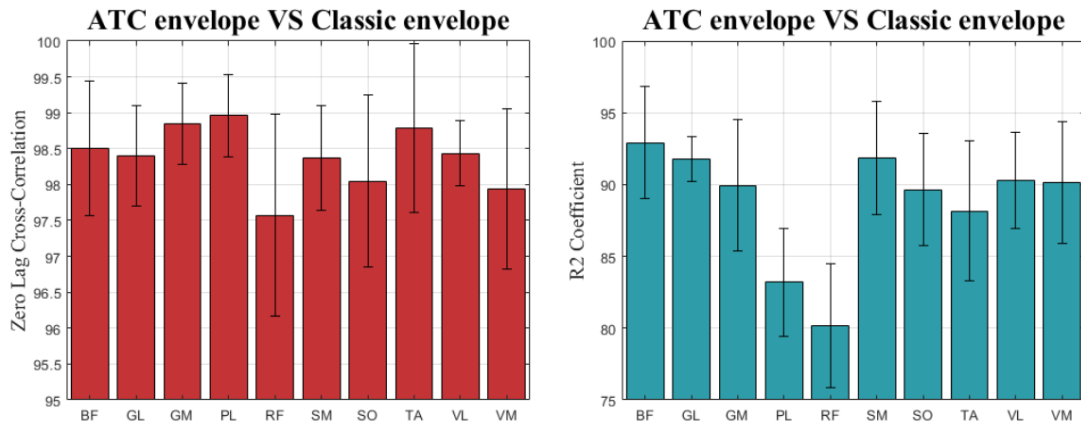


Figure 8.10: Similarity coefficient of classic envelope and ATC envelope.

normalized amplitude as the ATC. So, for this reason, the R^2 coefficient is so high. Instead, in the RF signal, the situation is a bit different. In the complex, the trend of the two signals is the same but they have a different level in the middle of the gait cycle. This difference is caused by the ATC because for technique everything below the threshold is not considered. On the contrary, the traditional envelope also reconstructs the baseline noise that is above the ATC threshold.

his problem, as will be shown later, does not involve problems in choosing the number of synergies and in the course of the temporal activations and muscle weights in the synergies extracted.

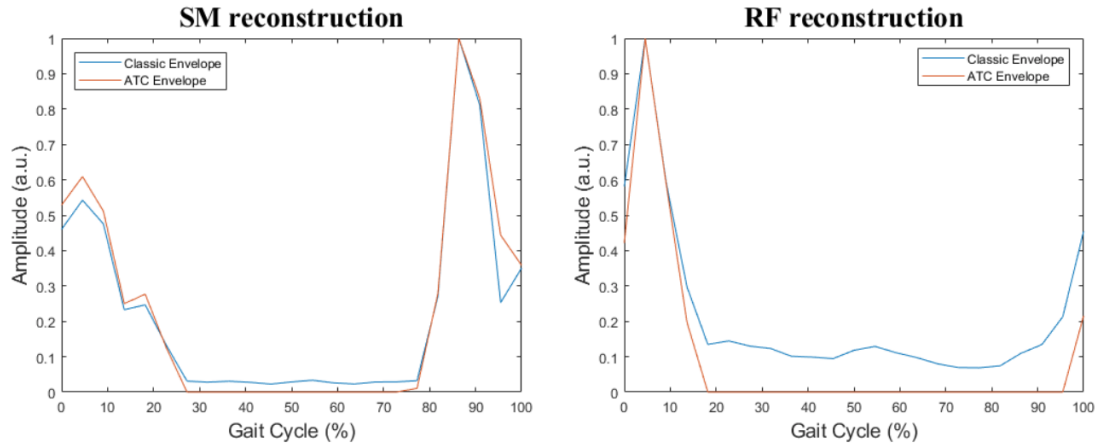


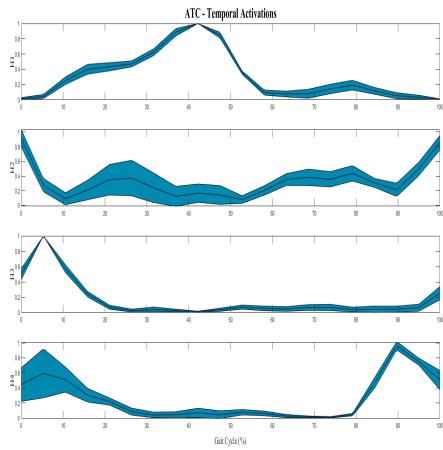
Figure 8.11: Example of ATC envelope Vs Classic envelope.

To test the synergies extraction with the ATC technique, the signals obtained from 6 recording sessions each containing 10 steps are used. From each recording session, an average ATC matrix was obtained which was used as nmmf input. So in total, we got 6 different matrices of time activation coefficients and 6 of weights. The mean and standard deviation of these matrices have been calculated. The results are shown in the figure 8.12 [a and b].

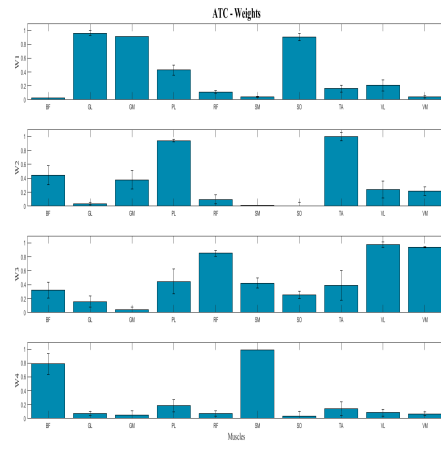
These results were compared with the synergies obtained by the same signals using the classic envelope and not the ATC (8.12 [c and d]).

The temporal activations of the synergies with the ATC are edgier because it is characterized by higher frequency components than the classic envelope. Besides this signal can be smoothed mediating more signals. To obtain similarity coefficients, as in the case of the traditional approach, the temporal activations obtained with classical envelopes have been interpolated to have the same number of points. In this way, it is possible to calculate the zero-lag cross-correlation between the mean temporal activations and the cosine similarity between the mean weights. The results obtained are shown in figure 8.13.

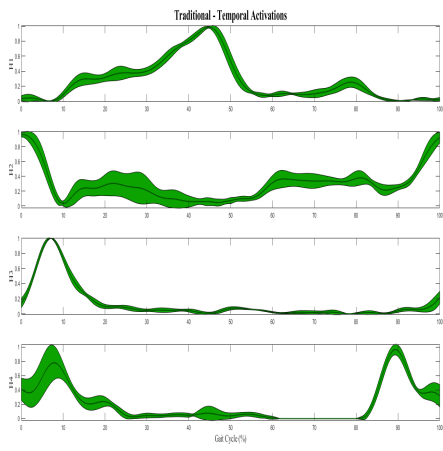
The results in terms of zero lag cross-correlation and cosine similarity have very high similarity. This implies that this intake can be used to give a good description of muscle synergies during the gait.



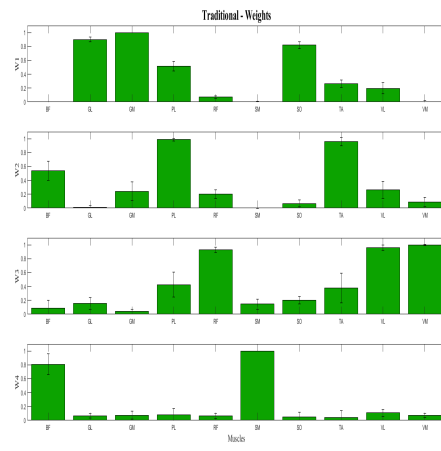
(a) ATC Timing Activation (H)



(b) ATC Weights (W)



(c) Envelope Timing Activation (H)



(d) Envelope Weights (W)

Figure 8.12: a) ATC Timing Activation (H); b) ATC Weights (W); c) Envelope Timing Activation (H); d) Envelope Weights (W).

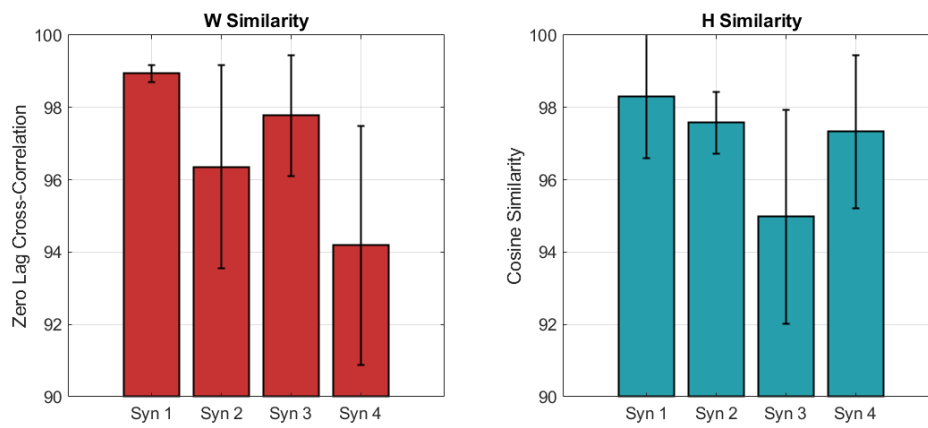


Figure 8.13: *left*) Zero-Lag Cross-Correlation between the time activation of the four synergies of ATC envelope and classic interpolated envelope; *right*) Cosine Similarity of the synergies weight of ATC envelope and classic interpolated envelope.

Chapter 9

Conclusion

The current MITOR system, consisting of 6 wearable boards, allows the monitoring of the sEMG signal with three different recording modes:

- acquisition of the sEMG signal, with a frequency of 1kHz and a resolution of 1mV.
- sEMG signal enveloping through the use of digital filters implemented in firmware.
- ATC signal, obtained by counting the number of events in the time unit (time window) generated by the hardware comparison between the sEMG signal and a threshold.

Particular attention was paid to testing ATC mode. The algorithm created to select the threshold works correctly positioning the threshold value very close to the signal baseline.

Boards work synchronously with an average delay of 10 μ s with a synchronization window of 5s. This allows the MITOR system to be used for long-term analysis without being affected by meter drift that would cause delays that would invalidate the analysis.

Besides, 20% energy savings were achieved by optimizing the choice of components and updating the microcontroller compared to the previous version. With a battery of 450mA/h, the system can record for 42 hours continuously the raw sEMG signal or for 80 hours the ATC signal.

The MITOR system has been validated using an EMG acquisition system on the market, the Motion Lab System. The signals recorded with both systems during a maximum voluntary contraction of arms muscles were compared in terms of SNR.

The values obtained are very high $>30\text{dB}$ with both systems and differ by a maximum of 2dB .

Mixing the MITOR system with the Motion Lab System, a hybrid system with 10 channels has been developed to carry out a study on muscle synergies during the journey. To validate the results, muscle synergies have also been obtained using the Motion Lab System only. The results show a zero-lag mean cross-correlation of $99.18\% \pm 0.59\%$ between the temporal activations of the synergies obtained with the two systems, and average cosine similarity between the weights equal to $98.20\% \pm 0.84\%$. Such values are consistent with the normal variability of the step.

A different approach has been tested to derive muscle synergies, using the classic sEMG signal envelope, but using the average envelope obtained by the ATC signal. To assess performance, synergies with ATC were compared with synergies extracted by the traditional method. Such synergies show a zero-lag cross-correlation of the activations time equal to $96.9\% \pm 1.94\%$ and a cosine similarity between the weights equal to $97.3\% \pm 1.40\%$.

These results show that the ATC approach is valid to extract muscle synergies on repetitive movements such as gait analysis. The limit of the approach with the ATC signal is right the need to have repeatability in the movements. This technique cannot be used (with the algorithm proposed in this thesis) on grasping exercises where for example there are so many degrees of freedom and little repeatability. As a result of the tests, it has been shown that the design specifications set out in the design part have been respected.

Chapter 10

Future Steps

The MITOR project is being developed so it is needed to define the possible future steps: those related to hardware and firmware changes and search for future applications.

As for the design of the boards, the future version should have smaller dimensions to make it easier to position the boards on the body of the subject during sEMG signal recording. It would, therefore, be appropriate to create a multi-layer structure of the PCB, taking care to maximize the mechanical stability of the device. As a result of the problems found on the inrush current that generates the peaks of tension during writing on the μ SD card, it is necessary to study in detail this phenomenon and improve the circuit of conditioning of the μ SD card.

One should introduce a way to have an adjustable gain in the amplification chain to enhance also muscles with low muscle activations.

To have an eco-friendly device, a charging circuit should be introduced so that rechargeable batteries can be used and the use of single-use batteries avoided.

An innovation to the system would be introduced by the use of the accelerometer and gyroscope introduced in the design phase of this new version. This component could be used as a system start and stop. This for a long-term analysis could be ideal. This way at the moment when the system does not move for a certain time the system could stop recording the sEMG signal to have an energy-saving. Moreover, the data of accelerometer and gyroscope can be useful, in post-processing, to realize an algorithm of recognition of the movements. This would be helpful to identify the times when repeatable movements like gait begin. In this way, we could figure out which signal windows to use for the study of synergies.

Further progress could be made by introducing wireless communication to see in real-time the signal that the device is recording. This option is useful to verify the correct electrode positioning and generally the signal quality that the system is

recording. In addition, via a wireless application, channel gain parameters could be set and ATC characteristic parameters (time window, threshold) modified or controlled. In this way, the system would be more adaptable to any type of movement and customizable for each individual.

As regards the application fields, the technique of extracting synergies with the ATC signal on other types of repeatable movements should be tested. An example of the upper limbs is the *kranking* movement. ATC should be analyzed in detail to find all limits to the use of this technique for extracting muscle synergies and possibly make changes to overcome them.

Appendix A

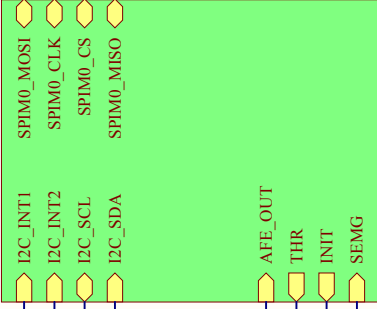
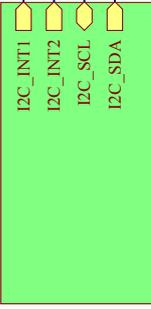
Circuit Diagram and Altium Design[®] Project

Power_management
power.SchDoc

Accelerometer
accelerometer.SchDoc

nRF52840
nRF52840.SchDoc

uSD_card
SD_card.SchDoc



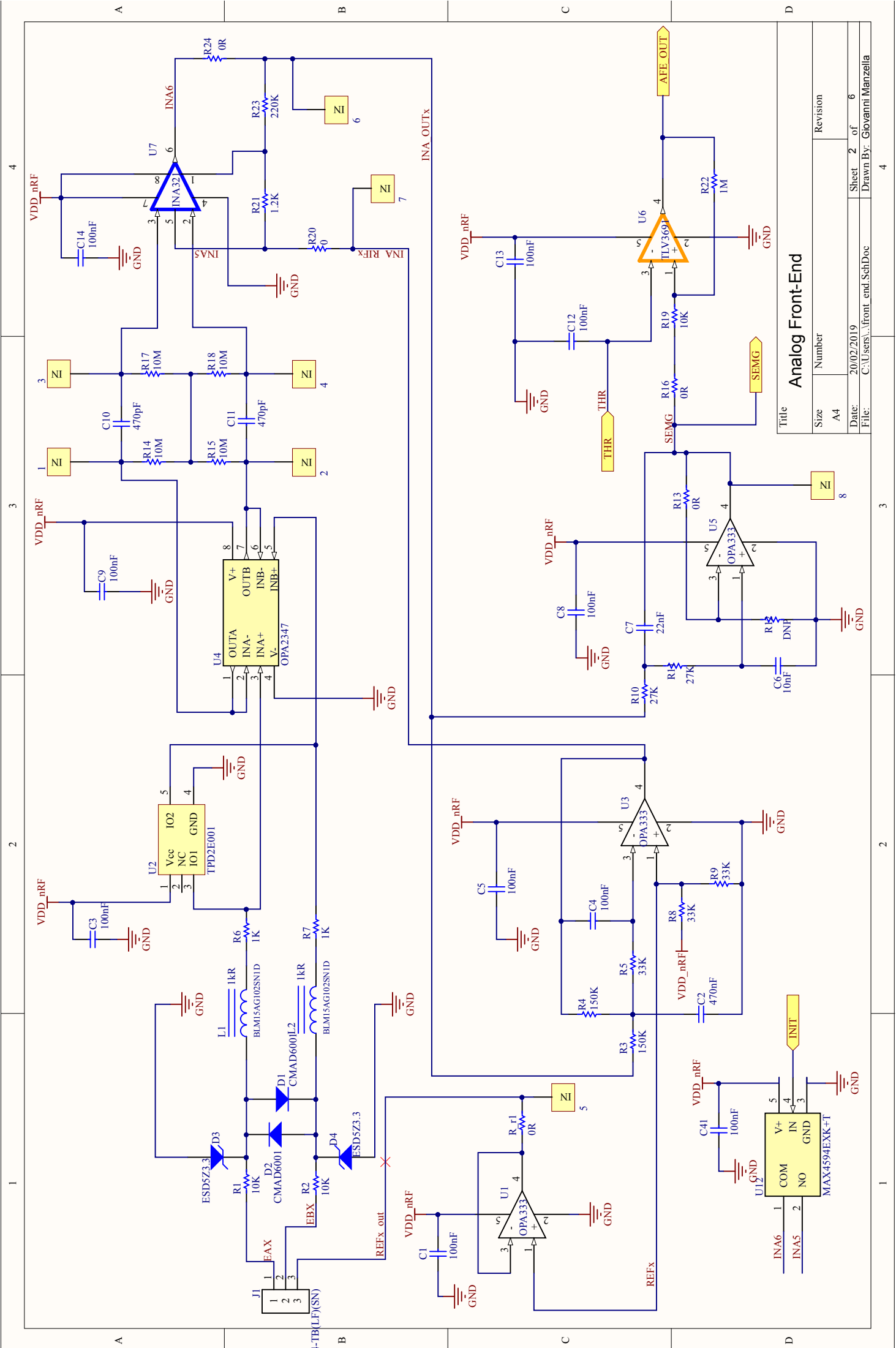
EMG
front_end.SchDoc



Title

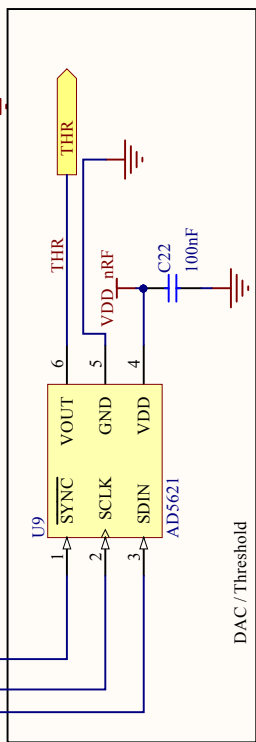
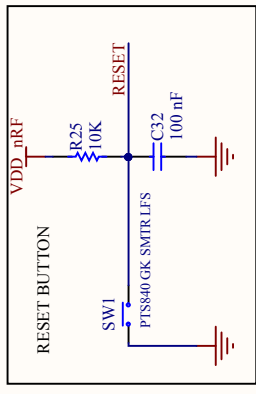
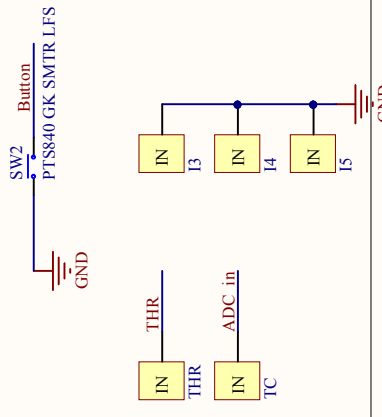
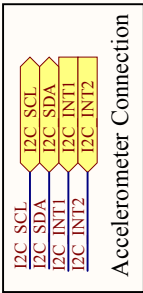
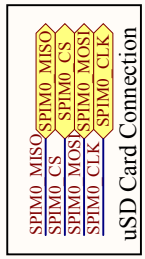
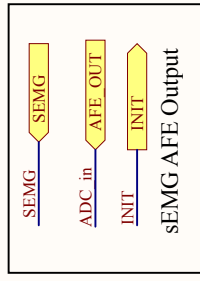
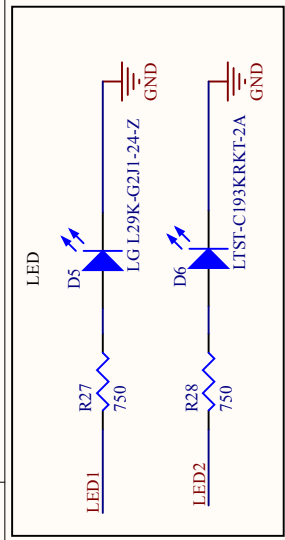
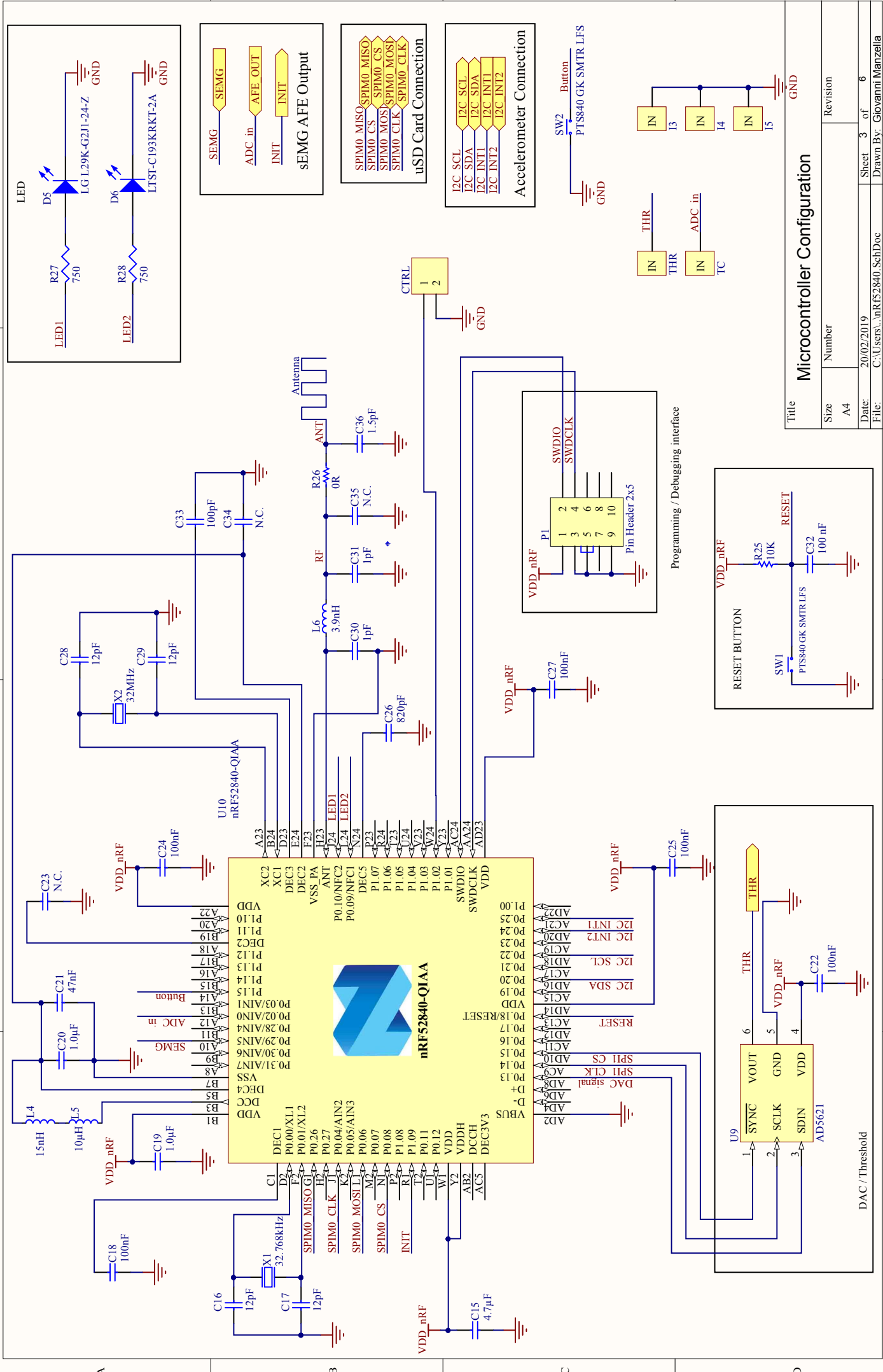
General Structure

Size	Number	Revision
A4		
Date:	20/02/2019	Sheet 1 of 6
File:	C:\Users\...general_structure.SchDoc Drawn By: Giovanni Manzella	

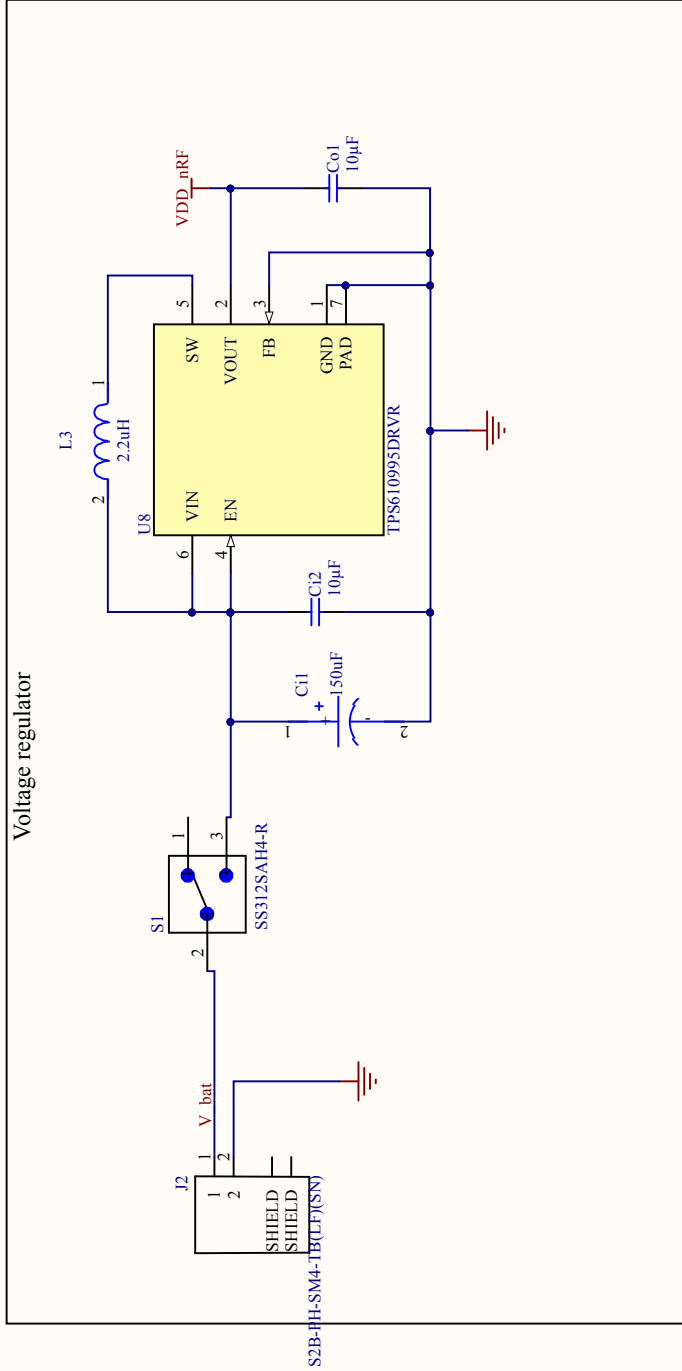


Title			
Size	Number	Revision	
A4			
Date:	20/02/2019	Sheet	2 of 6
File:	C:\Users\...\front_end.SchDoc		
		Drawn By:	Giovanni Manzella

Analog Front-End



Microcontroller Configuration			
Title	Size	Number	Revision
	A4		
Date:	20/02/2019	Sheet	3 of 6
File:	C:\Users\...nRF52840_SchDoc	Drawn By:	Giovanni Manzella



A

B

C

D

A

B

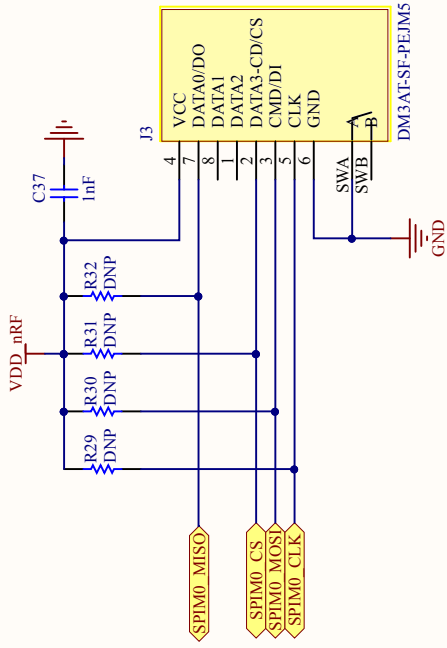
C

D

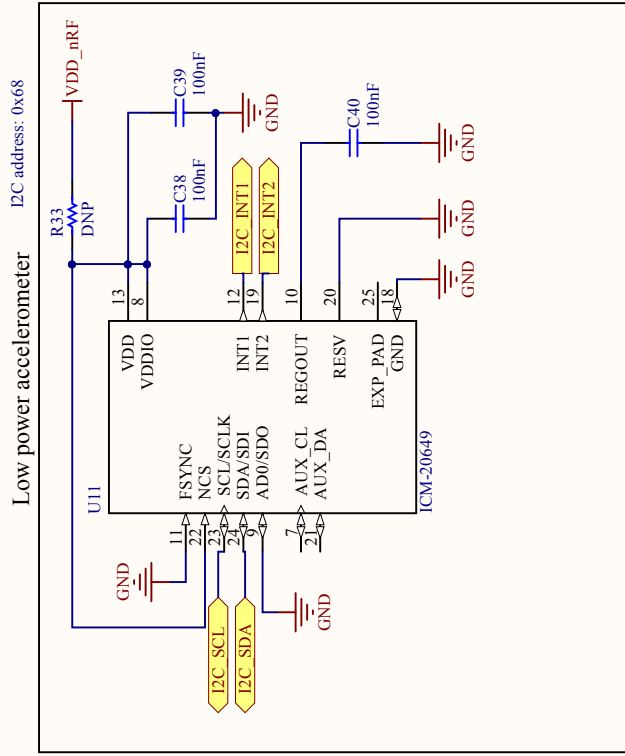
Title

Power Supply Management

Size	Number	Revision
A4		
Date:	20/02/2019	Sheet 4 of 6
File:	C:\Users\...power.SchDoc	Drawn By: Giovanni Manzella



Title		µSD Conditioning Circuits	
Size	Number	Revision	
A4			
Date:	20/02/2019	Sheet	5 of 6
File:	C:\Users\...\.SD_card.SchDoc	Drawn By: Giovanni Manzella	

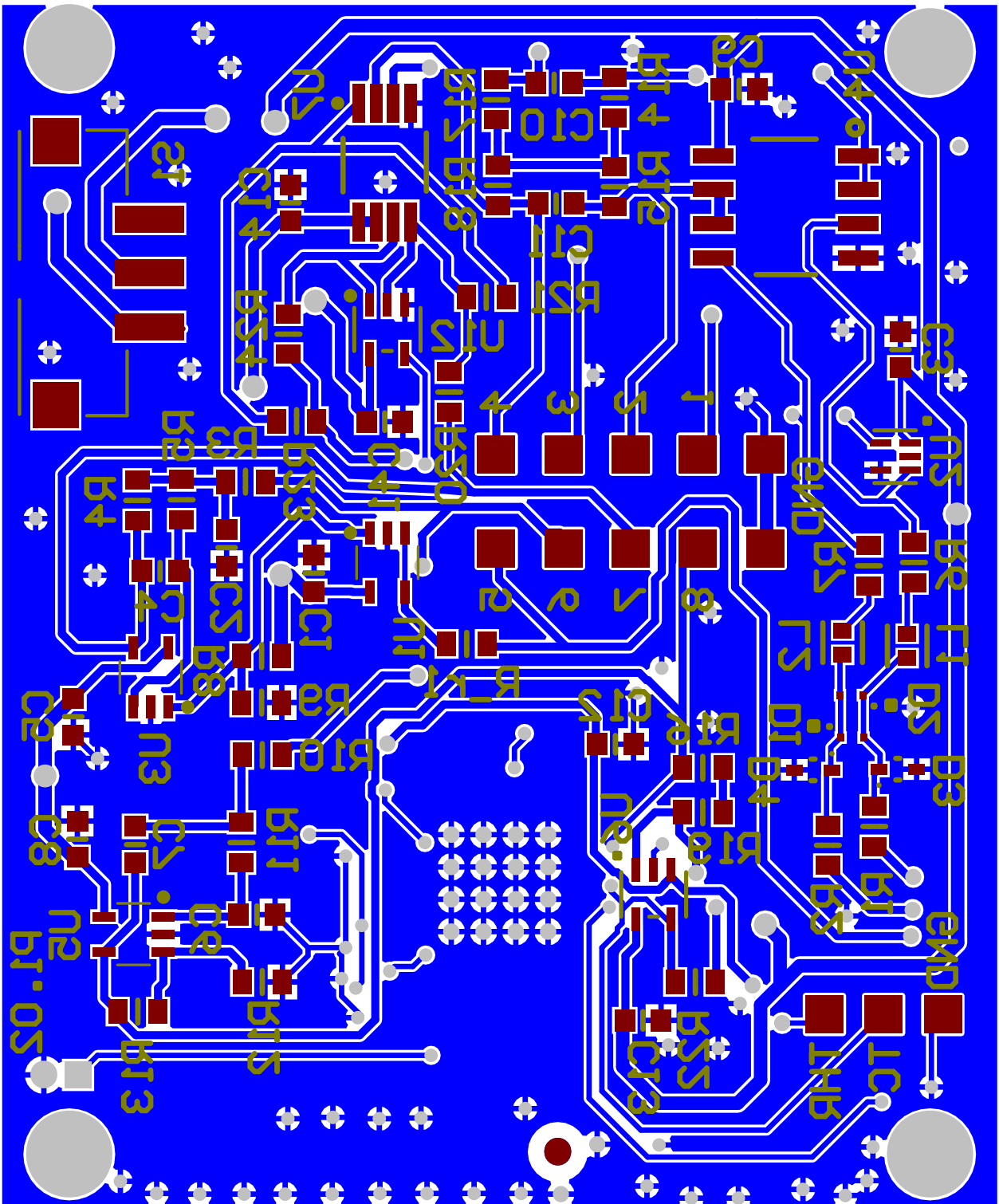


Title

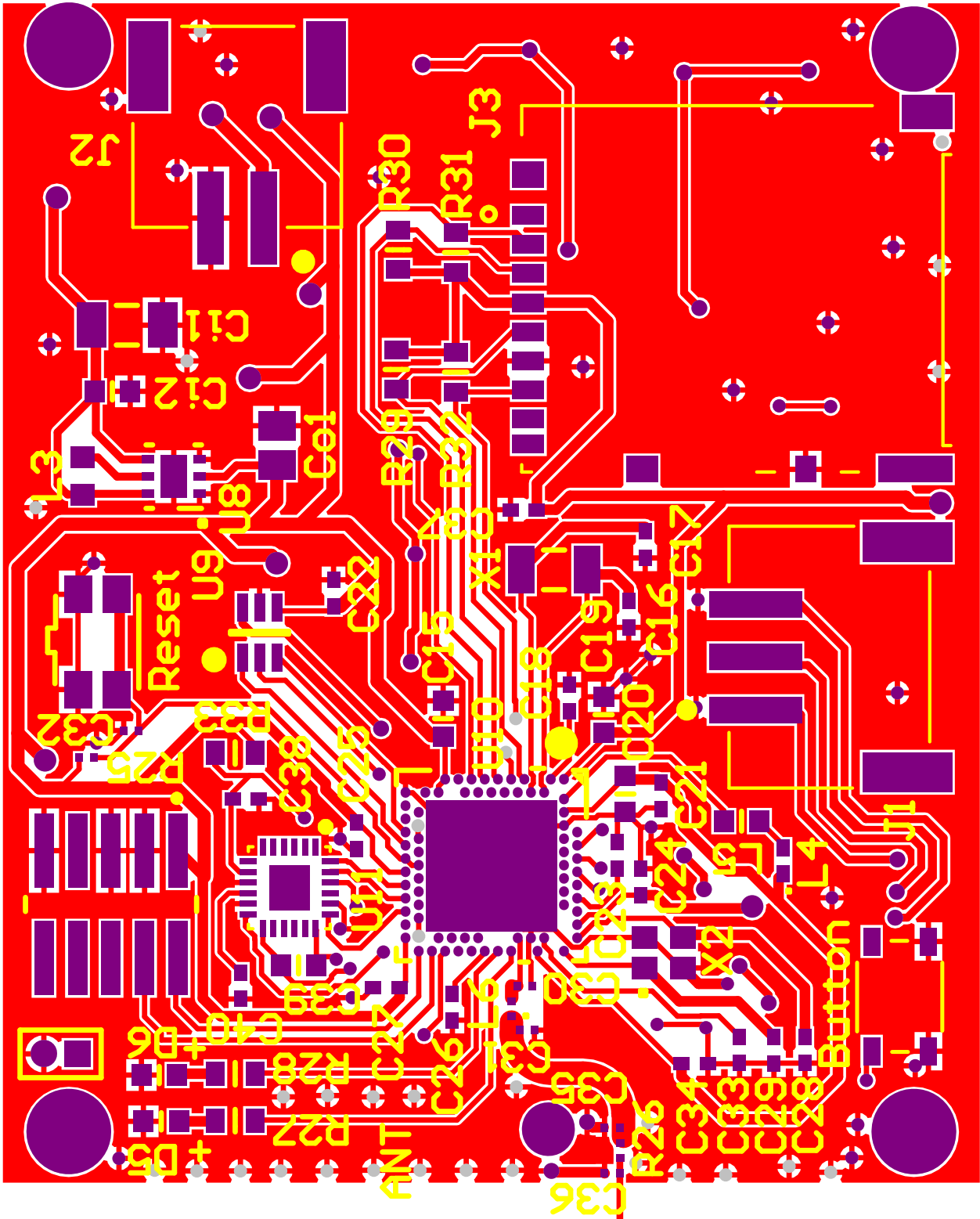
Accelerometer Conditioning Circuits

Size	Number	Revision
A4		
Date:	20/02/2019	Sheet 6 of 6
File:	C:\Users\... \accelerometer.SchDoc Drawn By: Giovanni Manzella	

2EMG-TC-Acd-v0.0



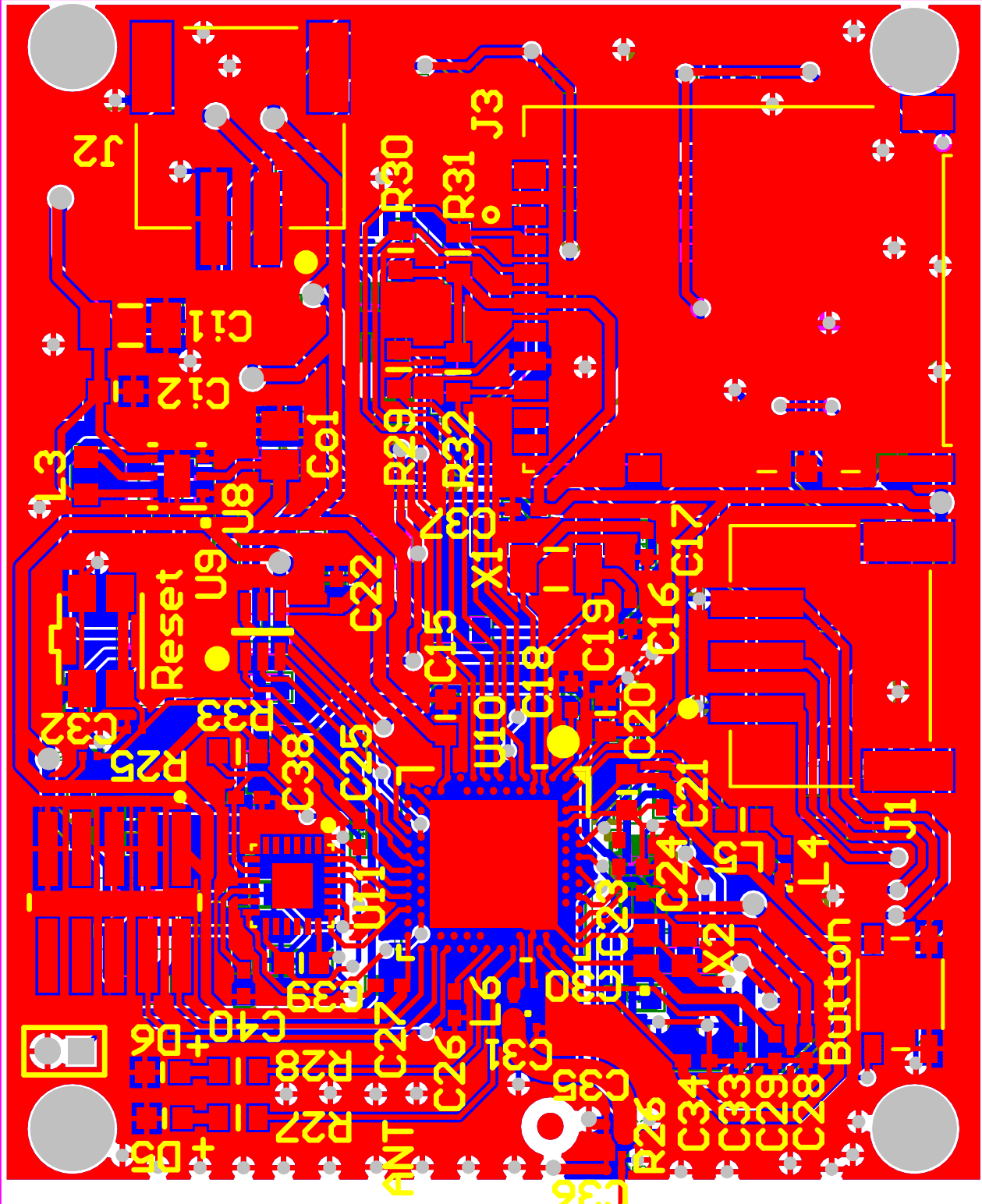
Bottom Layer



Top Layer

SISTER project MINES.polito.it

SISTER project MINEO.polito.it



PCB Overview

Acronyms

μC microcontroller.

μSD micro SD.

ADC Analog-to-Digital Converter.

ADP Adenosine DiPhosphate.

AER Address-Event Representation.

AFE Analog Front-End.

AP Action Potenzial.

ATC Average Threshold Crossing.

ATP Adenosine TriPhosphate.

CMRR Common Mode Rejection Ratio.

CNS Central Nervous System.

DAC Digital-to-Analog Converter.

ECG ElectroCardioGraphic.

EMG ElectroMyoGraphy.

ESB Enhanced ShockBurst.

ESD ElectroStatic Discharge.

FA Factorization Algorithm.

FES Functional Electrical Stimulation.

- FIFO** First Input First Output.
- FSR** Force Sensitive Resistor.
- I2C** Inter Integrated Circuit.
- IEC** International Electrotechnical Commission.
- iEMG** intramuscular ElectroMyoGraphy.
- IR-UWB** Impulse Radio Ultra Wide Band.
- JTAG** Joint Test Action Group.
- LED** Light Emitting Diode.
- MEMS** Micro Electro-Mechanical Systems.
- MISO** Master Input Slave Output.
- MLS** Motion Lab System.
- MOSI** Master Output Slave Input.
- MU** Motor Unit.
- MUAP** Motor Unit Action Potential.
- NFC** Near-Field Communication.
- NNMF** Non Negative Matrix Factorization.
- PCB** Printed Circuit Board.
- PSD** Power Spectral Density.
- QFN** Quad Flat No-leads.
- RAM** Random Access Memory.
- sEMG** Surface ElectroMyoGraphy.
- SNR** Signal to Noise Ratio.
- SPI** Serial Peripheral Interface.

TC Threshold Crossing.

THR THReshold.

USB Universal Serial Bus.

WBAN Wireless Body Area Network.

Bibliography

- [1] H. McGuinness, “Anatomy & physiology (5th edition),” pp. 128– 172, Hodder Education, 2018.
- [2] J. Moini, “Anatomy and physiology for health professionals (3th edition),” pp. 219 – 269, Jones & Barlett Learning, 2019.
- [3] J. E. Hall, “Guyton and hall textbook of medical physiology (12th edition),” pp. 71 – 90, Saunders, 2010.
- [4] R. Merletti and D. Farina, “Analysis of intramuscular electromyogram signals,” *Philosophical transactions. Series A, Mathematical, physical, and engineering sciences*, vol. 367, no. 1887, p. 357, 2009.
- [5] C. J. De Luca, A. Adam, R. Wotiz, L. D. Gilmore, and S. H. Nawab, “Decomposition of surface emg signals,” *Journal of neurophysiology*, vol. 96, no. 3, p. 1646, 2006.
- [6] C. G. M. A and V. T. M. M, “Surface electromyography: Why, when and how to use it,” *In: REVISTA ANDALUZA DE MEDICINA DEL DEPORTE*, 2011.
- [7] Carlo J. De Luca, *SURFACE ELECTROMYOGRAPHY: DETECTION AND RECORDING*, 2002. <https://www.delsys.com/downloads/TUTORIAL/semg-detection-and-recording.pdf>.
- [8] S. Sapienza, M. Crepaldi, P. Motto Ros, A. Bonanno, and D. Demarchi, “On integration and validation of a very low complexity atc uwb system for muscle force transmission,” *In: IEEE TRANSACTIONS ON BIOMEDICAL CIRCUITS AND SYSTEMS*, 2016.
- [9] S. Sapienza, P. Motto Ros, D. A. F. Guzman, F. Rossi, R. Terracciano, E. Cordedda, and D. Demarchi, “On-line event-driven hand gesture recognition based on surface electromyographic signals,” Institute of Electrical and Electronics Engineers Inc., 2018.
- [10] P. M. Ros, M. Paleari, N. Celadon, A. Sanginario, A. Bonanno, M. Crepaldi, P. Ariano, and D. Demarchi, “A wireless address-event representation system

- for atc-based multi-channel force wireless transmission,” IEEE - INST ELECTRICAL ELECTRONICS ENGINEERS INC, 2013.
- [11] M. Castagna, “Feasibility study of average threshold crossing (atc) technique application in muscle synergies analysis.,” 2019.
- [12] V. C. K. Cheung, A. Turolla, M. Agostini, S. Silvoni, C. Bennis, P. Kasi, S. Paganoni, P. Bonato, and E. Bizzi, “Muscle synergy patterns as physiological markers of motor cortical damage,” *Proceedings of the National Academy of Sciences of the United States of America*, vol. 109, no. 36, p. 14652, 2012.
- [13] Wikipedia contributors, “Coefficient of determination r2 Wikipedia, the free encyclopedia,” 2019. [Online; accessed 25-September-2019].
- [14] D. Rimini, V. Agostini, and M. Knaflitz, “Intra-subject consistency during locomotion: Similarity in shared and subject-specific muscle synergies,” *Frontiers in Human Neuroscience*, vol. 11, 2017.
- [15] M. Crepaldi, M. Paleari, A. Bonanno, A. Sanginario, P. Ariano, D. H. Tran, and D. Demarchi, “A quasi-digital radio system for muscle force transmission based on event-driven ir-uwband,” 2012.
- [16] A. Shahshahani, M. Shahshahani, P. M. Ros, A. Bonanno, M. Crepaldi, M. Martina, D. Demarchi, and G. Masera, “An all-digital spike-based ultra-low-power ir-uwband dynamic average threshold crossing scheme for muscle force wireless transmission,” in *2015 Design, Automation Test in Europe Conference Exhibition (DATE)*, pp. 1479–1484, EDAA, 2015.
- [17] I. Furfaro, “Integration and validation of average threshold crossing (atc) applied to surface electromyography (semg) / ivan furfaro ; rel. accademico danilo demarchi ; rel esterno silvestro micera,” 2015.
- [18] S. Cecchini, “Average threshold crossing validation for functional electrical stimulation applied to surface electromyographic signals,” 2018.
- [19] B. Sereni, “Desing and development of a low-power wearable device for the acquisition of surface electromyography (semg) signals with average threshold crossing (atc) / bianca sereni ; rel. danilo demarchi ; rel. aziendale paolo motto ros,” 2016.
- [20] F. Rossi, “Low power system for event-driven control of functional electrical stimulation/ fabio rossi ; rel. danilo demarchi ; rel. aziendale paolo motto ros,” 2017.
- [21] M. C. Tresch, V. C. Cheung, and A. d’Avella, “Matrix factorization algorithms for the identification of muscle synergies: evaluation on simulated and experimental data sets,” *Journal of neurophysiology*, vol. 95, no. 4, pp. 2199–2212, 2006.
- [22] J. Taborri, V. Agostini, P. K. Artemiadis, M. Ghislieri, D. A. Jacobs, J. Roh,

- and S. Rossi, “Feasibility of muscle synergy outcomes in clinics, robotics, and sports: A systematic review,” *Applied Bionics and Biomechanics*, vol. 2018, 2018.
- [23] D. Rimini, V. Agostini, S. Rosati, C. Castagneri, G. Balestra, and M. Knaflitz, “Influence of pre-processing in the extraction of muscle synergies during human locomotion,” *IEEE*, 2017.
- [24] P. Kieliba, P. Tropea, E. Pirondini, M. Coscia, S. Micera, and F. Artoni, “How are muscle synergies affected by electromyography pre-processing?,” *IEEE Transactions on Neural Systems and Rehabilitation Engineering*, vol. 26, no. 4, pp. 882–893, 2018.
- [25] G. Torres-Oviedo and L. H. Ting, “Muscle synergies characterizing human postural responses,” *Journal of neurophysiology*, vol. 98, no. 4, pp. 2144–2156, 2007.
- [26] D. Rimini, V. Agostini, and M. Knaflitz, “Evaluation of muscle synergies stability in human locomotion: A comparison between normal and fast walking speed,” in *2017 IEEE International Instrumentation and Measurement Technology Conference (I2MTC)*, pp. 1–5, IEEE, 2017.
- [27] V. C. Cheung, A. d’Avella, M. C. Tresch, and E. Bizzi, “Central and sensory contributions to the activation and organization of muscle synergies during natural motor behaviors,” *Journal of Neuroscience*, vol. 25, no. 27, pp. 6419–6434, 2005.
- [28] E. Morin, “Lower limb muscle synergies during gait in humans,” in *2006 International Conference of the IEEE Engineering in Medicine and Biology Society*, pp. 6667–6669, IEEE, 2006.
- [29] A. Tuoheti, “Smart embedded systems for biomedical applications,” 2019.
- [30] ON Semiconductor, *ESD5Z2.5T1G Series, SZESD5Z2.5T1G Series ESD Protection Diode*, Rev.15 2018. datasheet, <https://www.mouser.com/datasheet/2/308/ESD5Z2.5T1-D-74691.pdf>.
- [31] CENTRAL SEMICONDUCTOR, *CMAD6001 SURFACE MOUNT ULTRA LOW LEAKAGE SILICON SWITCHING DIODE*, Rev. 2010. datasheet, https://my.centralsemi.com/get_document.php?cmp=1&mergetype=pd&mergepath=pd&pdf_id=CMAD6001.PDF.
- [32] Murata Electronics, *Chip Ferrite Bead BLM15SN series*. datasheet, <https://www.murata.com/en-us/products/productdata/8796740059166/ENFA0018.pdf>.
- [33] Texas Instruments, *TPD2E001 Low-Capacitance 2-Channel ESD-Protection for High-Speed Data Interfaces*, Rev. 2016. datasheet, <http://www.ti.com/lit/ds/symlink/tpd2e001.pdf>.

- [34] Texas Instruments, *microPower, Rail-to-Rail Operational Amplifiers (OPA2347)*, Rev. 2007. datasheet, <http://www.ti.com/lit/ds/symlink/opa2347.pdf>.
- [35] E. Spinelli, R. Pallas-Areny, and M. Mayosky, "Ac-coupled front-end for biopotential measurements," *IEEE Transactions on Biomedical Engineering*, vol. 50, no. 3, pp. 391–395, 2003.
- [36] C. J. De Luca, L. Donald Gilmore, M. Kuznetsov, and S. H. Roy, "Filtering the surface emg signal: Movement artifact and baseline noise contamination," *Journal of Biomechanics*, vol. 43, no. 8, pp. 1573–1579, 2010.
- [37] J. Potvin and S. Brown, "Less is more: high pass filtering, to remove up to 99% of the surface emg signal power, improves emg-based biceps brachii muscle force estimates," *Journal of Electromyography and Kinesiology*, vol. 14, no. 3, pp. 389–399, 2004.
- [38] Texas Instruments, *microPower, Single-Supply, CMOS Instrumentation Amplifier (INA321)*, Rev. 2006. datasheet, <http://www.ti.com/lit/ds/symlink/ina2321.pdf>.
- [39] Maxim Integrated, *Low-Voltage, Single-Supply, 10 Ω SPST CMOS Analog Switches (MAX459)*, Rev.2 2004. datasheet, <https://datasheets.maximintegrated.com/en/ds/MAX4594-MAX4597.pdf>.
- [40] Texas Instruments, *OPAx3331.8-V, microPower, CMOS Operational Amplifiers, Zero-Drift Series (OPA333)*, Rev. 2015. datasheet, <http://www.ti.com/lit/ds/symlink/opa333.pdf>.
- [41] Texas Instruments, *TLV3691 0.9-V to 6.5-V, Nanopower Comparator*, Rev. 2015. datasheet, <http://www.ti.com/lit/ds/symlink/tlv3691.pdf>.
- [42] Analog Devices Inc., *2.7 V to 5.5 V, <100 A, 8-/10-/12-Bit nanoDAC, SPI Interface in LFCSP and SC70, AD5601/AD5611/AD5621*, Rev. 2019. datasheet, https://www.analog.com/media/en/technical-documentation/data-sheets/AD5601_5611_5621.pdf.
- [43] Interlink Electronics, *FSR[®] Force Sensing Resistors[®]*, Rev. C. Integration guide, <https://www.generationrobots.com/media/FSR400-Series-Integration-Guide.pdf>.
- [44] Texas Instruments, *TPS61099x Synchronous Boost Converter with Ultra-Low Quiescent Current*, Rev. 2018. datasheet, <http://www.ti.com/lit/ds/symlink/tps61099.pdf>.
- [45] "nrf52840 dongle." <https://www.nordicsemi.com/Software-and-Tools/Development-Kits/nRF52840-Dongle/Download#infotabs>.
- [46] TDK InvenSense, *World's First Wide-Range 6-Axis MEMS Motion-TrackingTM Device for Sports and High Impact Applications*, Rev.

2016. datasheet, https://product.tdk.com/info/en/documents/catalog_datasheet/motion/DS-000192-ICM-20649-v1.0.pdf.
- [47] Nordic Semiconductor, *nRF52840 Product Specification V1.1*, Rev. 2019. datasheet, https://www.nordicsemi.com/-/media/DocLib/Other/Product_Spec/nRF52840PSv11pdf.pdf.
- [48] “J-link edu mini.” <https://www.segger.com/products/debug-probes/j-link/models/j-link-edu-mini/>.
- [49] “Nrf52832, nrf52840 and nrf52810 comparison.” <https://devzone.nordicsemi.com/f/nordic-q-a/24919/nrf52832-nrf52840-and-nrf52810-comparison>.
- [50] “Altium designer templates with eurocircuits design rules.” <https://www.eurocircuits.com/altium-designer-templates-with-eurocircuits-design-rules/>.
- [51] L. Seung-Seok, L. J. Hyun, P. I. Keun, S. Sung-Jin, and C. M. Yong, “Development of a portable and wireless surface emg,” in *Advanced Nondestructive Evaluation I*, pp. 1–1, Trans Tech Publications Ltd, 2006.
- [52] Texas Instruments, *TPS63070 2-V to 16-V Buck-Boost Converter With 3.6-A Switch Current*, Rev. 2016. datasheet, <http://www.ti.com/lit/ds/symlink/tps63070.pdf>.
- [53] SparkFun Electronics, *SparkFun Buck-Boost Converter*. datasheet, https://media.digikey.com/pdf/Data%20Sheets/Sparkfun%20PDFs/COM-15208_Web.pdf.
- [54] Motion Lab Systems, *MA-300 EMG System User Guide*, Rev. 2012. User Guide, https://www.motion-labs.com/pdf/ma300_user_manual_harwin.pdf.
- [55] “Ma-411 emg preamplifier.” https://www.motion-labs.com/prod_preamp_ma411.html.
- [56] “Iec 60479-1:2018.” <https://webstore.iec.ch/publication/62980>.
- [57] J. Perry and B. Schoneberger, *Gait Analysis: Normal and Pathological Function*. SLACK, 1992.
- [58] R. Howard, *The application of data analysis methods for surface electromyography in shot putting and sprinting*. PhD thesis, 11 2017.